

ABSTRACT

Title of Dissertation: **FREQUENCY MODULATION SPECTROSCOPY
TECHNIQUES FOR DETECTION OF WATER VAPOR
ON MARS**

Mark Flanagan, Doctor of Philosophy, 2004

Dissertation directed by: Professor Christopher Davis
Department of Electrical Engineering

Remote measurements of atmospheric trace gases are critical to the understanding of both Earth and planetary meteorological systems. The conventional lidar technique currently applied is Differential Absorption lidar (DIAL). A potentially more sensitive method is Frequency Modulation (FM) spectroscopy. An original analysis will investigate the feasibility of using FM techniques for remote sensing of water vapor in the Martian atmosphere. Original mathematical models, both analytic and computer models, will be used in this effort. This analysis will establish the limitations of using scattered light for the return. Using FM sounding techniques will be shown to overcome these limitations. A SNR equation based on the FM sounding technique will be developed. A model of the Martian atmosphere will be described and used along with the SNR equation to evaluate the performance of an FM sounding system for detection of water vapor on Mars.

FREQUENCY MODULATION SPECTROSCOPY TECHNIQUES FOR
DETECTION OF WATER VAPOR ON MARS

by

Mark Flanagan

Dissertation submitted to the Faculty of the Graduate School of the
University of Maryland, College Park in partial fulfillment
of the requirements for the degree of
Doctor of Philosophy
2004

Advisory Committee:

Professor Christopher Davis, Chair
Professor Robert Gammon
Professor Julius Goldhar
Professor Ping-Tong Ho
Professor Thomas Murphy

© Copyright by

Mark Flanagan

2004

DEDICATION

To my mother and father,
Elisabeth Adeline Flanegan
and
William Clinton Flanegan

ACKNOWLEDGEMENTS

Without the educational programs available at GSFC and the willingness on the part of my managers to let me use them, it wouldn't have been possible for me to finish. Many of my colleagues at GSFC have encouraged and supported me throughout this task. I'm honored to have worked with them all and thankful for all their help. The education I received at the University of Maryland was excellent. I appreciate all the assistance provided by the professors and teaching assistants who have listened patiently to my questions and helped me work through the answers. In particular my advisor, Dr. Christopher Davis, has provided assistance at critical junctures.

I would especially like to thank my family, both Flanegans and Harpers, and the many friends who have encouraged me over the years. Those words of encouragement helped more than you know.

Mostly I would like to thank Abigail and Gwentyth, who shared in both the effort and accomplishment.

TABLE OF CONTENTS

1.	INTRODUCTION.....	1
2.	INTRODUCTION TO FREQUENCY MODULATION REMOTE SENSING ON MARS.....	4
2.1.	Why Measure Water Vapor on Mars?	4
2.2.	Introduction to Remote Sensing	7
2.3.	DIAL Remote Sensing	8
2.4.	Coherent Remote Sensing	10
2.5.	Laboratory FM Technique.....	12
2.6.	Remote Sensing Using FM	15
2.7.	Novel Contributions of Dissertation.....	18
2.8.	Organization of Dissertation.....	19
3.	WATER VAPOR IN THE MARTIAN ATMOSPHERE	21
3.1.	Introduction.....	21
3.2.	The Martian Atmosphere.....	21
3.3.	Modeling the Return on Mars using the LIDAR equation.....	25

3.4.	The Basic LIDAR Equation	26
3.5.	Technology Limited Parameters	28
3.5.1.	Quantum Efficiency and Detectors	29
3.5.2.	Laser Wavelength Selection	30
3.5.3.	Laser Energy	31
3.5.4.	Laser linewidth.....	32
3.5.5.	Summary of Technology restricted parameters	33
3.6.	Ranging Parameters	35
3.6.1.	Ranging Resolution.....	35
3.6.2.	Coherence length limits to pulsewidth.....	37
3.6.3.	Frequency of Laser Firing.....	38
3.6.4.	Summary of Ranging Parameters	38
3.7.	Science Limited Parameters.....	40
3.7.1.	Backscatter	41
3.7.2.	Attenuation.....	44
3.8.	LIDAR Equation Solution.....	48
3.9.	Summary of LIDAR Equation Results.....	50
4.	FM REMOTE SENSING EQUATIONS.....	51
4.1.	Introduction.....	51
4.2.	Laboratory FM equations.....	52
4.2.1.	Single Tone with external modulation.....	52
4.2.2.	Two tone with external modulation	54
4.2.3.	Single Tone with current modulation	58
4.2.4.	Two Tone with current modulation	59
4.2.5.	Summary and Limitations of Laboratory Equations.....	59
4.3.	Development of the Two Tone FM Remote Sensing Model.....	60
4.4.	Review of Two Tone FM Remote Sensing Model	68

4.5.	Comparison to Laboratory Equations.....	69
4.6.	Uses and Limits of Analytic Equation.....	72
4.7.	Description of Computer Model.....	73
4.8.	Summary.....	74
5.	FM REMOTE SENSING PHASE EFFECTS.....	75
5.1.	Introduction.....	75
5.2.	Phase effects introduction	75
5.3.	Lossless, equally spaced scatterers	79
5.4.	Lossy, Equally Spaced Scatterers.....	91
5.5.	Two Tone Results: Lossy, Equally Spaced Scatterers.....	97
5.6.	Summary.....	99
6.	EXPERIMENT DESCRIPTION AND RESULTS.....	101
6.1.	Introduction.....	101
6.2.	Comparison to Previously Published Experimental Data.....	101
6.3.	Current Modulation Phase Experiment Introduction.....	103
6.4.	Experiment Description and Preliminary Measurements	104
6.4.1.	Setup	104
6.4.2.	Laser Frequency Adjustment	107

6.4.3.	Linewidth Measurement	108
6.4.4.	Modulation Response of Laser vs Frequency	110
6.4.5.	Modulation Response of the Laser vs. Power.....	111
6.4.6.	Summary of preliminary results.....	113
6.5.	Experiment Results.....	114
6.6.	Discussion and Conclusions	116
7.	FM SOUNDING SNR EQUATION DEVELOPMENT.....	118
7.1.	Introduction.....	118
7.2.	Sounding	118
7.3.	Laboratory FM SNR Equation.....	119
7.3.1.	Return Current Term.....	120
7.3.2.	Q term	121
7.3.3.	Noise Terms	123
7.3.4.	Summary of Laboratory SNR Equation.....	125
7.4.	FM Remote Sensing Sounding Equation	126
7.4.1.	LIDAR equation modifications for sounding	126
7.4.2.	FN SNR modifications for sounding	127
7.4.3.	Calculating P_{RS}	129
7.4.4.	Calculating Q_{RS}	130
7.4.5.	FM Remote Sensing SNR equations summary.....	134
8.	FM SOUNDING SNR ANALYSIS	136
8.1.	SNR Parameters.....	136
8.2.	Noise Currents.....	139
8.3.	SNR Equation Analysis	144
8.3.1.	FM modulation index.....	144
8.3.2.	AM modulation index	145

8.3.3.	Laser power.....	147
8.4.	Summary.....	150
9.	SUMMARY	151
10.	CONCLUSIONS.....	155
11.	RECOMMENDATIONS FOR FUTURE WORK.....	157
12.	REFERENCES.....	159

LIST OF TABLES

Table 3.1. Composition of the lower atmosphere of Mars	23
--	----

LIST OF FIGURES

Figure 2.1. Hebes Chasm on Mars from Viking Orbiter	4
Figure 2.2. Olympic Mons volcano on Mars	5
Figure 2.3. Early Earth and Mars comparison	6
Figure 2.4. Basic Laser Remote Sensing Configuration.....	7
Figure 2.5. DIAL Signal and Absorption Profile.....	9
Figure 2.6. Coherent Detection System	10
Figure 2.7. Laboratory FM technique	13
Figure 2.8. Frequency Modulation Remote Sensing System (scattered return)	16
Figure 3.1. Viking 2 Lander site pressure and temperature	22
Figure 3.2. Profile of water vapor at the Viking Lander 2 site	24
Figure 3.3 Diagram of LIDAR equation parameters	27
Figure 3.4. Water vapor absorption lines at 1atm, 23°C, 50m path length.....	30
Figure 3.5. Water vapor absorption line at 935.68nm	31
Figure 3.6. 935.68 absorption line for 4.6 Torr and -30C.....	33
Figure 3.7. Ranging resolution.....	36
Figure 3.8. Altitudinal variation of backscatter	43
Figure 3.9. Atmospheric Transmission due to Backscatter	45
Figure 3.10. Atmospheric Transmission due to Absorption.....	47
Figure 3.11. Detector counts due to Martian return.....	49
Figure 4.1 Single Tone FM.....	53
Figure 4.3. Two tone in a laboratory configuration	55
Figure 4.4. Two tone FM	56

Figure 4.5. Electric Field Spectrum of FM signal with carrier in center	61
Figure 5.1. Time of flight.....	76
Figure 5.2. DubinskyFM signal from Two Scatterers	78
Figure 5.3. Source and Absorption	79
Figure 5.4. Sideband Absorption	80
Figure 5.5. Return current in time domain.....	81
Figure 5.6 Detector currents of different phases versus time	82
Figure 5.7. Time-Distance diagram	82
Figure 5.8. Summation of return.....	83
Figure 5.9. Detector current vs. distance induced phase difference of return waves	85
Figure 5.10. Interference of return currents for absorptions of 1 and 0.5.....	87
Figure 5.11. Interference of detector currents for summation of 10 waves	88
Figure 5.12. Interference of detector current for 100 waves (1).....	89
Figure 5.13. Interference of detector currents for 100 waves (2)	90
Figure 5.14. Return waveform including scattering loss	92
Figure 5.15. Return waveforms summed.....	93
Figure 5.16. Detector current vs. distance induced phase difference	94
Figure 5.17. Detector current vs. distance induced phase difference at 150 meters.....	95
Figure 5.18. Detector current vs. distance induced phase difference at	96
Figure 5.19. Current vs. distance induced phase difference, two tone	97
Figure 5.20. Detector current vs. distance induced phase difference at 150 meters.....	98
Figure 5.21. Detector current vs. distance induced phase difference at 150 meters (log scale)	98

Figure 6.1. Computed FM signal from Two Scatterers (top) compared to Dubinsky's laboratory data (bottom)	102
Figure 6.3. Laser and isolator	106
Figure 6.4. Beamsplitting, delay path and recombination	106
Figure 6.5. Entire Experimental Setup.....	107
Figure 6.6. Laser linewidth	109
Figure 6.7. Optical power as a function of frequency.....	111
Figure 6.8. Optical power as a function of RF power.....	112
Figure 6.9. Modulated laser	113
Figure 6.10. Delay-non Delay phase difference	114
Figure 6.11. Detector signal as a function of differential distance	115
Figure 7.1. FM Sounding	119
Figure 7.2. Transmission versus Relative Frequency	133
Figure 8.1. Martian Water Vapor Parameters.....	137
Figure 8.2. Science Requirements: Range Resolution and Firing Rate.....	138
Figure 8.3. Science Requirements: Laser	138
Figure 8.4. Science Requirements: Receiver/Detector	139
Figure 8.5. Noise Current vs Laser power for single mode FM sounding.....	140
Figure 8.6. Noise currents vs temperature for FM sounding at 1W laser power	141
Figure 8.7. RAM and shot noise comparison as a function of M	142
Figure 8.8. RAM/shot noise ratio as a function of laser power	143
Figure 8.9. SNR vs. Power showing maximum at $B=1.2$	145
Figure 8.10. SNR as a function of M for various B around 1.2.....	146

Figure 8.11. SNR as a function of power for various FM indices	148
Figure 8.12 SNR as a function of power for various AM indices	149

1. Introduction

Frequency Modulation (FM) spectroscopy has been shown to be a sensitive technique for measuring trace gases in the laboratory environment. Orders of magnitude improvement over conventional absorption spectroscopy techniques has been demonstrated. This demonstrated ability to sensitively measure trace gases in the laboratory raises the possibility that these techniques can be used to measure atmospheric trace gases in a remote sensing environment. The purpose of this paper is to conduct a detailed investigation, supported by analytic and computer models validated by experiment, of FM techniques for remote sensing. The focus of this effort is the measurement of water vapor in the Martian atmosphere.

The transition to a remote sensing environment is complex. The analysis and results obtained in the laboratory do not incorporate considerations that are crucial to a remote sensing application. The equations developed and the analysis performed for laboratory applications are not adequate to predict the behavior in a remote sensing environment. Inherent in these equations are assumptions concerning phase relationships and power levels, for example, that do not hold in remote sensing applications. In order to determine the feasibility of using FM techniques for remote sensing applications, this paper addresses these considerations which are ignored in the laboratory.

In order to evaluate remote sensing uses of FM techniques we develop more sophisticated models that include characteristics important to remote sensing. Initially we develop an analytic model. This is a model based on the development of equations to describe the behavior of the FM remote sensing system. This model is a significant

improvement over the laboratory version. It includes important considerations such as phase effects that allow the calculation of the FM remote sensing system behavior when the return light is produced by scattering off of atmospheric constituents. However, this model is also limited. To remedy this a computer model is developed. The computer model is significantly more sophisticated and flexible than the analytic model. The result of using this model to analyze a FM remote sensing system based on scattered returns is presented in detail. Various scenarios are calculated and described in this paper. The analysis presented supports the significant conclusion that FM remote sensing based on scattered light has severe limitations.

In order to verify that the models are valid and the conclusions, therefore, are also valid, we compare the results to previously published experimental data as well as conduct a unique experiment. The previously published data is shown to fit the model predictions. The experiment builds on that to verify another aspect of the model. Taken together, these results establish the validity of the model used. More than this, they both address important parts of the model that deal with the phase of the return light. They verify that the model correctly predicts the phase behavior of the return signal. This is a key verification since the phase dependent value of the detected signal is the key result obtained from the model.

The conclusion that FM techniques dependent on scattered light have severe limitations is an important one. The results obtained from the model and verified by experiment also indicate how these limitations can be avoided. We conclude that an FM system based on the return of light from a reflecting surface avoids the problems associated with the scattered light. This technique, called sounding, can be used to

sensitively measure the atmosphere, albeit without ranging data.

The key calculation for this FM sounding system is the Signal to Noise (SNR) ratio as a function of the key FM parameters. We develop an FM sounding SNR equation by making important modifications to the laboratory FM equation and combining it with the Mars LIDAR equation. From this equation and the noise current equations that are a part of it, we first calculate the noise currents to show that shot noise limited performance can be expected for a Martian FM sounding experiment. Varying the values of the critical FM parameters allows us to determine their optimal value and the behavior of the SNR as a function of those values. Based on this analysis we conclude that the FM sounding technique retains the advantageous of the laboratory FM technique while avoiding the disadvantageous of the FM remote sensing technique based on scattering for a FM remote sensing system to detect water vapor on Mars.

2. Introduction to Frequency Modulation Remote Sensing on Mars

2.1. Why Measure Water Vapor on Mars?

Mars used to have large amounts of water. Around three and a half billion years ago Mars likely had water in seas and rivers. Canyons, islands and river structures on Mars all testify to the former presence of water. Evidence of this can be seen below in a photograph of the 120 km long Hebes Chasm on Mars. The feature in the middle looks like an island, perhaps indicating the presence of a lake in the past that has since drained away.

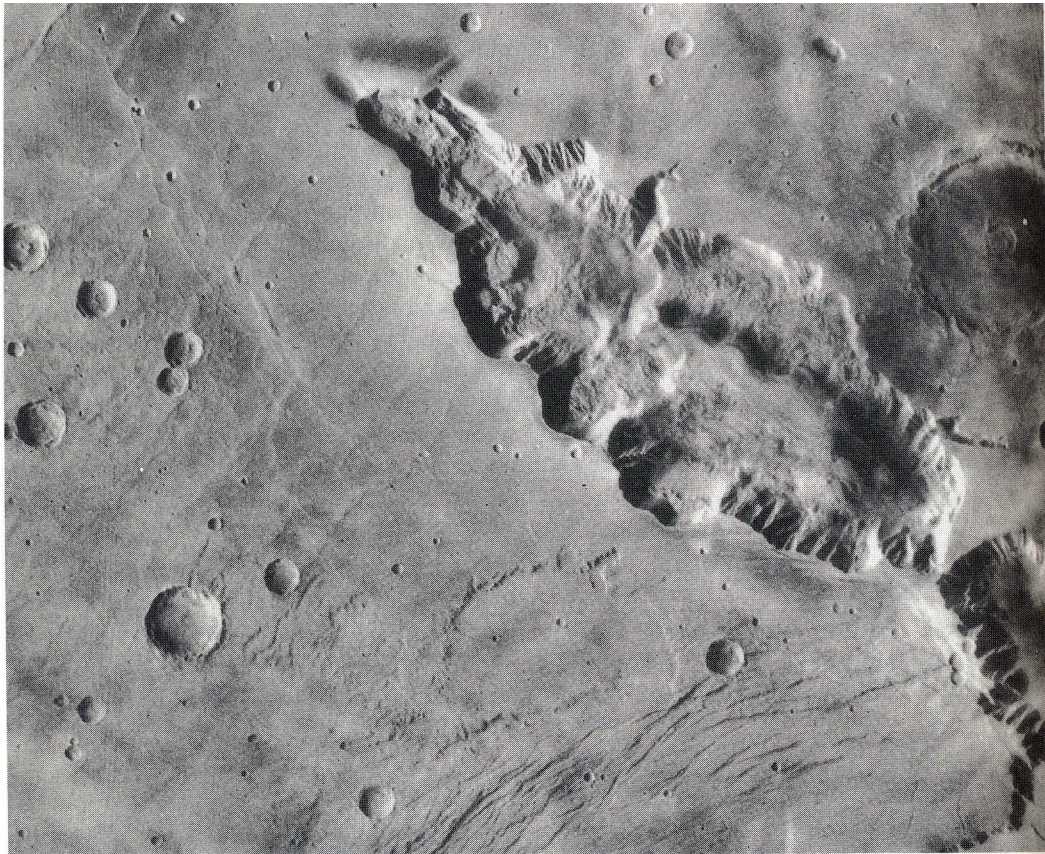


Figure 2.1. Hebes Chasm on Mars from Viking Orbiter [1]

The next photograph shows the Martian volcano Olympus Mons. A notable feature Olympus Mons has in common with other volcanoes on Mars is the relative absence of cratering. This indicates that these volcanoes are relatively young and possibly still spewing gasses, such as water vapor, into the atmosphere.

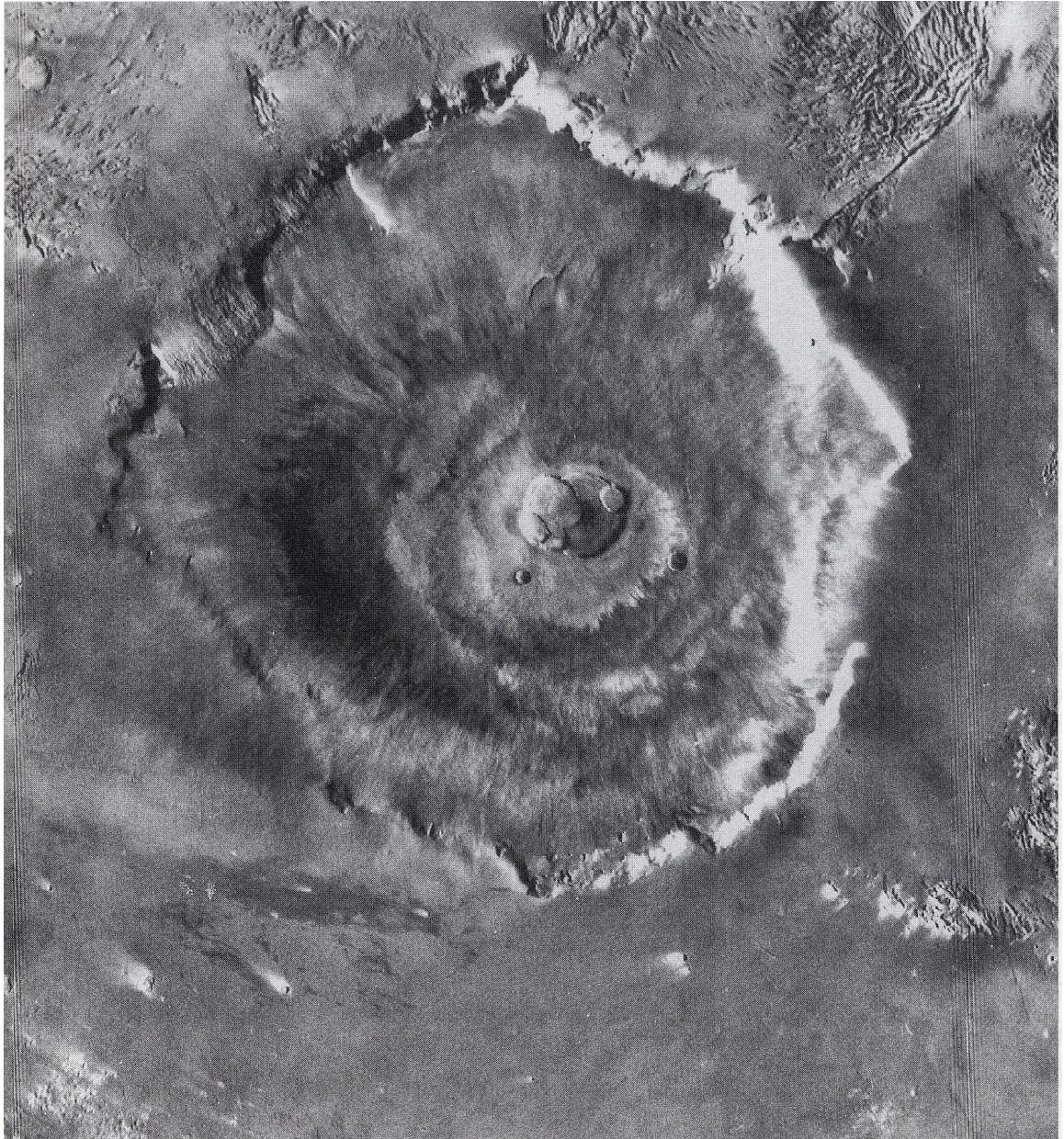


Figure 2.2. Olympus Mons volcano on Mars [2]

Perhaps most exciting is that the presence of water has great significance for the search for life on Mars. The early Earth and early Mars had some similarities that indicate the possibility that life developed on Mars as well as Earth.

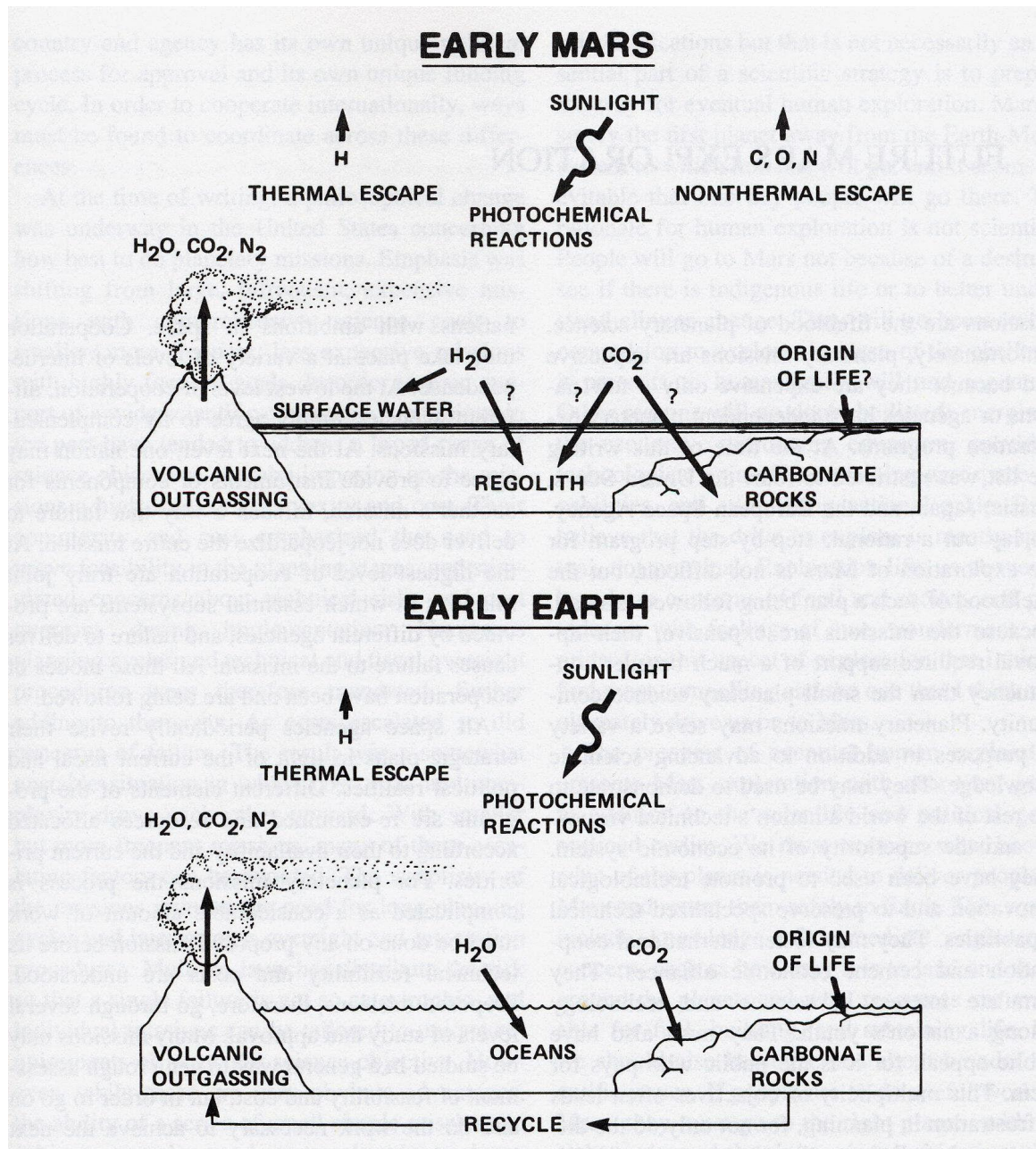


Figure 2.3. Early Earth and Mars comparison [3]

We can see from this diagram that the search for water plays a key role in the search for life on Mars. The search for water is also an essential part of the general scientific effort to gain an understanding of Mars atmospheric processes and climatological history. Knowing the distribution of water vapor on Mars over time would greatly expand our knowledge of Mar's development and the search for life on worlds other than Earth.

2.2. Introduction to Remote Sensing

Measuring water vapor on Mars will require a remote sensing system either on the Martian surface looking up or in space looking down.

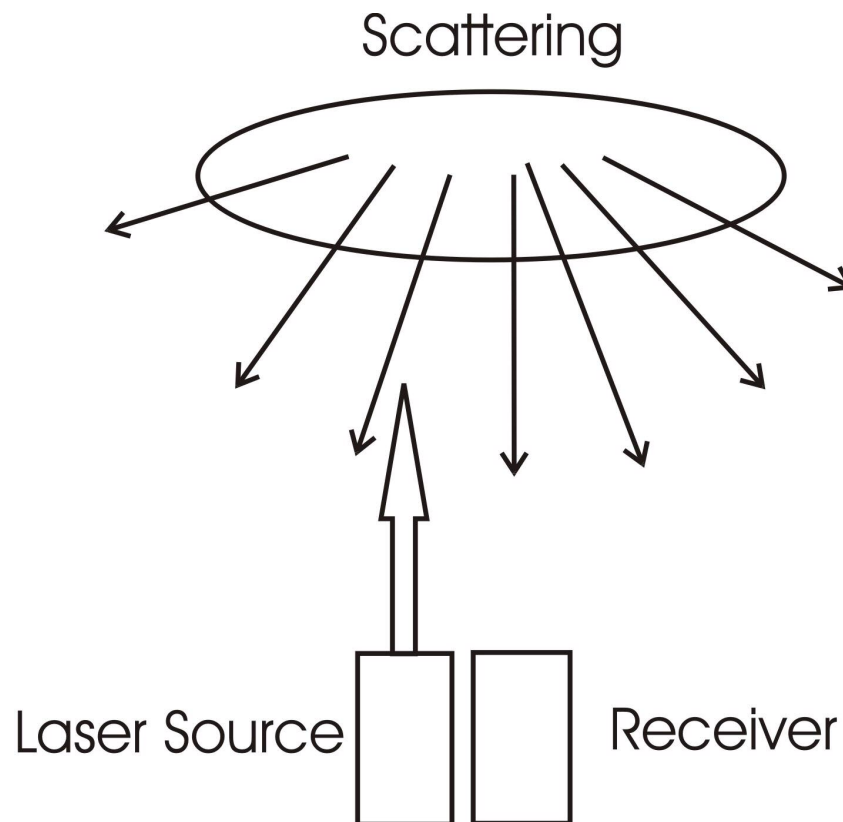


Figure 2.4. Basic Laser Remote Sensing Configuration

The above figure shows the basic configuration of a remote sensing system to measure atmospheric constituents. The laser source emits a laser beam that interacts with the atmosphere. The beam is scattered back to the receiver. The receiver consists of a telescope and detector and associated electronics. If the experiment is theoretically sound and constructed properly, the return signal will contain data on the concentration of the particular constituent of interest. This data can be extracted by feeding the received signal into a computer or another data analysis device. The result is scientific data on the constituent in question that can be used to better understand and model the planetary atmosphere. The specific type of remote sensing used can vary. DIAL and Coherent systems are two types of remote sensing that are in widespread use.

2.3. DIAL Remote Sensing

One commonly used laser remote sensing technique is called DIAL (Differential Absorption LIDAR) where LIDAR stands for Light Detection and Ranging. A DIAL system uses the selective absorption of light by an atmospheric constituent to detect that constituent. The plot of absorption versus wavelength (or frequency) gives the absorption profile of the constituent. If a laser is tuned to a frequency within the limits of the absorption profile, termed the online signal, it will be partially absorbed and attenuated as it passes through the atmosphere. A laser tuned to a frequency outside the absorption profile, the offline signal, won't undergo absorption. The offline return signal takes into account effects other than the absorption profile of interest. Thus, it can be used to remove those effects from the online return signal so that the result only reflects the effects of the absorption profile.

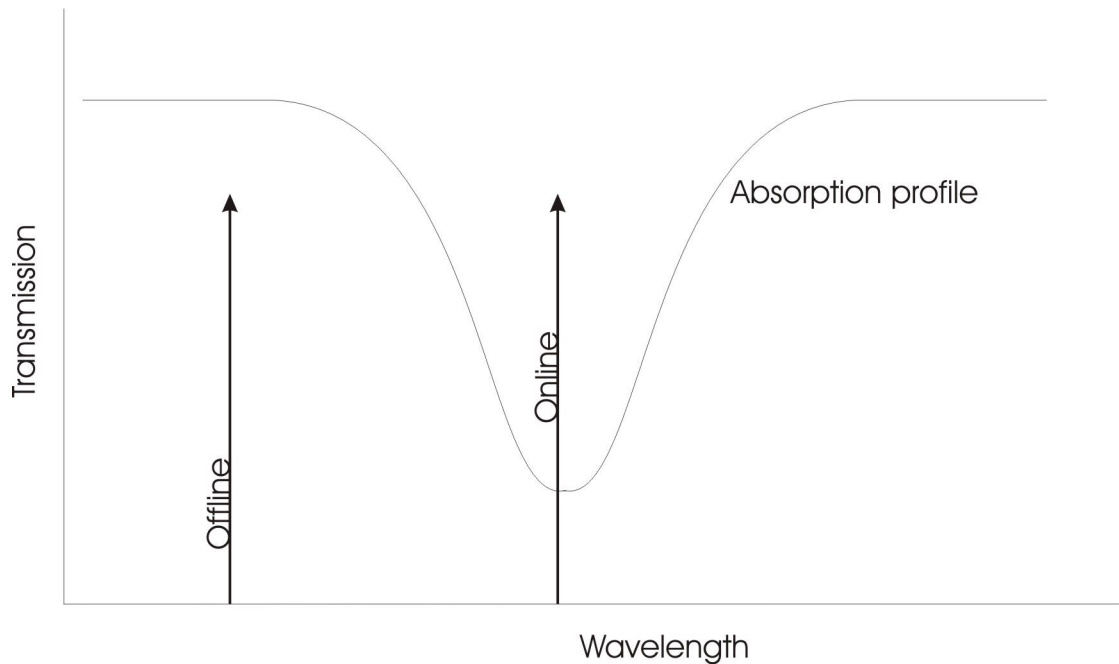


Figure 2.5. DIAL Signal and Absorption Profile

The online and offline signals can be produced by different sources or the online signal can be varied in frequency to sweep across the absorption feature and map it out. This frequency (or wavelength) sweeping can be accomplished in a semiconductor laser by varying the temperature of the laser, varying the size of the laser cavity or varying the current supplied to the laser.

In a DIAL system the absorption is measured by the difference between the online return signal and the offline return signal. Thus, the sensitivity of the system depends on how accurately the difference between the online and offline return photon counts can be determined. Since the difference is small compared to the magnitude of the return signals themselves it is difficult to measure accurately. A DIAL system will consequently have the ability to detect constituent concentrations down to a few percent. To measure Martian water vapor accurately, two to three orders of magnitude improvement in this

sensitivity is required.

2.4. Coherent Remote Sensing

Another remote sensing method is called coherent detection. Coherent detection is based on measuring the amplitude, frequency or phase of the electric field returned from the atmosphere rather than just the number of photons. Coherent detection systems direct the incoming return and a local optical oscillator onto a square law detector.

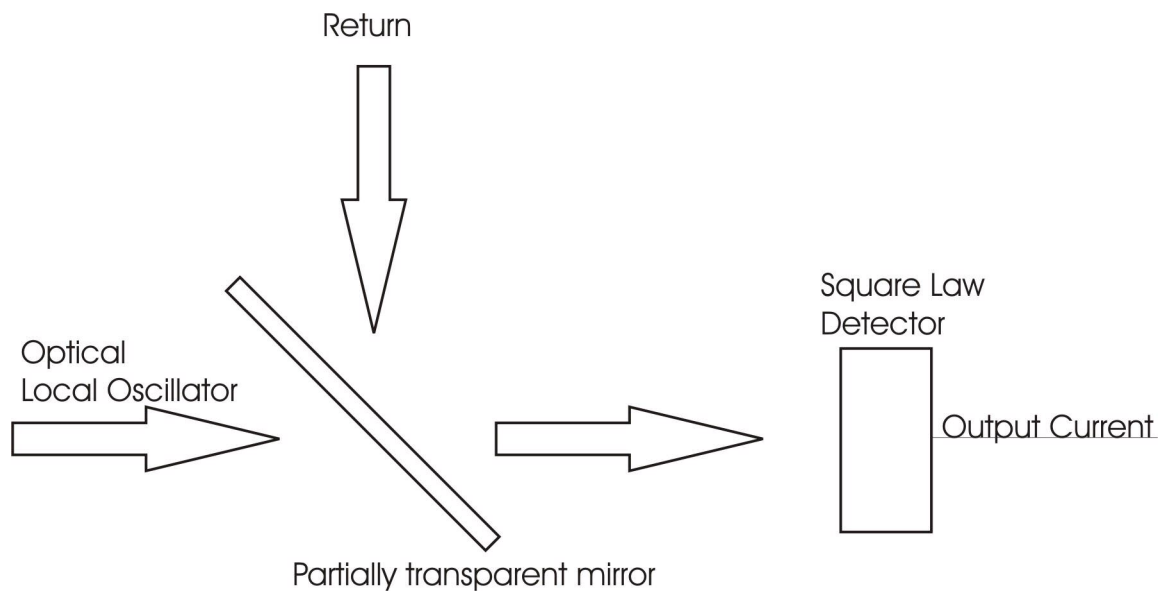


Figure 2.6. Coherent Detection System

The detector output is a current proportional to the square of the sum of the return and the local oscillator. The sum and difference frequencies in this current output are filtered to remove the optical frequencies by the slow response of the detector. The result is a dc term and an oscillating term dependent on the difference in frequency and phase between the incoming signal and the local oscillator. This is expressed as

$$i \propto \frac{(P_{return} + P_{lo})}{2} + \sqrt{P_{return} P_{lo}} \cos[(\omega_{return} - \omega_{lo})t + (\phi_{return} - \phi_{lo})] \quad (2.1)$$

where P is power, ω is the frequency in radians and ϕ is the phase of either the return or local oscillator, designated in the subscripts. In a DIAL system, the amplitude of the output of the detector is directly proportional to the power of the return. In a coherent system the amplitude of the output of the detector exhibits a gain dependent on the amplitude of the local oscillator as follows.

$$G_{coherent} = \sqrt{\frac{P_{lo}}{P_{return}}} \quad (2.2)$$

This is a distinct improvement over the DIAL system. Increasing the power of the local oscillator can raise the signal out of the noise due to the detector and associated electronics.

However there are disadvantages to coherent detection as well. The requirement for mixing on the detector means that the return and local oscillator signals must have well matched phase fronts at the detector. This requires that the optics be the best possible. In addition, the laser light will experience wavefront distortion as it passes through the atmosphere. This distortion is highly dependent on the state of the atmosphere when the light passes through it and can be quite complicated and rapidly changing. Removing the distortions effects at the receiver is, therefore, difficult. Using more laser power can help, but that partially defeats the advantage of Coherent over DIAL. For these reasons flying a coherent system to Mars and using it to detect water vapor presents serious difficulties. To address these difficulties while still improving on the performance of a DIAL system we propose to develop a new kind of laser remote sensing system called Frequency

Modulation (FM) Remote Sensing Spectroscopy.

2.5. Laboratory FM Technique

The general idea of FM remote sensing is to improve the performance over DIAL by using frequency detection methods like coherent systems, but to do so in the electrical domain to avoid wavefront distortion and optical design issues that would make it difficult to fly such a system to Mars. Using electrical techniques allows the use of readily available electrical mixing components and radio-frequency (RF) design techniques for spaceflight. As a result, a rugged, compact, low weight and low power system could be developed using FM techniques that can meet the requirements for measuring water vapor on Mars.

Frequency Modulation (FM) remote sensing is a significant extension of a simpler technique that has been used in laboratories since 1980 [4]. In laboratory FM techniques sidebands are impressed on a laser signal using an electrical local oscillator. This electrical local oscillator either modulates the current to the laser or phase modulates the laser beam itself using an external modulator. At their creation, the FM sidebands are equal in amplitude. If directed at a detector and the detector electrical output is mixed with the local oscillator and filtered down to the baseband, the output of the mixer will be zero because the sidebands are of equal amplitude. If, however, the signal is transmitted through a sample to a detector on the other side of the sample and one of its sidebands is attenuated by an absorption feature, then the return signal will develop an amplitude modulation as a result of the unbalanced sidebands. This can be accurately detected by mixing the current output of the detector with the electrical local oscillator again. This

time the output of the mixer will oscillate with amplitude proportional to the absorbance the sideband experienced.

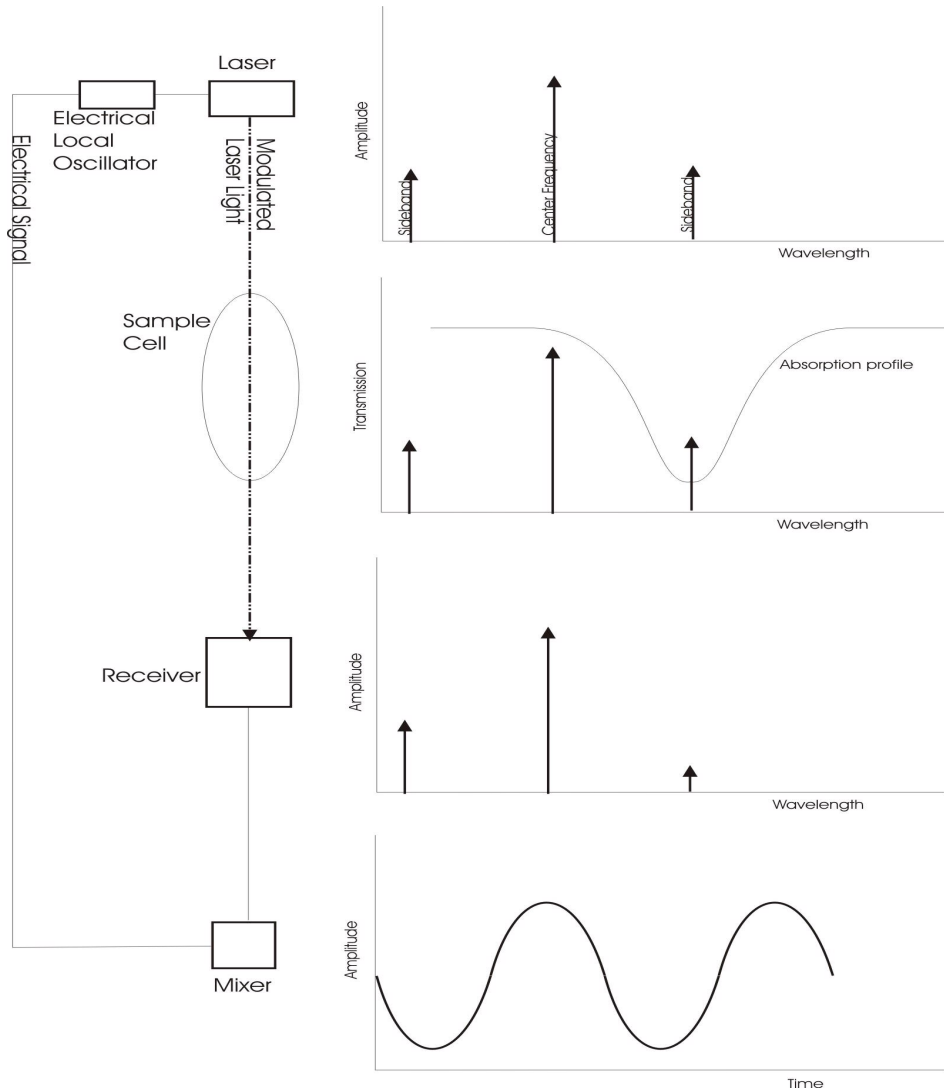


Figure 2.7. Laboratory FM technique

The diagram illustrates this method. The left side shows the components involved in the experiment. The right side shows the signals associated with each component. At the top the laser is modulated by an electrical local oscillator. The spectrum of the resultant laser beam is shown to the right, a center frequency and two equally spaced and equal

amplitude sidebands (there are actually an infinite number of sidebands of decreasing amplitude, but the first two are the most important for FM). Next down is the sample cell which contains a sample of the constituent, say water vapor. On its right is shown the absorption feature superimposed on the laser spectrum. The feature overlaps one of the sidebands. The next step down is the receiver. The signal is received and converted to an electrical signal here. The signal received is shown on the right, a center frequency and two sidebands. Now one of the sidebands is reduced in amplitude. The last step is the mixing of the local oscillator with the detected signal to give the time varying result shown on the right. The amplitude of this signal reflects the absorption experienced by the laser beam in traveling through the sample cell.

No time varying signal is received if no absorption occurs. This means that the background signal is ideally zero. As the absorption increases, the sideband undergoes greater absorption and the detected signal level increases. In addition, modulating the laser moves the sidebands away from the center frequency of the laser. The center frequency is where much of the laser noise is located. Moving away from center frequency reduces this noise to the point where the dominant noise term is the shot noise of the detector. Thus an FM system can detect the return limited only by the detector shot noise. This results in very sensitive detection systems. It would be advantageous if remote sensing systems could use these techniques to increase their sensitivity. A general description of what an FM remote sensing system would look like is contained in the next section.

2.6. Remote Sensing Using FM

The diagram below illustrates this combination of laboratory FM techniques with remote sensing methods. A local oscillator provides a modulating signal to the optical modulator as well as to one input of a mixer. The modulator modulates the light emitted from the laser and that FM modulated light travels into the atmosphere. The light interacts with the atmospheric constituent to reduce one of the sidebands. The scattered light returns and is collected in a telescope, focused onto a detector and converted into an electrical signal. The electrical signal is mixed with the local oscillator to produce the oscillating signal that contains the data on the atmospheric constituent of interest.

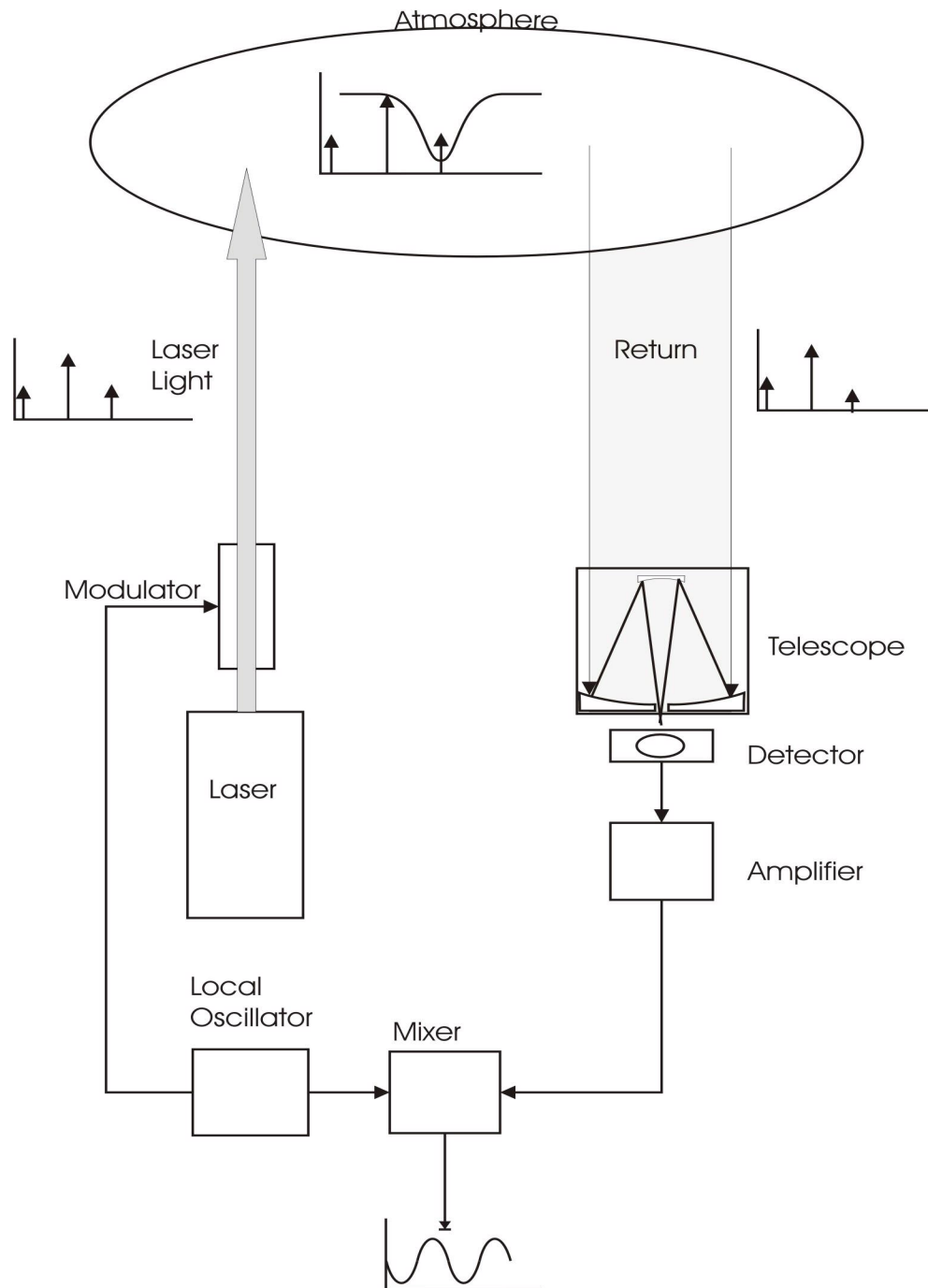


Figure 2.8. Frequency Modulation Remote Sensing System (scattered return)

There are several important features to note about remote sensing FM spectroscopy that distinguish it from laboratory techniques.

In the laboratory technique the light travels along a straight path to the receiver. As a result, all the light emitted at a given time from the laser source will arrive at the same time on the detector. Therefore, all the wavefronts arriving at the detector will be in phase. In a remote sensing application that uses scattered light the source laser light will scatter off of atmospheric constituents at different locations in the sky. The result is that the return signals detected at a given time will have traveled different distances. The wavefronts of these return signals will be different, they will be out of phase. It will be necessary to calculate the effect of these differing phase fronts on the total return signal. Another remote sensing technique that avoids this issue is called sounding. Sounding uses reflected light from a surface rather than scattered light for the return. In the above diagram the atmosphere is replaced by a planets surface or some other reflective surface for a sounding application. This technique avoids the phase issues associated with scattered light technique and will also be discussed further in a later section.

Another issue affecting the phase of the return is the coherence length of the laser source. In a laboratory configuration the distance between the source and the detector is small compared to the coherence length of the laser. In a remote sensing experiment the distances are much larger. If these distances are greater than the coherence length of the laser the return signal strength could be adversely affected.

Another important consideration is the power received at the detector. Due to the short, straight line path from emitter to receiver in a laboratory configuration the signal arriving at the receiver is almost the same as that emitted at the laser. A low power laser of only a few milliwatts will provide enough power to be easily detected at the receiver. In a scattering remote sensing application the laser light will be scattered off of

atmospheric constituents and will be significantly attenuated before arriving back at the detector. It will be necessary to detect the FM signal with a low number of photons. In a sounding application the returned light will be much higher.

This paper will use novel analytic and numerical simulations in conjunction with laboratory experiments to address these issues to determine the best method to use to apply FM techniques to remote sensing on Mars.

2.7. Novel Contributions of Dissertation

The overall goal of this dissertation is to resolve the issues that are required to transition from laboratory FM systems to a remote sensing FM system, using either scattered or reflected light, to detect water vapor in the atmosphere of Mars. In order to do this, it must be determined how the FM signal interacts with the atmosphere to produce a signal at the detector compared to how it is used in a laboratory configuration. Both analytic and computer models will be developed that allow the calculation of the detector currents with respect to the phases of the return wavefronts and the other parameters associated with the laser source and detection systems. This model will be used in a novel analysis of effects of phase on the return signal. It will then be possible to determine the feasibility of using scattered light for the return. The output of this model will be compared with previously published experimental data as well as an experiment performed by the author. The analysis using the model will lead to the conclusion that a sounding configuration is a better use of the FM technique for remote sensing.

To enabled analysis of the use of FM sounding, a novel SNR equation for the sounding method will be developed and combined with a Martian water vapor model to

calculated the important parameters associated with using FM sounding on Mars and predict the performance that can be expected from such a system.

2.8. Organization of Dissertation

Section 1 describes the goals of this research.

Section 2 has introduced the topic of FM remote sensing by describing the use of FM techniques in the laboratory environment and the extensions of the technique required for use in a remote sensing environment.

Section 3 will describe the atmosphere of Mars to better define the problem FM remote sensing is proposed to solve. A general description of the water vapor concentration on Mars will be followed by a detailed model of that distribution developed using data from earlier scientific missions and observations. The LIDAR equation will be used to model the return. Modifications to the model have been made by the author to allow its incorporation into the FM computer model developed later. The result will be an estimate of the return that can be expected from various altitudes on Mars. This information both defines the problem more clearly in terms of low return and low concentration of water vapor as well as provides a model that can be used as part of the models developed in later sections.

Section 4 introduces the equations that describe the laboratory FM configuration. A novel analytic model is developed that will be used in later sections to model the simpler cases. The limitations of this model will be discussed. As a result, a computer model will be used to augment the analytic model. This computer model will be described.

Section 5 uses the analytic and computer models to perform a novel analysis of the

return of a scattering based FM remote sensing system. The conclusion is that this method presents severe difficulties for practical use.

Section 6 compares the model to previously published data as well as an experiment conducted by the author. This validates the model.

Section 7 transitions to the discussion of the FM sounding system by developing an SNR equation for FM sounding. The laboratory FM equation is significantly modified by the author to include parameters and terms that are necessary to model a sounding system. These terms are equated with terms in the Martian water vapor LIDAR equation developed in section 2 to form an SNR equation that models the FM sounding method for Martian water vapor detection.

Section 8 uses the SNR model to determine the performance of an FM sounding system for Martian water vapor detection using values for the parameters based on available technology.

Section 9 is the summary.

Section 10 is the conclusion.

Section 11 is the recommendations for future work.

3. Water Vapor in the Martian Atmosphere

3.1. Introduction

The first step to developing an FM remote sensing system is to understand the scientific measurement that is required. In this case the measurement required is water vapor concentration versus altitude on Mars. This section describes the Martian atmospheric water vapor modeled developed as a result of previous scientific investigations, especially spacecraft missions to Mars. Then the LIDAR equation is introduced and combined with the Martian atmospheric model to mathematically model the return of a laser light signal traveling through the atmosphere and scattering back to the detector, which is near the source. The parameters that go into the LIDAR equation are discussed. All these equations have been numerically solved by the author to give various plots indicating how important parameters vary by altitude on Mars. The final result is a prediction of the signal intensity expected at a remote sensing detector used on Mars. This model will be used as an input in later sections into the FM computer model to give results predicting performance of an FM system on Mars. This provides a basic understanding of water vapor distribution on Mars for the purposes of evaluating FM remote sensing for that purpose.

3.2. The Martian Atmosphere

Data gathered from the Viking I and II spacecraft, both of which orbited and landed on Mars in 1976, provide detailed information on the pressure and temperature profiles at

the landing sites.

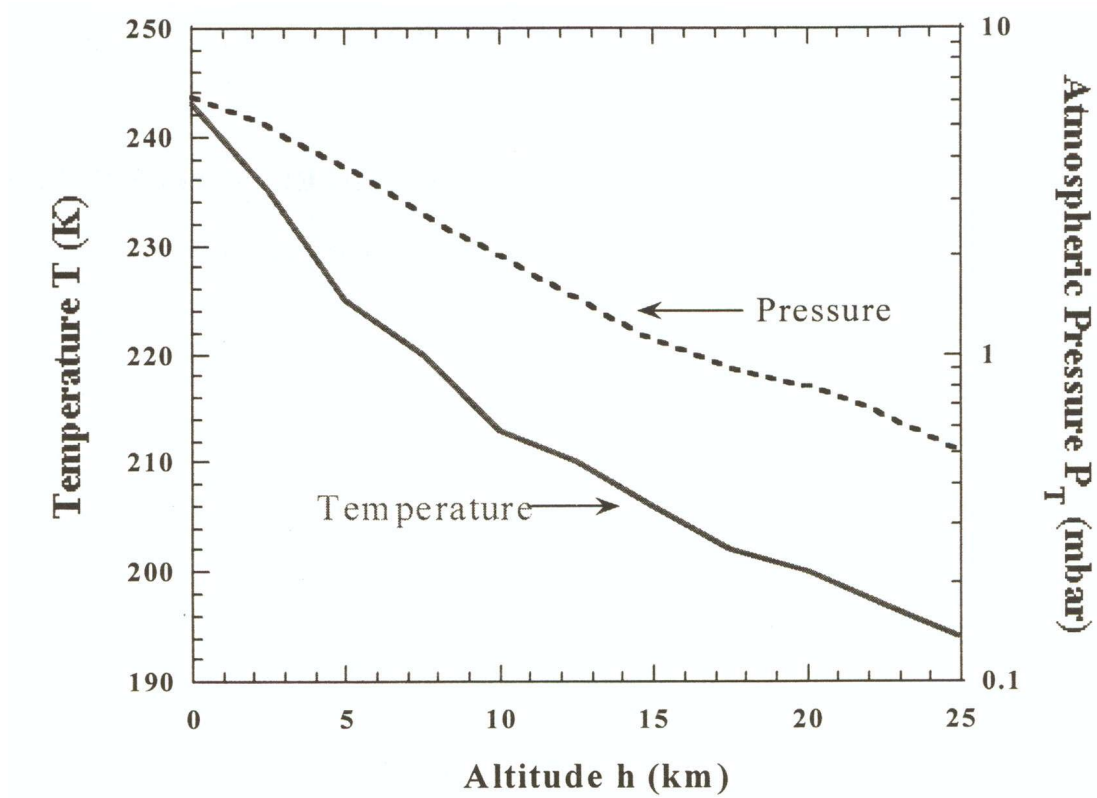


Figure 3.1. Viking 2 Lander site pressure and temperature [5]

The pressure on Mars between ground level and 25km is less than 10mbar, with 1bar being Earth's surface pressure. In addition, water vapor is a small part of this already thin atmosphere as can be seen from the next chart.

Table 3.1. Composition of the lower atmosphere of Mars [6]

Species	Abundance by volume
CO ₂	0.9532
N ₂	0.027
Ar	0.016
O ₂	0.0013
CO	0.0007
H ₂ O	0.0003
Ne	2.5 ppm
Kr	0.3 ppm
Xe	0.08 ppm
O ₃	0.04 to 0.2 ppm

Water vapor is, therefore, only .03% of an atmosphere that is 1% of Earth's pressure. The vertical profile of water vapor density of Mars is illustrated in the next figure.

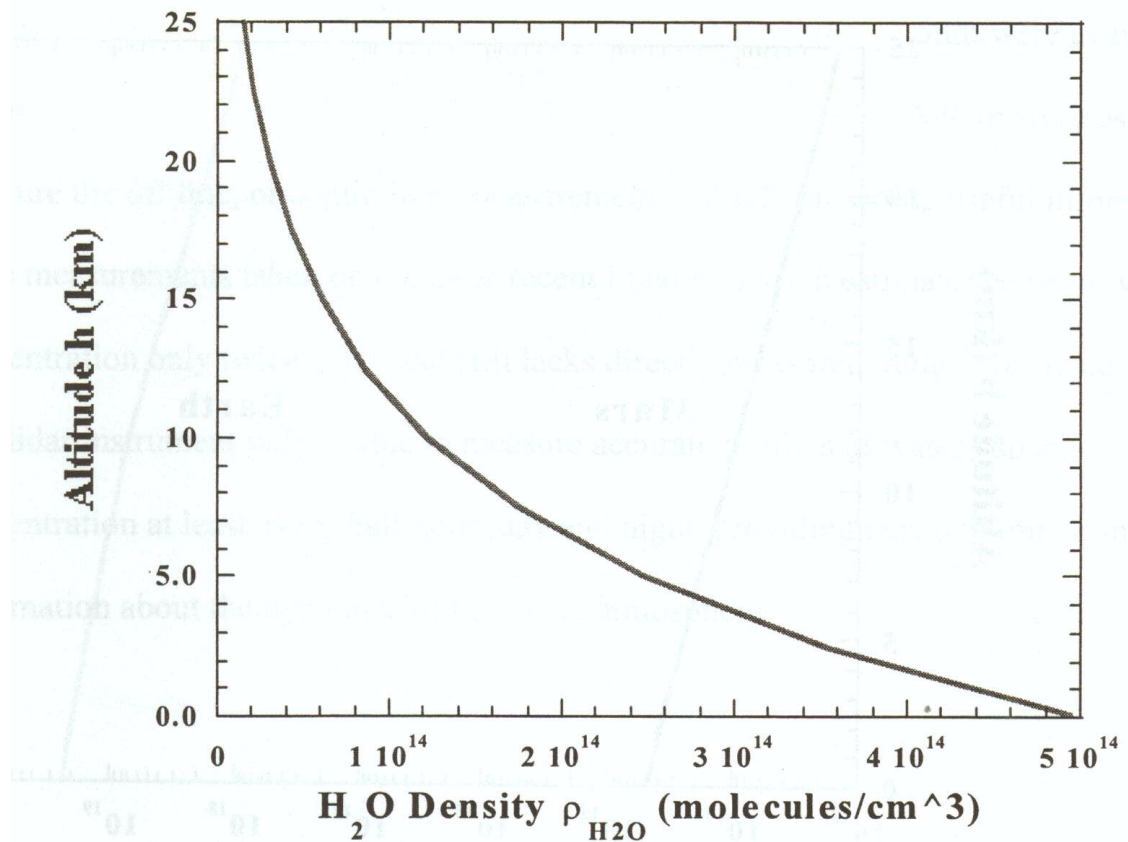


Figure 3.2. Profile of water vapor at the Viking Lander 2 site

At all altitudes the Martian atmosphere is less than 1/100 the density of the Earth's.

As these charts show, the Martian atmosphere is very thin and contains only a small amount of water compared to Earth. Clearly, sensitive techniques will be required to accurately measure water vapor on Mars. Just how sensitive can be illustrated by quantitatively determining the return signal expected for a given source signal. This data for the temperature, pressure and water vapor density of the Martian atmosphere obtained from missions to Mars can now be used to determine how light can propagate and scatter in the Martian atmosphere and how much light will return to the source. In the rest of this

section, the LIDAR equation will be used along with Martian atmospheric parameters to quantitatively describe the Martian atmosphere and determine the magnitude of the return.

3.3. Modeling the Return on Mars using the LIDAR equation

Here a mathematical model of the laser return signal based on the LIDAR equation is developed. This model has been implemented in a computer model by the author. This computer model is used to calculate the variations of various important parameters over the altitude of a Martian atmospheric experiment, from 0 to 25 km. The final result of this section is a plot of the photon count at the receiver versus altitude. This plot illustrates the required sensitivity limits for any remote sensing experiment on Mars. This model will ultimately be used in conjunction with the SNR equation developed later to evaluate the performance of an FM system on Mars.

In the following sections the LIDAR equation will be introduced and each parameter identified and described. The limitations of current technology will be used to restrict the choices available to a designer. The terms for backscatter and attenuation through the atmosphere require additional development which is provided. These terms depend on the specifics of the atmosphere probed, in this case Mars, and the atmospheric constituent probed for, in this case water vapor. The data on the Martian atmosphere discussed in an earlier section will be used to determine these terms. These terms as well as the values for the other parameters discussed will then be put back into the LIDAR equation for a final result of counts expected at the detector relative to altitude.

3.4. The Basic LIDAR Equation

The LIDAR equation models the transmission, backscatter and absorption of laser light passing through an atmosphere. It also includes parameters to model the basic characteristics of the transmission and receiving optical and electronic systems. The result is a calculation of the number of photons counted by the detector given a number of photons sent into the atmosphere by the source. For the case where the source light and detected light have the same wavelength, the rate of photon capture at the receiver can be expressed using the following LIDAR equation [7]:

$$N_{photons}(\lambda_L, R) = \frac{E_L}{hc/\lambda_L} \frac{A}{R^2} \xi(R) \xi(\lambda_L) \eta_{qe} \beta(\lambda_L, R) \Delta R f e^{-2 \int_0^R \kappa(\lambda_L, R) dR} \quad (3.1)$$

The following diagram illustrates this equation. A physical location of a device is associated with each of the parameters in the LIDAR equation.

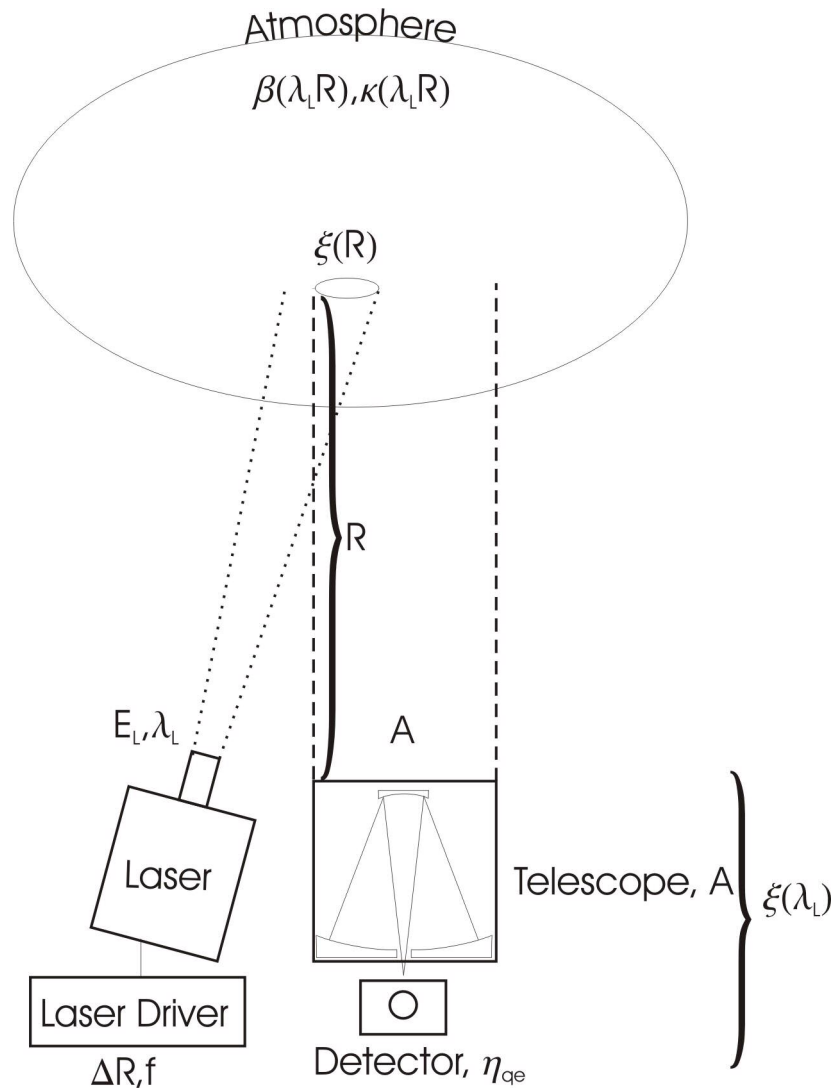


Figure 3.3 Diagram of LIDAR equation parameters

E_L is the energy per pulse from the laser. The wavelength of the emitted laser radiation is λ_L . The LIDAR equation term hc/λ_L is therefore the energy per laser photon. The energy output of the laser and its wavelength are parameters determined by the laser chosen. The driver of the laser in conjunction with the laser controls the rate of laser firing, f , and the resolution of the range cell, ΔR .

As the laser light travels through the atmosphere it is scattered and attenuated

according to the atmospheric backscatter coefficient, $\beta(\lambda_L, R)$, and the atmospheric attenuation coefficient, $\kappa(\lambda_L, R)$.

At the target the field of view of the receiving telescope overlaps with the illumination of the laser beam. The parameter describing this overlap is $\xi(R)$. After the light is scattered it travels a distance R back to the receiver.

The receiving telescope collects the incoming scattered light in an area A . As the received light passes through the receiving system it experiences optical filtering that is represented by the spectral transmission of the receiver, $\xi(\lambda_L)$. The light strikes the detector and is counted with an efficiency represented by the quantum efficiency of the detector, η_{qe} . The output of the detector is the number of counts received per second as the result of a given energy pulse sent into the atmosphere.

In the next section these parameters will be evaluated further to determine values for them that can be used in the LIDAR equation to give a value for the counts expected on Mars for a remote sensing experiment. For this purpose it will be useful to divide them into three types. The first type is the technology limited parameters. These are the parameters that are heavily constrained by the limits of current available lasers and detectors. The second type is the ranging parameters. These are limited by what ranging resolution is desired. The third is the atmospheric parameters. These parameters describe the Martian atmosphere.

3.5. Technology Limited Parameters

These are the size of the telescope (A), the transmission through the receiver system ($\xi(\lambda_L)$), the quantum efficiency (η_{qe}), the laser energy (E_L) and the laser linewidth.

Since the size of an optical system will be limited by the requirements for a spacecraft mission to Mars, we will assume that the size of the telescope and the transmission through the system are optimized for that mission and are fixed. The size of the rocket used to launch the spacecraft to Mars in conjunction with the allocation given this particular instrument will determine the size of the telescope. A reasonable telescope size would be around 0.3 meter.

The quantum efficiency, laser energy and laser linewidth are restricted by the limits of current technology and the requirements for spaceflight. A mission to Mars requires a rugged, small, low power device. A few Watts and a few kilograms is about the limit for long duration missions with low power supply capability and low launch weight requirements, such as a mission to Mars. These parameters are also interrelated due to the limits of current technology. Determination of one severely limits the determination of the others. Each will now be discussed in turn. A summary of the results will be provided at the end of this section.

3.5.1. Quantum Efficiency and Detectors

Single Photon Counting Detectors (SPCMs) based on silicon Avalanche Photodiodes (APD) are most sensitive and least noisy in silicon. Silicon APDs operating in the Geiger Mode are available with gains approaching 10^8 , quantum efficiencies of 50 to 70 percent (dependent on wavelength) and dark counts as low as 1 count/second [8]. These detectors operate in the wavelength range from 300nm to 1100nm. Germanium and InGaAs can be used to extend the range up to 1700nm. However, the current technology in these devices limits the gains to orders of magnitude below that of silicon. The range of wavelengths

available for use in water vapor absorption is therefore restricted to between 300nm to 1100nm. Unless the laser source power above 1100nm is 200 or more times that of lasers below that limit, the choice of wavelength will be restricted to be within the range of a silicon detector.

3.5.2. Laser Wavelength Selection

The wavelength chosen is most strongly determined by the absorption lines for water vapor. Clearly, no matter what the limitations given by the detector, a line with strong absorption is necessary due to the thinness of the Martian atmosphere.

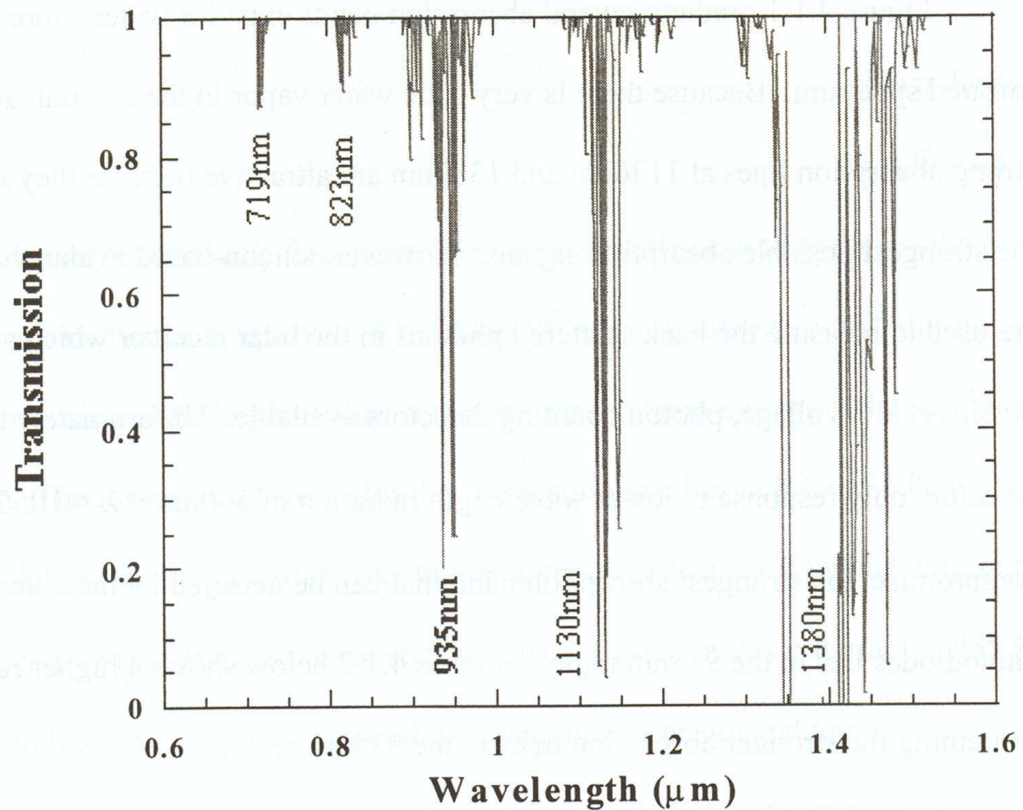


Figure 3.4. Water vapor absorption lines at 1atm, 23°C, 50m path length [9]

There are strong lines above 1100nm, two in particular at 1130nm and 1380nm, which would be much easier to reach with current technology semiconductor or solid state lasers. There are continuing efforts to develop room temperature detectors at these wavelengths to make it possible to use the more powerful lasers. The strongest line within the restricted range is at 935.68nm.

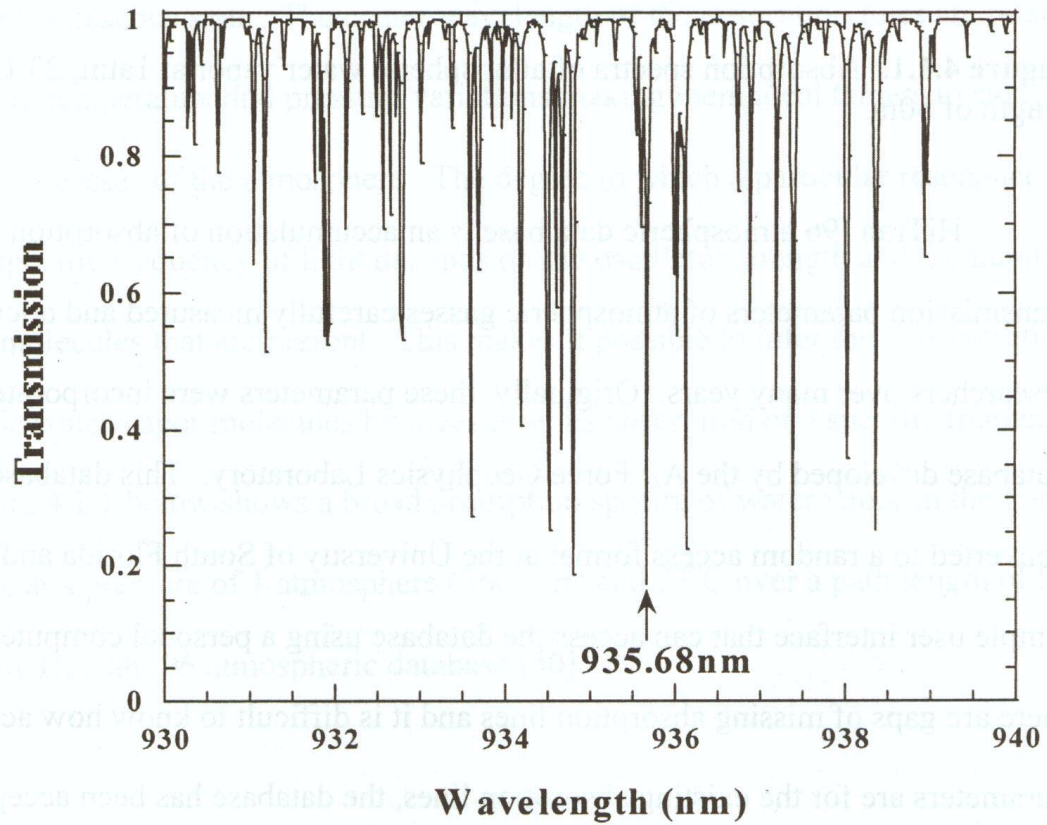


Figure 3.5. Water vapor absorption line at 935.68nm [10]

3.5.3. Laser Energy

A semiconductor or solid state laser suitable for spaceflight that operates at 935.68nm is not a widely available commercial technology. They are available at low powers, up to

100mW at the most, usually more like 10mW. If more power is needed to improve the SN ratio, then optical amplifiers will have to be added to increase the power output.

3.5.4. Laser linewidth

One important parameter not explicitly addressed in the LIDAR equation is the linewidth of the absorption feature. The absorption feature width limits the linewidth of the laser. In order to map out the absorption feature accurately, it is necessary that the linewidth of the probe be much smaller than the width of the feature. The absorption feature shape can be determined using the HiTran program [11]. HiTran (High-Resolution Transmission Molecular Absorption) is a program that uses spectroscopic parameters to calculate the transmission and emission of light in the atmosphere. Using HiTran to calculate the absorption feature parameters gives:

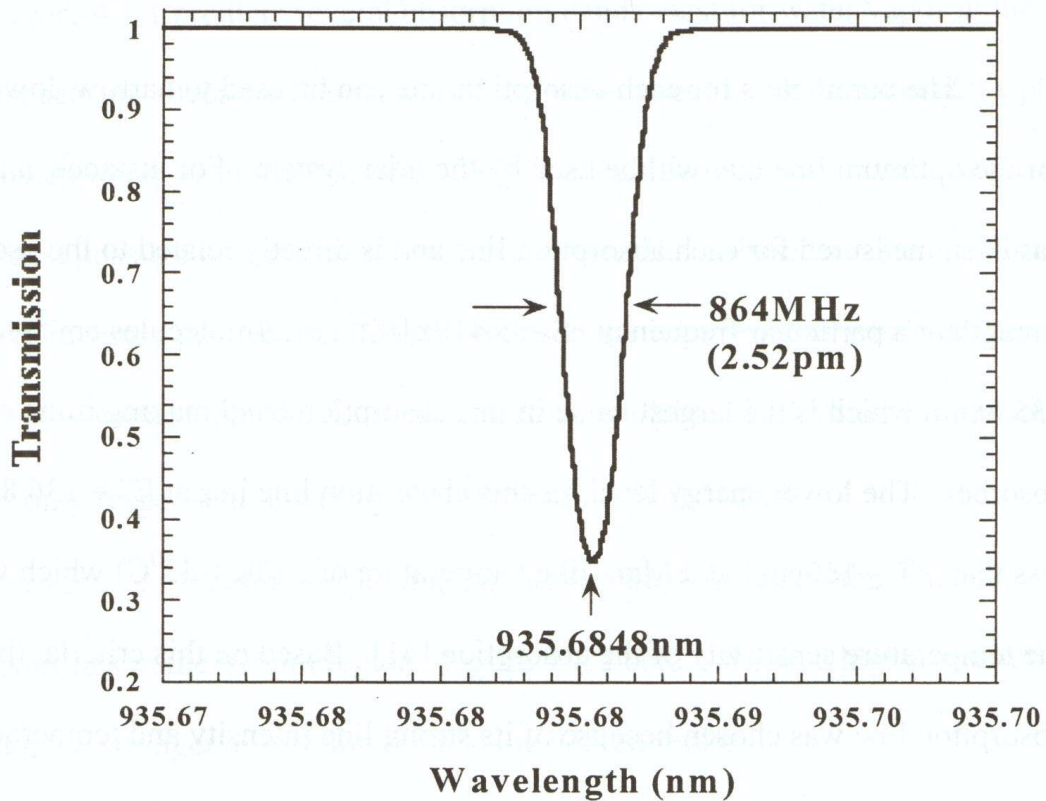


Figure 3.6. 935.68 absorption line for 4.6 Torr and -30C

This is representative of what would be expected on Mars. The 864MHz width of this absorption feature (2.52pm at 935.68nm) limits the linewidth of the laser source to less than 25MHz. With this laser linewidth, the profile of the absorption can be mapped out accurately.

3.5.5. Summary of Technology restricted parameters

In the discussion of the technology limitations on some of the LIDAR equation parameters for a Martian water vapor mission the values of certain parameters have been set. The telescope size can be about 0.3 m. The wavelength of the laser light is that of a

strong absorption line in the range of a silicon detector, which is 935.68nm. The power of lasers at this wavelength can be from 10 to 100 mW CW. The linewidth required is 25MHz or less. Current technology can provide semiconductor devices with these specifications that are suitable for a Martian mission.

3.6. Ranging Parameters

The second set of parameters includes the ranging parameters. Both ΔR and f are limited by the resolution required of the measurement. To see how, it is necessary to discuss ranging in a little more detail.

3.6.1. Ranging Resolution

Ranging is the added ability to a remote sensing system that allows a researcher to divide a vertical sampling region into sections and gather data on each section. Instead of obtaining data integrated over the entire vertical column, the data is broken down into segments representing specific distances from the source/detector. Ranging is done at the detector by dividing the return signal into range bins. These are equally sized periods of time during which photons are collected. Each of these bins represents a range of distances from the source, determined by its width. If the output pulse from the laser is a given time interval wide, then the bins are usually sized to equal that laser pulse width. In this way the laser pulse width and bin size are equal and determine the resolution of the ranging measurement.

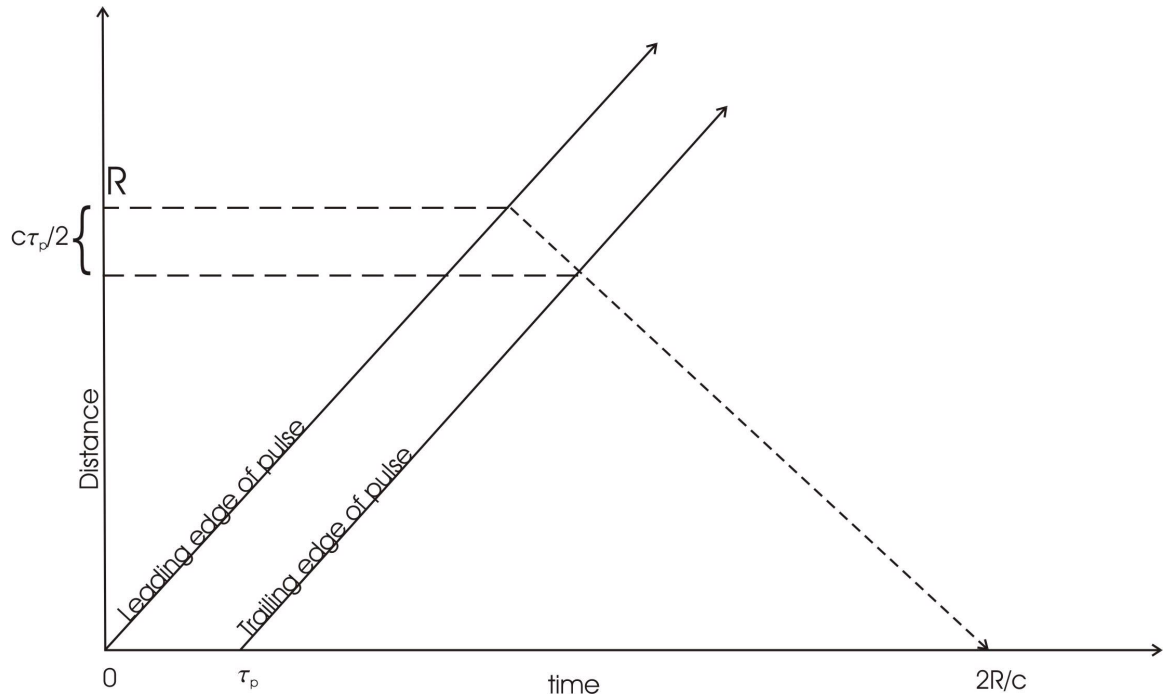


Figure 3.7. Ranging resolution

The resolution limit can be seen from the figure above. In that figure, the distance from the laser source is on the y axis and time on the x axis. The leading edge of the pulse is scattered at distance R and returns to the source at time $2R/c$. This is represented by the triangle formed by the “leading edge of pulse” line going up and the dotted line going back down to $2R/c$ on the x axis. At that time $2R/c$ the rest of the pulse hasn’t traveled as far as R since it got started a little later. The rest of the pulse up to its pulsewidth scatters at shorter distances and returns to the source such that the travel time is $2R/c$. The result is that the light received at $2R/c$ is scattered from a distance range equal to:

$$\Delta R = \frac{c \tau_p}{2} \tag{3.2}$$

This is the resolution of the range measurement. A common value for this is $1.28 \mu\text{s}$. This

corresponds to a range resolution of 192 meters. This value will be used later to complete the LIDAR equation.

3.6.2. Coherence length limits to pulsewidth

The presentation so far assumes an ideal monochromatic source. Real laser sources will have finite bandwidths. As a result the laser light isn't coherent over an infinite length. As the light propagates, the phases of its constituent waves diverge. The coherence length (or time) is determined by the linewidth of the laser.

$$l_c = ct_c = \frac{c}{\Delta f} \quad (3.3)$$

In order for the light to retain its phase characteristics, the distance over which the measurement is being made must be less than the coherence length of the laser. The measurement length is related to the pulsewidth as follows:

$$l_m = \tau_p c \quad (3.4)$$

The coherence condition required is:

$$l_m < l_c \quad (3.5)$$

Substituting the expression for the measurement length gives:

$$\tau_p < \frac{1}{\Delta f} \quad (3.6)$$

The earlier discussion of the width of the absorption feature has limited this linewidth to less than 25MHz. A linewidth of 25MHz limits the pulsewidth to 40 ns. A lower bandwidth than this can support larger pulsewidths. For the pulsewidth of 1.28 μ s mentioned earlier a linewidth of 780 kHz would be required.

This is a narrow linewidth, but not state of the art. External cavity lasers in our laboratory at GSFC produce linewidths near this value. They are relatively low power devices, of at most 100 mW, that could be used to seed amplifiers to get both the linewidth and power needed for a given application.

Lasers with linewidths much more narrow have been developed with 100mW of power at 1550nm [12] but aren't currently available at frequencies around 935.68nm. However, a vendor named Kohares makes custom fiber lasers with narrow linewidths, some around 1kHz [13]. It may be possible to develop fiber lasers with these required linewidths in conjunction with one or more of these vendors if longer pulsewidths are desired.

For the remainder of this paper the 1.28 μ s will be used as a standard pulsewidth.

3.6.3. Frequency of Laser Firing

The frequency of laser firing, f , has to be small enough that two pulses don't overlap during a single measurement. If a second pulse is sent before the scatter from the first pulse is completely collected, then energy from both pulses will arrive at the detector at the same time and confuse the results. For a Martian atmospheric mission the altitude will be about 25 km. A round trip to this altitude at the speed of light is 83 μ s. This corresponds to a maximum repetition frequency of 12 kHz. Keeping the rate below this and well within the capability of semiconductor lasers would allow rates from tens of Hertz to a few kHz.

3.6.4. Summary of Ranging Parameters

The ranging resolution of the system is determined by the laser source pulsewidth.

For a commonly used pulsewidth of 1.28 μs results a range resolution ΔR of 192m. The frequency of laser firing can be up to 12 kHz without causing pulses to overlap in a Martian atmospheric experiment going to an altitude of 25 km.

3.7. Science Limited Parameters

The rest of the parameters in the LIDAR equation are determined by the characteristics of the planet studied. These parameters are used in the terms for backscatter and attenuation. The Martian temperature profile, water vapor density and pressure profile discussed earlier will now be used to determine the backscatter and attenuation terms in the LIDAR equation. Although the results of the following treatment is not original, the author has taken the basic data on Mars obtained from the analysis of the Martian space missions and independently created a computer model that was then used to generate all results in these sections.

3.7.1. Backscatter

Having established the parameters that the experimenter has some ability to choose, it is now necessary to focus in on the terms in the LIDAR equation that are determined by the Martian atmosphere. The first of these in this section is the backscatter.

The backscatter, β_{π} , includes components from scattering off of aerosols and molecules.

$$\beta_{\pi}(\lambda, h) = \beta_a(\lambda, h) + \beta_m(\lambda, h) \quad (3.7)$$

The backscatter coefficients are in units of $\text{m}^{-1}\text{sr}^{-1}$. These coefficients can be expressed in terms of the scattering cross sections, σ_a and σ_m , which are in units of $1/\text{m}$, as a function of height for aerosols and molecules [14]:

$$\beta_a(\lambda, h) = \frac{\sigma_a(\lambda, h)}{S_p} \quad (3.8)$$

$$\beta_m(\lambda, h) = \frac{3}{8\pi} \sigma_m(\lambda, h) \quad (3.9)$$

S_p is the extinction to backscatter ratio in units of steradians. It represents the efficiency of light scattering from an aerosol and is dependent on scattering direction and absorptive properties of the aerosol. $S_p = 30$ sr for Mars [15].

The expressions for the scattering require sophisticated modeling of the Martian atmosphere. An aerosol scattering model has been developed based on LIDAR experiments on Earth which has been extended to Mars [16,17,18,19]. The aerosol scattering cross section distribution with altitude is:

$$\sigma_a(\lambda, h) = \lambda_{cal} \sigma_0 \left(1 + a\right) \frac{e^{\frac{h}{b}}}{\left(a + e^{\frac{h}{b}}\right)} + \lambda_{cal} f \left(1 + a'\right) \frac{e^{\frac{h}{b'}}}{\left(a' + e^{\frac{h}{b'}}\right)^2} \quad (3.10)$$

where:

$$\lambda_{cal} = \left(\frac{694.3nm}{\lambda}\right) * 1.5 \quad (3.11)$$

adjusts for the shift from the wavelength the model assumes, 694.3 nm. The model parameters for Mars are $\sigma_0 = 0.025 \text{ km}^{-1}$, $a = 0.4$, $b = 3.2 \text{ km}$, $f = 6 \times 10^{-6} \text{ km}^{-1}$, $a' = 2981$ and $b' = 5.0 \text{ km}$. The equation for the molecular scattering distribution as a function of altitude is [20,21]:

$$\sigma_m(\lambda, h) = \frac{8\pi}{3} (5.45) \left(\frac{550}{\lambda(nm)}\right)^4 \times 10^{-28} \times \left(\frac{\sigma_{Mars}}{\sigma_{mixture}}\right) \times \rho_{air}(h) \quad (3.12)$$

where $\sigma_{mixture}$ and σ_{Mars} have been inserted into the equation to allow for adjusting the value for a particular gas. For a mixture of gases, $\sigma_{mixture} = 2.15 \times 10^{-28} \text{ cm}^2 \text{ sr}^{-1}$ is the effective cross section at 694.3nm. Since most of the Martian atmosphere is CO_2 , σ_{Mars} can be set to the value for CO_2 , or $6.36 \times 10^{-28} \text{ cm}^2 \text{ sr}^{-1}$ [22]. This gives:

$$\sigma_m(\lambda, h) = \frac{8\pi}{3} (16.12) \left(\frac{550}{\lambda(nm)}\right)^4 \times 10^{-28} \times \rho_{air}(h) \times \frac{m^2}{sr} \quad (3.13)$$

The molecular density, $\rho(h)$, on Mars has been calculated based on Martian data:

$$\rho(h) = 1.818 \times 10^{17} \times e^{-(0.9h + 0.0002 * h^2)} \times \text{molecules} / \text{cm}^{-3} \quad (3.14)$$

Using these equations to determine $\beta(\lambda_L, h)$ results in the following plot:

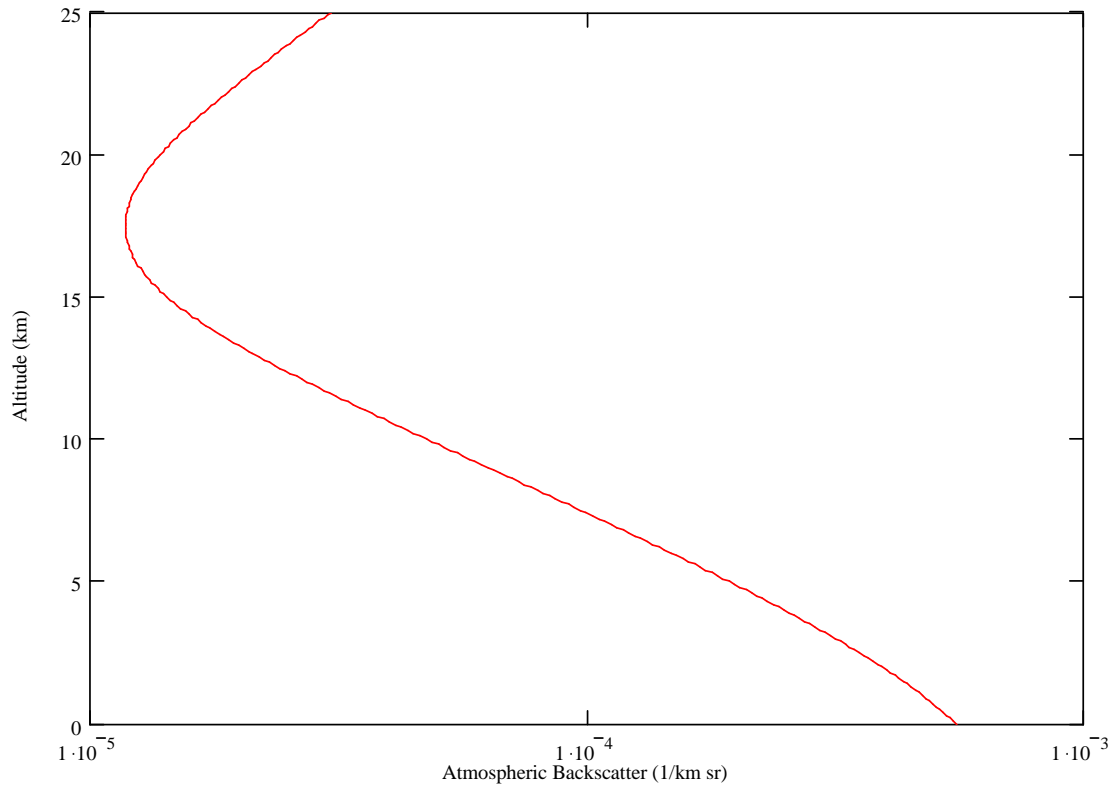


Figure 3.8. Altitudinal variation of backscatter

This plot is essentially just the aerosol backscatter, which dominates the backscatter at all altitudes. At the point of minimum return, at about 17.5 km, only about 1/85,000 photons return to the source. In addition to this low rate of return due to backscatter, there are losses that occur as the light passes through the atmosphere.

The results obtained for the backscatter will be used at the end of this section to help solve the LIDAR equation for a Martian atmospheric experiment. The next term that needs to be discussed is the attenuation term.

3.7.2. Attenuation

Now that the calculation of the backscatter term has been completed, the attenuation term can be calculated.

The attenuation of a signal passing through the Martian atmosphere is now modeled. The intensity of a signal traveling through an atmosphere will experience an exponential attenuation according to Beer's Law [23]:

$$I(\lambda, R) = I(\lambda, 0) e^{-2 \int_0^R \kappa(\lambda, R) dR} \quad (3.15)$$

Where κ is a coefficient representing scattering and absorption effects that reduce the signal as it propagates. This is the last multiplicative term in the Lidar equation. The attenuation coefficient represents a summation of the coefficients for separate individual effects:

$$\kappa = \kappa_a + \kappa_m + \kappa_\lambda \quad (3.16)$$

The first term is due to aerosol backscatter, the second to molecular backscatter and the last due to specific absorption at the wavelength of the light. The first two terms are equivalent to the corresponding scattering cross sections, for aerosols and molecules, as a function of altitude, are:

$$\kappa_a(\lambda, h) = \sigma_a(\lambda, h) \quad (3.17)$$

$$\kappa_m(\lambda, h) = \sigma_m(\lambda, h) \quad (3.18)$$

These two terms, when inserted into the Beer's Law equation, give the atmospheric attenuation caused by backscatter. Calculating this attenuation using equation 3.14 results in the plot:

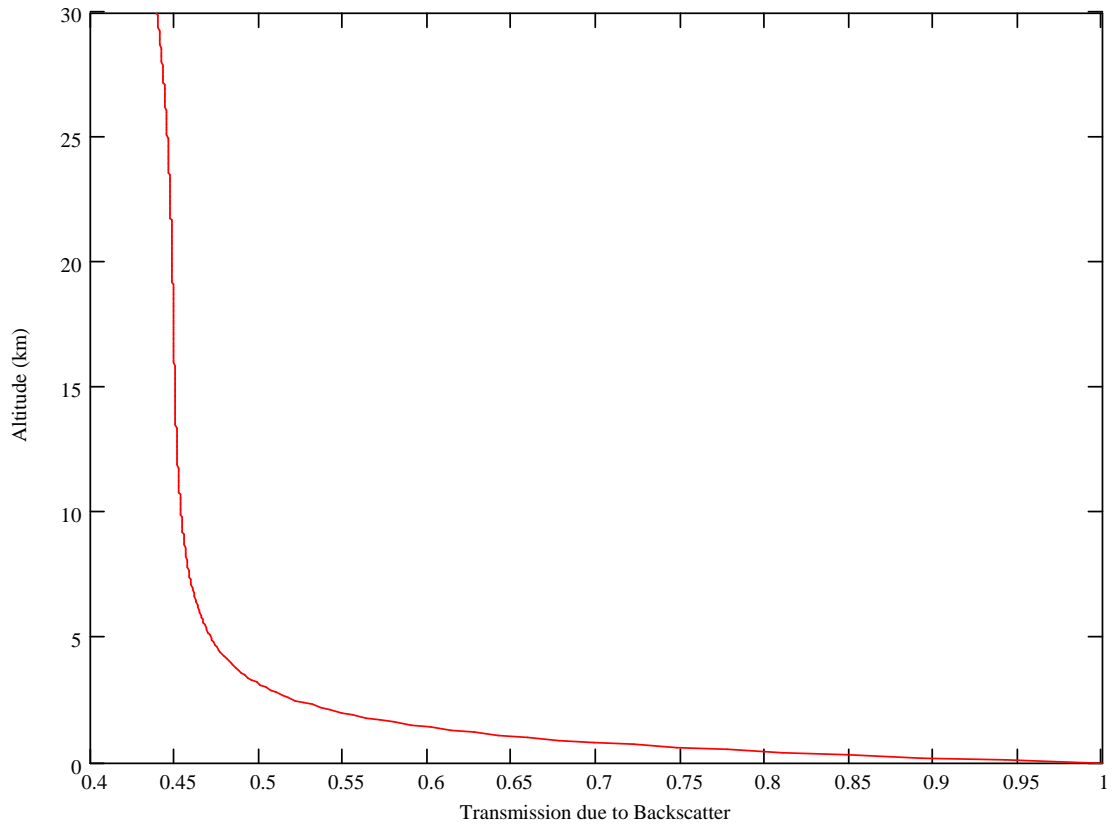


Figure 3.9. Atmospheric Transmission due to Backscatter

The absorption coefficient term depends on the absorption cross section as well as the density of a given atmospheric constituent:

$$\kappa_{\lambda}(\lambda, h) = \sigma_{H_2O}(\lambda, h)\rho_{H_2O}(h) \quad (3.19)$$

Where, for the particular case of water, σ_{H_2O} is the absorption cross section and ρ_{H_2O} is the molecular density of water vapor on Mars. The molecular density has been calculated based on the plot in Figure 1.2:

$$\rho_{H_2O}(h) = 4.9913 \times 10^{14} e^{-0.13987 \cdot h} \text{ molecules} / m^3 \quad (3.20)$$

The absorption cross section term is the line intensity, S in m^2/sec , multiplied by the absorption, $g(h)$ in sec:

$$\sigma_{H_2O}(h, \lambda) = S \cdot g(h, \lambda) \quad (3.21)$$

The absorption is dependent on the linewidth [24] of the feature, $\gamma_D(h, \lambda)$:

$$g(h, \lambda) = \frac{1}{\gamma_D(h, \lambda)} \left(\frac{\ln(2)}{\pi} \right)^{1/2} \quad (3.22)$$

where:

$$\gamma_D(h, \lambda) = \frac{v_0}{c} \left(2kT(h) \frac{\ln(2)}{m_{H_2O}} \right)^{1/2} 10^{3/2} \quad (3.23)$$

and m_{H_2O} is the molecular mass of water, 2.993×10^{-23} g/molecule, and k is the Boltzman constant, 1.381×10^{-23} J K^{-1} . The absorption $g(h, \lambda)$ is the peak absorption of a Gaussian distribution. Later in this paper a absorption profile will be substituted to modify the model for FM remote sensing applications.

The temperature profile, $T(h)$, has been calculated for Mars:

$$T(h) = 243.43 - 4.1600h + 0.14341h^2 - 0.0022379h^3 \cdot K \quad (3.24)$$

The attenuation due to the absorption feature is calculated from equation 3.14 to be:

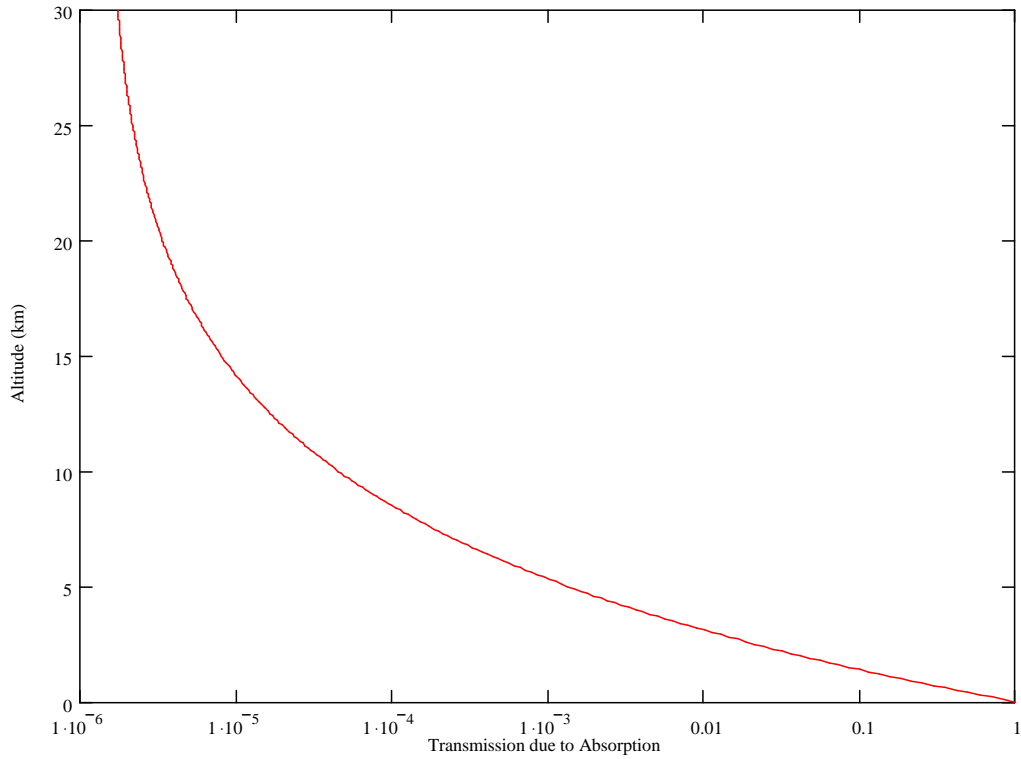


Figure 3.10. Atmospheric Transmission due to Absorption

With this determination of the attenuation term all the terms in the LIDAR equation have now been determined. The technology limited parameters, the ranging parameters and the science limited terms can now be combined in the LIDAR equation to give a measure of the expected return signal in a Martian water vapor remote sensing experiment.

3.8. LIDAR Equation Solution

All the terms and parameters for the LIDAR equation for laser light passing through the Martian atmosphere have been determined in the preceding sections. These results can now be combined in the LIDAR equation to determine the intensity of the return signal.

Some of the parameters were given in ranges. A typical value for the efficiency of a detector is 0.45. Lasers developed at GSFC for water vapor testing on Mars produce up to 100mW of power. Amplifiers are capable of boasting that to around 1W. A commonly used pulsewidth is 1.28 μ s. This gives an energy per pulse of 1.28 μ J. The range resolution, ΔR , is determined by the pulsewidth:

$$\Delta R = \frac{c}{2} \tau_{pulsewidth} \quad (3.25)$$

Using this equation gives ΔR of 192m. We'll assume that the transmitter and receiver overlap is unity, the receiver area is 0.292m and that the transmission through the receiver optical system is 0.30. The resulting plot:

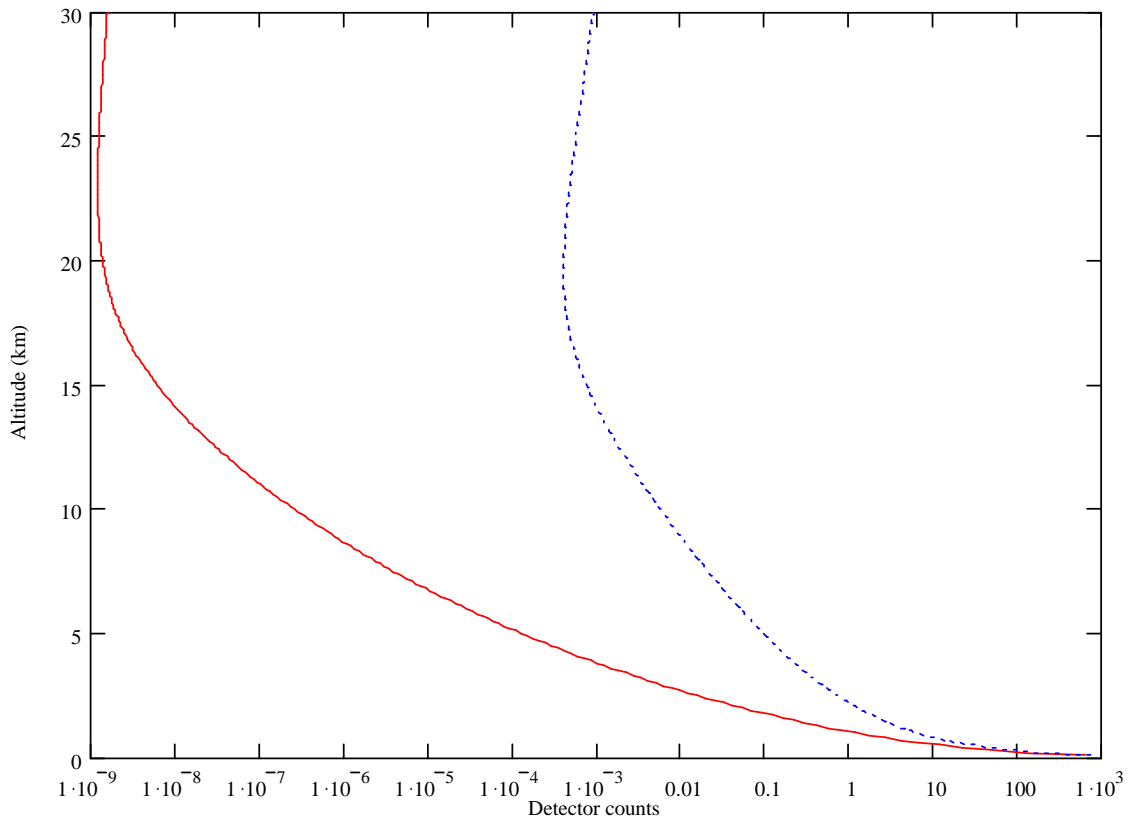


Figure 3.11. Detector counts due to Martian return

This final result is the number of detector counts recorded for each output pulse of the laser. The solid line is the return including the attenuation due to water vapor absorption of the signal on both its outward and return path. The dotted line is the return without water vapor absorption effects. These two curves distinguish two different wavelength regions, one at an absorbing wavelength and one at a non-absorbing wavelength. In this particularly case, one at 935.68nm and one nearby but not on the absorption feature.

The output pulse contains about 10^{12} photons. Close to the surface the return is about 10^3 photons making the efficiency on the order of 10^{-9} . The lowest return is around 10^{-9}

giving an efficiency of 10^{-21} at 23km altitude. This establishes the requirement of the sensitivity of any remote sensing system used on Mars to detect water vapor. It can be seen that the sensitivity required is high. At the minimum return, from 23km, there are only on the order of 10^{-9} counts per second. A very sensitive technique is required to extract the data out of such a small return signal.

3.9. Summary of LIDAR Equation Results

In this section the parameters for current available lasers and detectors have been combined with data on the Martian atmosphere and the LIDAR equation to model the transmission of laser light through the atmosphere and its scattering back to a detector. The result gives the number of counts that can be expected at the detector. This value can be used to set a lower limit on how sensitive a system must be to detect water vapor at all altitudes in the Martian atmosphere. This model will later be used to provide input to a novel FM specific model that will allow determination of performance for an FM remote sensing system on Mars. Before going to that it is necessary to introduce the laboratory FM technique and how it is different from the FM remote sensing technique developed in this paper. The next section will turn to a description of the frequency modulation technique as it exists in a laboratory setting. The limitations of the equations describing the laboratory technique will be discussed. A set of equations that can be used for remote sensing applications will be developed. This will set the stage for the analysis of FM for remote sensing which follows.

4. FM remote sensing equations

4.1. Introduction

In the proceeding sections the LIDAR equation has been solved to quantitatively describe the concentration and distribution as a function of altitude of Martian water vapor. In this section, laboratory FM will be briefly reviewed. The limitations of the laboratory FM equations will be described, demonstrating the requirement for a set of FM remote sensing equations.

This will set the stage for the author's development of the two tone equation for remote sensing to complete the simple model of FM remote sensing represented by these sets of equations. The equations developed by another author [25] for single tone FM remote sensing will be used as the basis for the two tone FM remote sensing development. The result will be a complete set of equations covering both single and two tone FM remote sensing.

The single tone and two tone FM remote sensing equations will then be discussed, showing the limitations in using them for system design of a practical FM remote sensing system. This will demonstrate the necessity of developing a computer model remedying these deficiencies. That computer model will be described in the last part of this section. Later sections will use both these models to evaluate FM remote sensing system performance.

4.2. Laboratory FM equations

There are two types of FM spectroscopy that will be discussed, single tone and two tone. Each of these requires the laser signal to be phase modulated. The modulation can be impressed on a diode laser output through the modulation of the supply current or the use of an external phase modulator. Both methods cause side bands to be produced on either side of the carrier. One side band is tuned to overlap the absorption line. The absorption causes the FM signal to become unbalanced and detectable as an AM signal. The detected AM signal strength is directly proportional to the unbalance and, therefore, to the magnitude of the absorption. The two types of modulation (single and two tone) combined with the two methods of modulation (current and external) result in four basic possibilities for implementing the FM technique.

4.2.1. Single Tone with external modulation

The earliest theories of FM techniques in laser spectroscopy describe what would later be called single tone spectroscopy using an external modulator. B is the FM index, ω_c is the central peak and ω_m is the modulation frequency. Passing an FM signal through a medium with an absorption δ and phase shift ϕ and assuming that $B \ll 1$ so that the sidebands other than for n of 1 or -1 are negligible gives:

$$E_{transmitted}(t) = E_0 \left[T_0 e^{i\omega_c t} + T_1 \frac{B}{2} e^{i(\omega_c + \omega_m)t} - T_{-1} \frac{B}{2} e^{i(\omega_c - \omega_m)t} \right] \quad (4.1)$$

The central peak and two sidebands of the basic single tone FM can be clearly distinguished in the three terms of the Fourier transform of this equation. Each sideband is shifted away from the central peak by the modulation frequency, with one sideband on

each side. Without the absorption the values the sidebands would be of equal amplitude, as shown in the figure. With the T_n factors the sidebands have unequal amplitudes. The following diagram shows a plot of the FM signal numerically generated from the above equation. The central peak and sidebands can be readily seen.

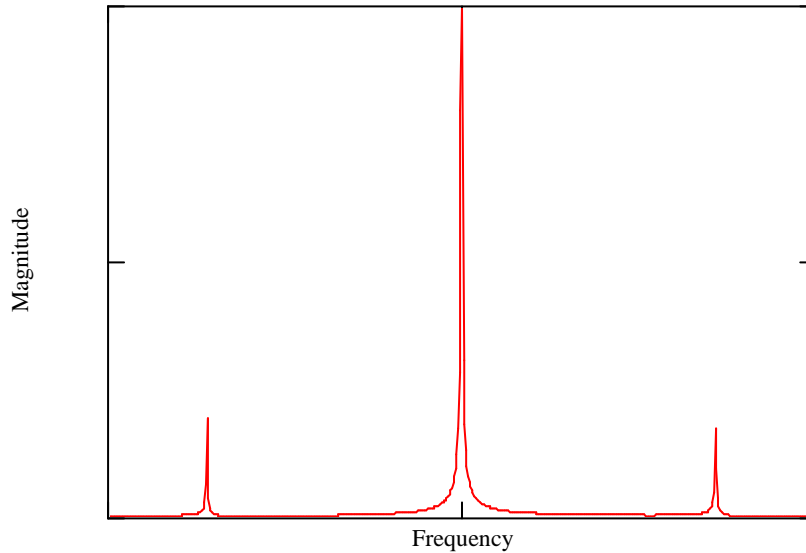


Figure 4.1 Single Tone FM

After the signal has interacted with the atmosphere it impinges on a square law detector. If the differential absorptions and phase changes are less than 1, the detector current can be approximated as:

$$I_{\text{detector}}(t) = \frac{cE_0^2}{8\pi} e^{-2\delta_0} \left[1 + (\delta_{-1} - \delta_1)B \cos \omega_m t + (\phi_1 + \phi_{-1} - 2\phi_0)B \sin \omega_m t \right] \quad (4.2)$$

The in-phase or cosine term is proportional to the loss due to the absorption feature and the quadrature or sine term is proportional to the phase change caused by the feature. That is, the cosine term measures the absorption and the sine term the dispersion caused by the absorbing species. If the absorption and dispersion is equal for both sidebands,

only a dc term is left. If they are unequal, a term oscillating at the modulation frequency is present that can be mixed with a local oscillator to sensitively detect the absorption magnitude. This is the basic conception of FM presented in the introduction to this paper. The modulating frequency can be relatively high, however, leading to an alteration of this method that allows the use of lower detection frequencies. This is two tone modulation.

4.2.2. Two tone with external modulation

The size of the absorption feature determines the size of the modulation frequency. This width will be around 1GHz for water vapor on Mars. A modulation frequency of 1GHz or greater requires detectors, cables, mixers and filters that operate at 1GHz or greater. Detectors at those frequencies tend to be easily damaged and relatively harder to handle than lower frequencies. Controlling noise at 1GHz frequencies is significantly harder than MHz frequencies. Cables and other RF equipment will have to be carefully designed to avoid cross coupling of RF signals and noise pickup from power supplies and detection electronics. To get the most rugged option for spaceflight, it would be desirable to use lower frequencies [26,27,28,29,30].

Two tone FM is designed to address these issues. In the two tone technique two closely spaced modulation frequencies are used. They both are larger than the absorption feature width, but the difference between them is relatively small. The difference between these two frequencies is kept small enough so that they sample essentially the same part of the absorption feature. In the figure, the distance between the sidebands has been exaggerated to make them visible. For an actual two tone signal the difference is not enough to be seen on such a plot.

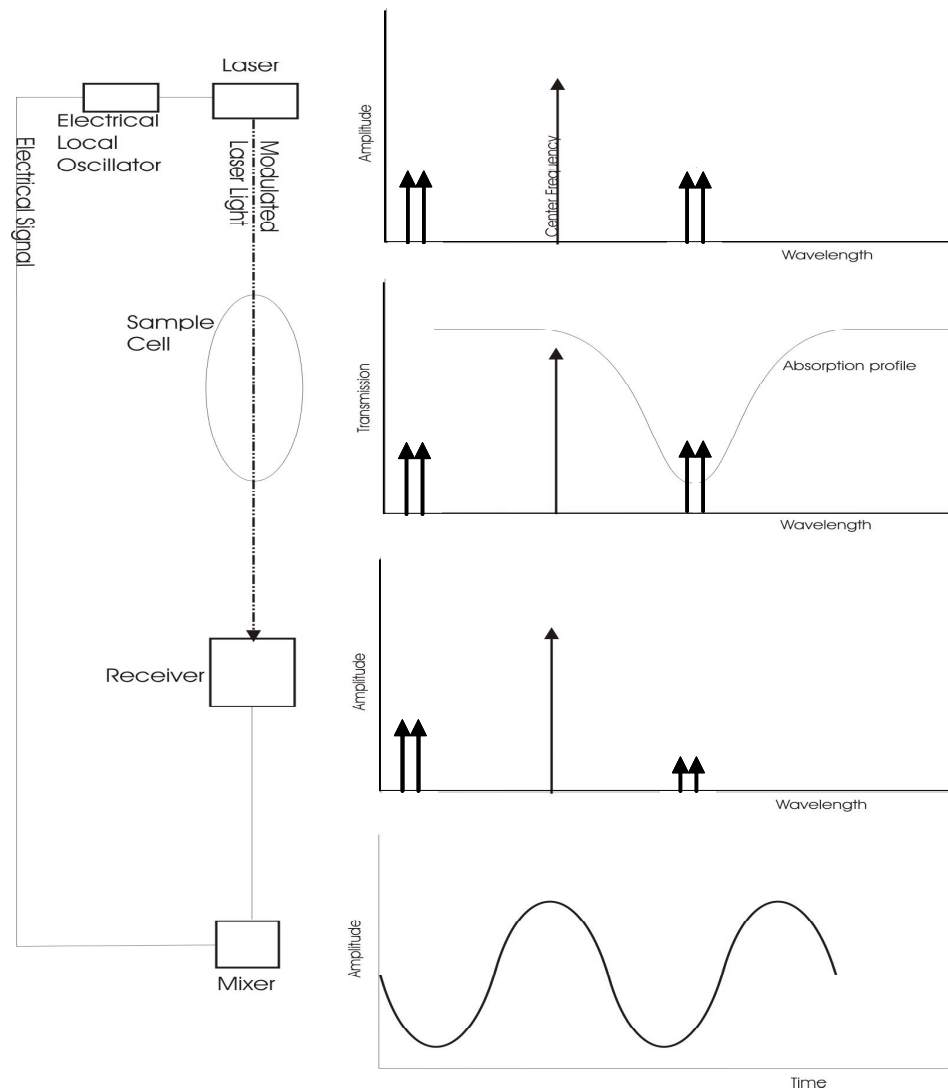


Figure 4.2. Two tone in a laboratory configuration

In the following equation, B_1 and B_2 are the modulation indices, ω_c is the central peak and ω_{m1} and ω_{m2} are the modulation frequencies. This signal is more complex than the single tone signal. Not only are there two frequencies, the products of these frequencies create intermodulation frequencies at $n\omega_1 + m\omega_2$. Passing this through a medium with an absorption δ and phase shift ϕ and assuming that $B_1=B_2 \ll 1$ so that the sidebands for $-1 < n, m > 1$ are negligible gives:

$$E_{transmitted}(t) = E_0 \left[\begin{array}{l} T_0 \left(e^{i\omega_c t} - \frac{B^2}{4} e^{i(\omega_c + (\omega_{m1} - \omega_{m2}))t} - \frac{B^2}{4} e^{i(\omega_c - (\omega_{m1} - \omega_{m2}))t} \right) + \\ T_{+1} \left(\frac{B}{2} e^{i(\omega_c + \omega_{m1})t} - \frac{B}{2} e^{i(\omega_c + \omega_{m2})t} \right) + \\ T_{-1} \left(-\frac{B}{2} e^{i(\omega_c - \omega_{m1})t} - \frac{B}{2} e^{i(\omega_c - \omega_{m2})t} \right) \end{array} \right] \quad (4.3)$$

This equation is plotted in the Fig 4.2 showing the electric field of the beam.

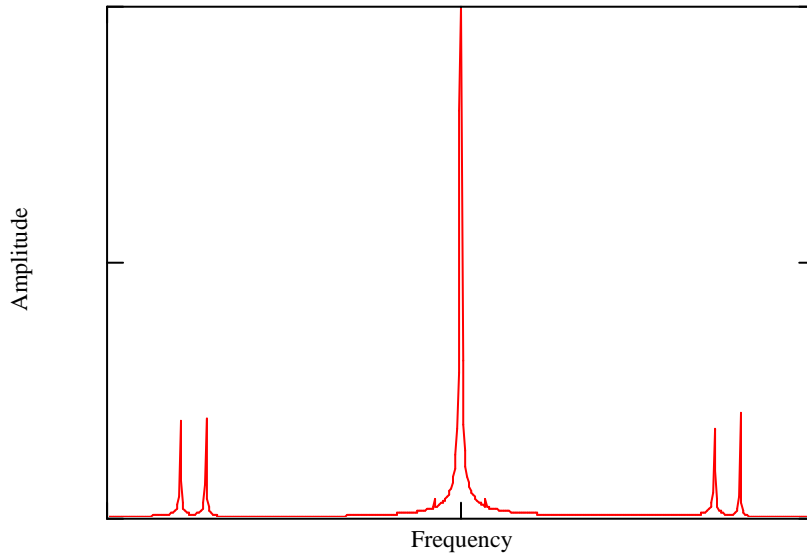


Figure 4.3. Two tone FM

The two sidebands can be seen in this plot. The difference between the sidebands has been exaggerated from a real case so that they can be distinguished. On a plot scaled for a real case, the two sidebands on either side are much closer together than the distance from the center frequency.

For Martian water vapor studies, the frequencies could reasonably be 1GHz and 1.01 GHz, a difference of 10MHz. The detector can then operate at the much lower 10 MHz frequency rather than in the GHz range. Cable requirements are much less stringent at

MHz rather than GHz frequencies, allowing the use of standard laboratory coax cables rather than more expensive rigid or semi-rigid cables. Detectors at these frequencies are relatively inexpensive. Noise due to the radiated and conducted emissions will also be much easier to control. This is of particular importance when looking ahead to the eventual spaceborne design, which would have to be small and tightly packed. Avoiding high frequencies is always desirable, especially under those circumstances.

For absorptions that are small:

$$I_{\text{detector}}(t) = \frac{cE_0^2 B^2}{8\pi} e^{-2\delta_0} (2\delta_0 - \delta_+ - \delta_-) \cos(\omega_{m1} - \omega_{m2}) \quad (4.4)$$

Here we've assumed that the closely spaced sidebands experience the same absorption. This result shows the dependence on the difference in frequency rather than the modulating frequencies themselves. In addition, two other differences distinguish this expression from the single tone result. The first is that the amplitude depends on B^2 rather than B . Consequently the value of B chosen is slightly more critical, since a small B results in a smaller B^2 and a smaller return signal. The second difference is that there is no phase information.

Like single tone, if the absorptions are equal the result is zero. If one sideband is absorbed more than the other the result is an oscillating term at the difference frequency. This can be mixed with a local oscillator to get a measure of the absorption magnitude.

The FM signal formulas and plots given up to this point assume a pure FM signal. The signal undergoes pure phase modulation without any corruption due to amplitude modulation. However, any method we actually use to phase modulate the signal will create some amplitude modulation. This Residual Amplitude Modulation (RAM) is a

noise source for an FM signal. The process of FM remote sensing converts a theoretically pure FM signal into one with an AM component, which is measured using heterodyne technique. Adding an AM signal at the source causes errors that must be accounted for and, ideally, calibrated out of the measured return.

In addition, it is better to have fewer parts in any remote sensing system sent to Mars. One way to reduce the parts count and simplify the system is to eliminate the external modulator and modulate the current to the laser directly. Although, as shall be seen in the next section, modulating the current to the laser adds noise to the signal, the gains in simplification may outweigh that consideration. In the following sections the basic equation describing current modulated FM signals will be presented.

4.2.3. *Single Tone with current modulation*

Under current modulation the semiconductor laser's injection current is directly modulated at the required frequency [31,32,33]. This modulates the optical frequency, an effect called chirping. Unfortunately, the current modulation also directly modulates the amplitude of the laser output, adding RAM. It is necessary to calculate the effect of current modulation on the previously developed pure FM signal.

The equations for pure FM can be modified to include RAM. For a single tone signal:

$$E_{source}(t) = E_0 \left(1 + M \sin(\omega_m t + \Psi) \right) e^{i(\omega_0 t + B \sin(\omega_m t))} \quad (4.5)$$

where M is the AM modulation index and Ψ is the phase difference between the AM and FM.

Assuming $M, B \ll 1$, we have and M isn't zero and the sideband and absorption phase differences are the same results in the detector current:

$$I(t) = \frac{cE_0^2}{8\pi} e^{-2\delta_0} \{1 + [M(2 + 2\delta_0)\sin\Psi]\cos\omega_m t + [M(2 + 2\delta_0)\cos\Psi]\sin\omega_m t\} \quad (4.6)$$

This reduces to the pure FM equation when $M=0$. There are still two terms, in-phase and quadrature, but they are complicated by the M terms which are noise on the signal.

4.2.4. Two Tone with current modulation

A similar analysis can be done for two tone. Starting with [34]:

$$E_{source}(t) = E_0 [1 + M_1 \sin(\omega_{m1}t + \Psi_1)][1 + M_2 \sin(\omega_{m2}t + \Psi_2)] e^{i(\omega_0 t + B_1 \sin(\omega_{m1}t) + B_2 \sin(\omega_{m2}t))} \quad (4.7)$$

Here it will be assumed that $M_1 = M_2 = M$ and similarly for B .

Again when the absorptions are equal, we are left with an oscillating signal:

$$I(t) = \frac{cE_0^2}{8\pi} e^{-2\delta_0} [M^2(2 - 2\delta_0)] \cos\omega_m t \quad (4.8)$$

The expression is more complicated than that for pure FM, reducing to it if $M = 0$.

There is still only an in-phase term for two tone whether or not RAM is included.

4.2.5. Summary and Limitations of Laboratory Equations

The basic equations for laboratory remote sensing have been presented. They are limited to situations where the FM modulation index (B), the AM modulation index (M) and the absorption are small. They also neglect the phase difference due to path length since it is unimportant in a laboratory FM setting. In addition, all the power emitted from the laser is received by the detector. There are no scattering losses included. These limitations are not acceptable for an FM remote sensing model.

It will be necessary to investigate FM and AM modulation indices greater than one.

Since the laser beam in a remote sensing application travels long distances through the atmosphere and encounters varying concentrations of a given atmospheric constituents it can't be guaranteed that the absorption will be small. Significant scattering will occur. In fact, the return is a scattered signal in one form of remote sensing. The phase difference between waves arriving back at the detector after being scattered off of the atmosphere will be important and cannot be neglected.

For these reasons an alternate set of equations will be developed for two tone FM remote sensing that doesn't include these approximations. They will build in work done by Dubinsky in developing a model for single tone FM remote sensing. This will result in a model for both single tone and two tone FM remote sensing.

4.3. Development of the Two Tone FM Remote Sensing Model

The results used in the introductory section of this paper are approximations. To better evaluate FM remote sensing, it is necessary to develop a more comprehensive model, without these approximations. Such a model has been developed by Dubinsky for single tone FM. The following is the novel addition to the model of the additional complexities for two tone FM.

We start with the expression for the source emission:

$$E_{source}(t) = E_0 e^{i[(\omega_0 t - kx) + B_1 \sin(\omega_{m1} t - k_n x) + B_2 \sin(\omega_{m2} t - k_l x)]} \quad (4.9)$$

which can be expanded using Bessel functions:

$$E(t) = E_0 e^{i(\omega_0 t - kx)} \sum_{n,l=-\infty}^{\infty} J_n(B_1) J_l(B_2) e^{i[B_1 \sin(n\omega_{m1} t - k_n x) + B_2 \sin(l\omega_{m2} t - k_l x)]} \quad (4.10)$$

This spectrum of the electrical field described by this equation is plotted below.

The electric field spectrum is an infinite sum of terms. Each term represents one frequency line determined by $(n\omega_{m1} + l\omega_{m2})$ with amplitude of $J_n(B_1)J_l(B_2)$. Therefore, each pair of values (n, l) determines a single line in the spectrum.

The center cluster is the carrier and its immediate sidebands. These are the zeroth order sidebands. The lines within the carrier cluster are $(\omega_{m1} - \omega_{m2}) = \Delta\omega$ away from each other. To the right and left of the carrier cluster are the first order sideband clusters. The first order clusters are centered on a frequency that is $(\omega_{m1} + \omega_{m2})/2$ from the carrier. Since the absolute values of the modulating frequencies ω_{m1} and ω_{m2} are much greater than the difference between them, namely $\Delta\omega$, the clusters are much farther apart than the lines within the clusters. In the plot the difference frequency has been exaggerated. If it were true to scale, the clusters would look like very tightly packed groups of lines with

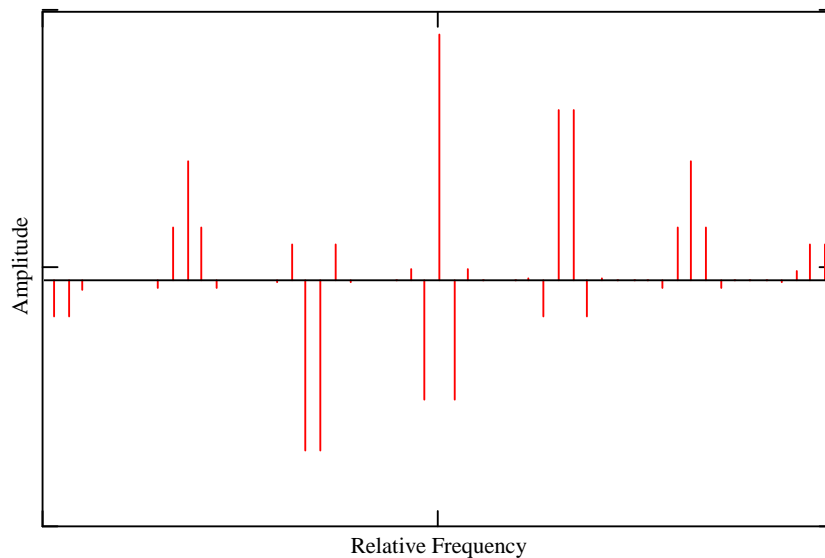


Figure 4.4. Electric Field Spectrum of FM signal with carrier in center

lots of space between them.

Further out to the right and left are the second order sidebands that are $(\omega_{m1} + \omega_{m2})/2$ away from the first order sidebands. This continues out to infinity on either side. However, the amplitude of the sidebands rapidly decreases as the distance from the carrier increases, so that they can and will be neglected.

It can be seen that there are lots of lines that are $\Delta\omega$ apart. All these lines contribute to the signal detected by the two tone system. Only one set of lines, however, will overlap the absorption feature. This is chosen to be the first order sidebands since they are the maximum amplitude sidebands and will contribute the most to the two tone detected signal. Now that the outbound signal has been characterized it is necessary to add the atmospheric effects.

The atmosphere modifies the return through absorption and phase change. This process can be modeled as an exponential containing a real term for the absorption and an imaginary term for the phase change. These terms are indexed by n and l to identify the absorption and phase change for a specific modulation frequency.

$$T_{nl} = e^{(-\delta_n - \delta_l - i\phi_n - i\phi_l)} = T_n T_l \quad (4.11)$$

This expression gives the total of the absorption and phase change experienced by each frequency line as it travels through the atmosphere. Multiplying this by the $E(t)$ gives the return signal. When this signal is received at the detector it will impinge on a square law device. A general term for the current output of the square law detector with a responsivity of Q_{det} is:

$$I(t) = \frac{Q_{det}}{2} E_{ret}(t) E_{ret}^*(t) \quad (4.12)$$

Multiplying E(t) by T to get the return and inserting into this expression for I(t) results in:

$$I(t) = \frac{Q_{\text{det}}}{2} E^2 \left(\sum_{n,l=-\infty}^{\infty} J_n(B_1) J_l(B_2) e^{i(n\omega_{m1} + l\omega_{m2} - k_{nl}x)t} T_{nl} \right) \left(\sum_{n',l'=-\infty}^{\infty} J_{n'}(B_1) J_{l'}(B_2) e^{-i(n'\omega_{m1} + l'\omega_{m2} - k_{n'l'}x)t} T_{n'l'}^* \right) \quad (4.13)$$

where k_{nl} has been defined to be equal to $k_n + k_l$.

The complex conjugation and multiplication has eliminated the center frequency. The prime designation on n and l allows the separation of the E field and conjugate E field.

The result is cross products of the each of the modulation frequency terms.

To make these expressions more compact and easier to understand, the B's will left out and the constants in the front of the summations will be defined as A. Collecting the terms into one summation gives:

$$I(t) = A \sum_{n,l,n',l'=-\infty}^{\infty} J_n J_l J_{n'} J_{l'} e^{i[(n-n')\omega_{m1}t + (l-l')\omega_{m2}t - (k_{nl} - k_{n'l'})x]} T_{nl} T_{n'l'}^* \quad (4.14)$$

This is the general term for the current output of the detector without approximations. To make this expression easier to use and understand some approximations will now be made and the expression rearranged.

The detector response and the filtering in the receiver will limit the detected current to only the terms corresponding to the difference frequency between the modulation frequencies. These are the ones where:

$$\begin{aligned} |n - n'| &= 1 \\ |l - l'| &= 1 \end{aligned} \quad (4.15)$$

That is, these are the frequencies which give $\omega_{m1} - \omega_{m2}$ when subtracted. The higher order multiples of this are filtered out. This relationship also allows the expression of n`

and Γ in terms of n and l . Using the approximation of only difference frequencies and expressing in terms of n and l gives:

$$I(t) = A \sum_{n,l=-\infty}^{\infty} J_n J_l J_{n+1} J_{l-1} e^{-i[(\omega_{m1}-\omega_{m2})t-k_{RF}x]} T_{nl} T_{n+1,l-1}^* + \sum_{n,l=-\infty}^{\infty} J_n J_l J_{n-1} J_{l+1} e^{+i[(\omega_{m1}-\omega_{m2})t-k_{RF}x]} T_{nl} T_{n-1,l+1}^* \quad (4.16)$$

where for convenience the RF wavenumber has been defined as:

$$k_{RF} = k_{nl} - k_{n'l'} = \frac{2\pi}{c} (\omega_{m1} - \omega_{m2}) \quad (4.17)$$

This can be further rearranged and the indices modified again to group the Bessel functions together and give a more compact expression:

$$I(t) = A \sum_{n,l=-\infty}^{\infty} J_n J_l J_{n+1} J_{l-1} \left[T_{nl} T_{n+1,l-1}^* e^{-i[(\omega_{m1}-\omega_{m2})t-k_{RF}x]} + T_{nl}^* T_{n+1,l-1} e^{+i[(\omega_{m1}-\omega_{m2})t-k_{RF}x]} \right] \quad (4.18)$$

The receiving system will beat this current with a local oscillator to extract the component at the difference modulation frequency. This mixing process can be represented as [35]:

$$I_{det}(t) = I(t) \cos(\Delta\omega + \phi_{RF}) \quad (4.19)$$

Here $\Delta\omega$ is the modulation difference frequency generated from the frequencies that were used to modulate the outgoing beam and ϕ_{RF} is the phase of this signal. Let:

$$A' = A \frac{1}{2} = \frac{Q_{det}}{4} E^2 \quad (4.20)$$

Letting A' equal this will combine all the constants in one term. Then, expressing the cosine in its exponential form, inserting the expression for $I(t)$ in the term for $I_{det}(t)$ and collecting terms results in:

$$I_{det}(t) = A' \sum_{n,l=-\infty}^{\infty} J_n J_l J_{n+1} J_{l-1} \left[T_{nl} T_{n+1,l-1}^* \left(e^{i(\phi_{RF} + k_{RF}x)} + e^{-i(2\Delta\omega - i(\phi_{RF} - k_{RF}x))} \right) + T_{n+1,l-1} T_{nl}^* \left(e^{-i(\phi_{RF} + k_{RF}x)} + e^{+i(2\Delta\omega + i(\phi_{RF} - k_{RF}x))} \right) \right]$$

(4.21)

The $2\Delta\omega$ term will be filtered out due to the detector's bandwidth limitations, leaving only the dc term:

$$I_{\text{det}}(t) = A' \sum_{n,l=-\infty}^{\infty} J_n J_l J_{n+1} J_{l-1} \left[T_{nl} T_{n+1,l-1}^* e^{i(\phi_{RF} + k_{RF}x)} + T_{n+1,l-1} T_{nl}^* e^{-i(\phi_{RF} + k_{RF}x)} \right] \quad (4.22)$$

To simplify further, let:

$$\phi = \phi_{RF} + k_{RF}x = \phi_{RF} + \frac{2\pi}{c}(\omega_1 - \omega_2)x \quad (4.23)$$

Using this expression gives the result:

$$I_{\text{det}}(t) = A' \sum_{n,l=-\infty}^{\infty} J_n J_l J_{n+1} J_{l-1} \left[T_{nl} T_{n+1,l-1}^* e^{i(\phi)} + T_{n+1,l-1} T_{nl}^* e^{-i(\phi)} \right] \quad (4.24)$$

It will prove to be convenient to separate this into cosine and sine terms of the phase.

As a first step, the lower summation limit can be changed to zero by adding two terms with negative indices compared to the two terms above. Setting the lower limit of index l to zero results in:

$$I_{\text{det}}(t) = A' \sum_{n=-\infty}^{\infty} \sum_{l=0}^{\infty} J_n J_{n+1} \left[J_l J_{l-1} \left(T_{nl} T_{n+1,l-1}^* e^{i(\phi)} + T_{n+1,l-1} T_{nl}^* e^{-i(\phi)} \right) + J_{-l} J_{-(l-1)} \left(T_{n,-l} T_{n+1,-(l-1)}^* e^{i(\phi)} + T_{n+1,-(l-1)} T_{n,-l}^* e^{-i(\phi)} \right) \right] \quad (4.25)$$

Repeating this process to set the lower limit of index n to zero gives:

$$I_{\text{det}}(t) = A' \sum_{n,l=0}^{\infty} \left[J_n J_{n+1} \left[J_l J_{l-1} \left(T_{nl} T_{n+1,l-1}^* e^{i(\phi)} + T_{n+1,l-1} T_{nl}^* e^{-i(\phi)} \right) + J_{-l} J_{-(l-1)} \left(T_{n,-l} T_{n+1,-(l-1)}^* e^{i(\phi)} + T_{n+1,-(l-1)} T_{n,-l}^* e^{-i(\phi)} \right) \right] + J_{-n} J_{-(n+1)} \left[J_l J_{l-1} \left(T_{-n,l} T_{-(n+1),l-1}^* e^{i(\phi)} + T_{-(n+1),l-1} T_{-n,l}^* e^{-i(\phi)} \right) + J_{-l} J_{-(l-1)} \left(T_{-n,-l} T_{-(n+1),-(l-1)}^* e^{i(\phi)} + T_{-(n+1),-(l-1)} T_{-n,-l}^* e^{-i(\phi)} \right) \right] \right] \quad (4.26)$$

The Bessel functions can now be recollected using the identity:

$$J_{-n} = (-1)^n J_n \quad (4.27)$$

to give:

$$I_{\det}(t) = A' \sum_{n=0}^{\infty} \sum_{l=0}^{\infty} J_n J_{n+1} J_l J_{l-1} \left[\begin{array}{l} (T_{nl} T_{n+1,l-1}^* e^{i(\phi)} + T_{n+1,l-1} T_{nl}^* e^{-i(\phi)}) \\ - (T_{n,-l} T_{n+1,-(l-1)}^* e^{i(\phi)} + T_{n+1,-(l-1)} T_{n,-l}^* e^{-i(\phi)}) - \\ (T_{-n,l} T_{-(n+1),l-1}^* e^{i(\phi)} + T_{-(n+1),l-1} T_{-n,l}^* e^{-i(\phi)}) \\ + (T_{-n,-l} T_{-(n+1),-(l-1)}^* e^{i(\phi)} + T_{-(n+1),-(l-1)} T_{-n,-l}^* e^{-i(\phi)}) \end{array} \right] \quad (4.28)$$

The T function can now be expanded back into its exponential form and the terms collected to form cosine terms. This results in:

$$I_{\det}(t) = A' \sum_{n=0}^{\infty} \sum_{l=0}^{\infty} J_n J_{n+1} J_l J_{l-1} \left[\begin{array}{l} e^{-\delta_{nl} - \delta_{n+1,l-1}} \cos(\phi_{nl} - \phi_{n+1,l-1} - \phi) \\ - e^{-\delta_{n,-l} - \delta_{n+1,-(l-1)}} \cos(\phi_{n,-l} - \phi_{n+1,-(l-1)} - \phi) \\ - e^{-\delta_{-n,l} - \delta_{-(n+1),l-1}} \cos(\phi_{-n,l} - \phi_{-(n+1),l-1} - \phi) \\ - e^{-\delta_{-n,-l} - \delta_{-(n+1),-(l-1)}} \cos(\phi_{-n,-l} - \phi_{-(n+1),-(l-1)} - \phi) \end{array} \right] \quad (4.29)$$

where ϕ_{nl} is defined as:

$$\phi_{nl} = \phi_n + \phi_l \quad (4.30)$$

Now the following trigonometric equations can be used:

$$\begin{aligned} \cos(x \pm y) &= \cos x \cos y \mp \sin x \sin y \\ \sin(x \pm y) &= \sin x \cos y \pm \sin y \cos x \end{aligned} \quad (4.31)$$

These serve to isolate ϕ within sine and cosine terms:

$$I_{\text{det}}(t) = A' \sum_{n,l=0}^{\infty} J_n J_{n+1} J_l J_{l-1} \begin{bmatrix} e^{-\delta_{nl} - \delta_{n+1,l-1}} \left(\cos(\phi_{nl} - \phi_{n+1,l-1}) \cos \phi \right) \\ + \sin(\phi_{nl} - \phi_{n+1,l-1}) \sin \phi \\ - e^{-\delta_{n,-l} - \delta_{n+1,-(l-1)}} \left(\cos(\phi_{n,-l} - \phi_{n+1,-(l-1)}) \cos(\phi) \right) \\ + \sin(\phi_{n,-l} - \phi_{n+1,-(l-1)}) \sin \phi \\ - e^{-\delta_{-n,l} - \delta_{-(n+1),l-1}} \left(\cos(\phi_{-n,l} - \phi_{-(n+1),l-1}) \cos \phi \right) \\ + \sin(\phi_{-n,l} - \phi_{-(n+1),l-1}) \sin \phi \\ + e^{-\delta_{-n,-l} - \delta_{-(n+1),-(l-1)}} \left(\cos(\phi_{-n,-l} - \phi_{-(n+1),-(l-1)}) \cos \phi \right) \\ + \sin(\phi_{-n,-l} - \phi_{-(n+1),-(l-1)}) \sin \phi \end{bmatrix} \quad (4/32)$$

It is now possible to express $I_{\text{det}}(t)$ as in-phase and quadrature parts:

$$I_{\text{det}}(t) = I^{\text{in}}(t) \cos \phi + I^{\text{out}}(t) \sin \phi \quad (4.33)$$

The final result is the following two equations:

$$I^{\text{in}}(t) = \frac{Q_{\text{det}}}{4} E^2 \sum_{n,l=0}^{\infty} J_n J_{n+1} J_l J_{l-1} \begin{bmatrix} e^{-\delta_{nl} - \delta_{n+1,l-1}} \cos(\phi_{nl} - \phi_{n+1,l-1}) \\ - e^{-\delta_{n,-l} - \delta_{n+1,-(l-1)}} \cos(\phi_{n,-l} - \phi_{n+1,-(l-1)}) \\ - e^{-\delta_{-n,l} - \delta_{-(n+1),l-1}} \cos(\phi_{-n,l} - \phi_{-(n+1),l-1}) \\ + e^{-\delta_{-n,-l} - \delta_{-(n+1),-(l-1)}} \cos(\phi_{-n,-l} - \phi_{-(n+1),-(l-1)}) \end{bmatrix} \quad (4.34)$$

$$I^{\text{out}}(t) = \frac{Q_{\text{det}}}{4} E^2 \sum_{n,l=0}^{\infty} J_n J_{n+1} J_l J_{l-1} \begin{bmatrix} e^{-\delta_{nl} - \delta_{n+1,l-1}} \sin(\phi_{nl} - \phi_{n+1,l-1}) \\ - e^{-\delta_{n,-l} - \delta_{n+1,-(l-1)}} \sin(\phi_{n,-l} - \phi_{n+1,-(l-1)}) \\ - e^{-\delta_{-n,l} - \delta_{-(n+1),l-1}} \sin(\phi_{-n,l} - \phi_{-(n+1),l-1}) \\ + e^{-\delta_{-n,-l} - \delta_{-(n+1),-(l-1)}} \sin(\phi_{-n,-l} - \phi_{-(n+1),-(l-1)}) \end{bmatrix} \quad (4.35)$$

These are the final equations defining the current output of the detector for a two tone FM remote sensing application. As such they are a new and significant addition to the theory compared to the approximate equations for laboratory FM spectroscopy and the single tone derivation for FM remote sensing spectroscopy. With these equations for two tone, there now are analytic tools to address both single tone and two tone FM remote sensing. Before proceeding, this result will be reviewed.

4.4. Review of Two Tone FM Remote Sensing Model

There are two equations, one representing the in-phase current and one the out-of-phase current. The time variation is contained in the ϕ term that is expressed in the total current, $I_{\text{det}}(t)$, equation. The I^{out} and I^{in} equations are the amplitudes of the in-phase and out-of-phase terms in this equation. These amplitudes are dependent on the absorption and phase change the signal experiences as it passes through the atmosphere.

These expressions demonstrate how both the attenuation and the phase change of the signal can be measured using FM remote sensing spectroscopy. If there is no absorption and no phase change then the cosines, the sine and exponential terms equal one and cancel each other out. So there is no signal. This zero baseline is exactly what should be the case for FM spectroscopy. Differential absorptions or phase changes result in an oscillating current at the detector. The differential phase changes within the cosines and sines cause the current to increase and decrease cyclically as the difference frequencies go in and out of phase relative to each other.

To further evaluate the effect of nonzero differential phase changes and absorptions it is helpful to express the phase changes and absorptions in terms of attenuation coefficients, distance and frequency. The phase change and absorption terms can be written as:

$$\delta_{nl} = \frac{\alpha_{nl}L}{2} \quad (4.36)$$

$$\phi_{nl} = \phi_n + \phi_l = n \frac{n_n L \omega_n}{c} + l \frac{n_l L \omega_l}{c} \quad (4.37)$$

where L is the distance the light travels, n_n and n_l are the indices of refraction for light at

$n\omega_{m1}$ and $l\omega_{m2}$, respectively. The absorption coefficient $\alpha_{nl} = \alpha_n + \alpha_l$ is the absorption coefficient for the light at those wavelengths.

Inserting these equations into the detector output current equations gives:

$$I^{in}(t) = \frac{Q_{det}}{4} E^2 \sum_{n,l=0}^{\infty} J_n J_{n+1} J_l J_{l-1} \begin{bmatrix} e^{-\frac{L}{2}(\alpha_{nl} + \alpha_{n+1,l-1})} \cos \frac{L}{c} (-n_n \omega_n + n_l \omega_l) \\ - e^{-\frac{L}{2}(\alpha_{n,-l} + \alpha_{n+1,-(l-1)})} \cos \frac{L}{c} (-n_n \omega_n - n_l \omega_l) \\ - e^{-\frac{L}{2}(\alpha_{-n,l} + \alpha_{-(n+1),l-1})} \cos \frac{L}{c} (n_n \omega_n + n_l \omega_l) \\ + e^{-\frac{L}{2}(\alpha_{-n,-l} + \alpha_{-(n+1),-(l-1)})} \cos \frac{L}{c} (n_n \omega_n - n_l \omega_l) \end{bmatrix} \quad (4.38)$$

$$I^{out}(t) = \frac{Q_{det}}{4} E^2 \sum_{n,l=0}^{\infty} J_n J_{n+1} J_l J_{l-1} \begin{bmatrix} e^{-\frac{L}{2}(\alpha_{nl} + \alpha_{n+1,l-1})} \sin \frac{L}{c} (-n_n \omega_n + n_l \omega_l) \\ - e^{-\frac{L}{2}(\alpha_{n,-l} + \alpha_{n+1,-(l-1)})} \sin \frac{L}{c} (-n_n \omega_n - n_l \omega_l) \\ - e^{-\frac{L}{2}(\alpha_{-n,l} + \alpha_{-(n+1),l-1})} \sin \frac{L}{c} (n_n \omega_n + n_l \omega_l) \\ + e^{-\frac{L}{2}(\alpha_{-n,-l} + \alpha_{-(n+1),-(l-1)})} \sin \frac{L}{c} (n_n \omega_n - n_l \omega_l) \end{bmatrix} \quad (4.39)$$

It is now possible to see the specific influences on the differential absorption and differential phase change that cause the detector current to change. The differential absorption increases with increasing distance traveled, producing a larger signal. The differential phase cyclically increases and decreases as the distance increases. In addition, the index of refraction contributes to the effective pathlength at a given frequency.

4.5. Comparison to Laboratory Equations

It's possible to reduce these solutions to the laboratory ones discussed earlier. Those simpler equations used only the terms corresponding to the center frequency and first

order sidebands. The corresponding assumption here is that only the terms containing J_0 and J_1 will be summed, all others will be assumed too small to contribute. For the in-phase component the result is:

$$I_{\text{det}}^{\text{in}}(t) = A' \left\{ \begin{array}{l} J_0 J_1 J_0 J_{-1} \left[\begin{array}{l} e^{-\delta_{00}-\delta_{+1,-1}} \cos(\phi_{00} - \phi_{+1,-1}) - e^{-\delta_{0,0}-\delta_{+1,+1}} \cos(\phi_{0,0} - \phi_{+1,+1}) \\ - e^{-\delta_{0,0}-\delta_{-1,-1}} \cos(\phi_{0,0} - \phi_{-1,-1}) + e^{-\delta_{0,0}-\delta_{-1,+1}} \cos(\phi_{0,0} - \phi_{-1,+1}) \end{array} \right] + \\ J_0 J_1 J_1 J_0 \left[\begin{array}{l} e^{-\delta_{0,+1}-\delta_{+1,0}} \cos(\phi_{0,+1} - \phi_{+1,0}) - e^{-\delta_{0,-1}-\delta_{+1,0}} \cos(\phi_{0,-1} - \phi_{+1,0}) \\ - e^{-\delta_{0,+1}-\delta_{-1,0}} \cos(\phi_{0,+1} - \phi_{-1,0}) + e^{-\delta_{0,-1}-\delta_{-1,0}} \cos(\phi_{0,-1} - \phi_{-1,0}) \end{array} \right] \end{array} \right\} \cos(\phi) \quad (4.40)$$

The out-of-phase current is the same except that the cosine function is replaced by the sine function.

One of the approximations for the simpler equations is that the phase changes caused by the feature are all very small. It's important to note here that this will not be true for a remote sensing application since the distances traveled are large. The simpler equations that make this assumption cannot be used for a remote sensing application.

For this approximation, the difference between any two of the phases is, therefore, always very close to zero. Since the cosine of zero is one, this expression can be written:

$$I_{\text{det}}^{\text{in}}(t) = A' \left\{ J_0 J_1 J_0 J_{-1} \left[\begin{array}{l} e^{-\delta_{00}-\delta_{+1,-1}} - e^{-\delta_{0,0}-\delta_{+1,+1}} \\ - e^{-\delta_{0,0}-\delta_{-1,-1}} + e^{-\delta_{0,0}-\delta_{-1,+1}} \end{array} \right] + J_0 J_1 J_1 J_0 \left[\begin{array}{l} e^{-\delta_{0,+1}-\delta_{+1,0}} - e^{-\delta_{0,-1}-\delta_{+1,0}} \\ - e^{-\delta_{0,+1}-\delta_{-1,0}} + e^{-\delta_{0,-1}-\delta_{-1,0}} \end{array} \right] \right\} \cos \phi \quad (4.41)$$

The expression for the remaining phase term is:

$$\phi = \phi_{\text{RF}} + \frac{2\pi}{c} (\omega_1 - \omega_2)x = \phi_{\text{RF}} + \frac{2\pi x}{c} \Delta \omega \quad (4.42)$$

The phase of the local RF source isn't specifically used in the approximate solution so it'll be set to zero.

Also using:

$$J_{-n} = (-1)^n J_n \quad (4.43)$$

The in-phase current can be expressed:

$$I^{in}(t) = A' J_0^2 J_1^2 \left[\begin{array}{l} \left[\begin{array}{l} e^{-\delta_{0,+1}-\delta_{+1,0}} \cos\left(-\frac{2\pi x}{c} \Delta\omega\right) - e^{-\delta_{0,-1}-\delta_{-1,0}} \cos\left(-2\frac{2\pi x}{c} \Delta\omega\right) \\ - e^{-\delta_{0,+1}-\delta_{-1,0}} \cos\left(2\frac{2\pi x}{c} \Delta\omega\right) + e^{-\delta_{0,-1}-\delta_{-1,0}} \cos\left(\frac{2\pi x}{c} \Delta\omega\right) \end{array} \right] \\ \left[\begin{array}{l} e^{-\delta_{0,0}-\delta_{+1,-1}} \cos\left(-\frac{2\pi x}{c} \Delta\omega\right) - e^{-\delta_{0,0}-\delta_{+1,+1}} \cos\left(-2\frac{2\pi x}{c} \Delta\omega\right) \\ - e^{-\delta_{0,0}-\delta_{-1,-1}} \cos\left(2\frac{2\pi x}{c} \Delta\omega\right) + e^{-\delta_{0,0}-\delta_{-1,+1}} \cos\left(\frac{2\pi x}{c} \Delta\omega\right) \end{array} \right] \end{array} \right] \quad (4.44)$$

Again, the out-of-phase current has sine's instead of cosine's.

The $2\Delta\omega$ will be filtered out, so those terms can be removed from the approximation.

The cosine is a even function, so the negative signs inside the cosine can be removed and those terms can be grouped together. In addition, the approximation for the exponential for small values of the exponent will be used since the absorptions are assumed small:

$$e^{-x} \approx 1 - x \quad (4.45)$$

Also:

$$\frac{2\pi x}{c} = t \quad (4.46)$$

Making these approximations and substitutions reduces the equation to:

$$I^{in}(t) = 2A' J_0^2 J_1^2 \cos(\Delta\omega t) [2\delta_0 + \delta_{+1,-1} + \delta_{-1,+1} - \delta_{0,1} - \delta_{1,0} - \delta_{0,-1} - \delta_{-1,0}] \quad (4.47)$$

In a similar fashion, the out-of-phase current is approximated by:

$$I^{out}(t) = A' J_0^2 J_1^2 \cos(\Delta\omega t) [\delta_{1,-1} - \delta_{-1,-1} + \delta_{-1,+1} - \delta_{-1,1} + \delta_{1,0} - \delta_{1,0} + \delta_{0,1} - \delta_{0,1} + \delta_{-1,0} - \delta_{-1,0} + \delta_{0,-1} - \delta_{0,-1}] \quad (4.48)$$

It will now also be assumed that frequencies separated by $\Delta\omega$ will experience the same absorption, so that:

$$\begin{aligned}\delta_0 &\approx \delta_{+1,-1} \approx \delta_{-1,+1} \\ \delta_{01} &\approx \delta_{10} \equiv \delta_1 \\ \delta_{0,-1} &\approx \delta_{-1,0} \equiv \delta_{-1}\end{aligned}\tag{4.49}$$

All terms within brackets for the out-of-phase signal cancel and the entire equation goes to zero. This is consistent with the simpler forms. If those assumptions are used, the two tone out-of-phase FM signal disappears.

The in-phase equation can be reduced further. The Bessel functions can be approximated for small x by:

$$\begin{aligned}J_0(x) &\approx 1 \\ J_1(x) &\approx \frac{x}{2}\end{aligned}\tag{4.50}$$

Using these and substituting back for A' gives the final result:

$$\begin{aligned}I^{in}(t) &= \frac{Q_{det}}{4} E^2 B^2 \cos(\Delta\omega t) [2\delta_0 - \delta_1 - \delta_{-1}] \\ I^{out}(t) &= 0\end{aligned}\tag{4.51}$$

This is the same result obtained earlier using the single sideband, small M and small B assumptions obtained earlier.

4.6. Uses and Limits of Analytic Equation

The two tone FM remote sensing equation developed in this section along with the single tone equations developed by Dubinsky can be used to model basic FM remote sensing configurations. However, there are other parameters that are necessary in a remote sensing model that even this model will not be able to accommodate. The most

important items missing from the analytic model include losses due to scattering, the effects of current modulation on the output of the laser and the ability to calculate the return using complex atmospheric models such as the one for Mars developed earlier in this paper. In order to accommodate these requirements, a computer model has been developed by the author. This model will be used extensively in the work that follows.

4.7. Description of Computer Model

The computer model developed by the author starts from the power output of the laser in the form of an equation that describes the electric field that represents the local oscillator modulated light output from the laser. These equations include both the frequency modulation and the undesirable side effect of amplitude modulation of the laser light electric field.

The light is mathematically propagated through the atmosphere, scattered and returns to the detector located at the same location as the source all. The signal undergoes attenuation of one sideband due to absorption and reduction of the entire signal due to scattering losses. This computer model allows for the use of sophisticated or simple absorption and scattering models. In this paper the model of the Martian atmosphere explained earlier will be used to give accurate results of the performance expected on Mars. The analytic model only includes the capability for simple attenuation, without losses like scattering losses.

The return signal is detected and filtered by the detector bandwidth. The resulting electrical current is mixed with the local oscillator. The result is filtered to leave the local oscillator frequency component of the return signal. The amplitude of the remaining

current contains the absorption information. The result will be used to evaluate FM phase effects, loss effects and system performance.

4.8. Summary

Analytic equations have been developed to describe the remote sensing FM techniques. These analytic equations have limitations. These limitations can best be overcome by developing a computer model that eliminates the approximations of the analytic model and adds parameters to cover additional considerations such as complex atmospheric models, scattering and laser current modulation. Doing this in an analytic model would result in complex and lengthy equations that would be difficult to interpret and use. A computer model has been developed to overcome these limitations. During the development of the computer model, the analytic model was used to validate the computer model results where the analytic model applied. This verification process was important as part of the overall effort, along with experimental results reported later in this paper, to validate the computer model. The analytic model and computer model will both be used to derive the results in the following sections.

5. FM Remote Sensing Phase Effects

5.1. Introduction

In the introduction it was stated that the effects of the RF (not optical) phase of the returning waves would be a critical component of the determination of the viability of FM remote sensing. In this section the analytic and computer models developed in earlier sections will be used to model the propagation of the laser light through the atmosphere, the scattering of the light and its addition at the detector. The resulting detector current will be determined as it depends on the number of waves added and the phase difference between them. Both lossless and lossy cases will be discussed to show the effect of loss on the return signal. The models will then be used to compare calculated results to the results from experimental data from other authors. The data from experiments will also be used to compare to calculated results. These comparisons will demonstrate that the model reflects reality and the results obtained from it are valid.

5.2. Phase effects introduction

The basic case is that of a single tone FM signal emitted from the laser source, directed up into the atmosphere and reflected back. If all the power is reflected back into the detector the situation is like that of a laboratory FM experiment except for one major exception. The phases of the wavefronts returning to the detector are dependent on the distance the wave has traveled, and so will be different upon reaching the detector.

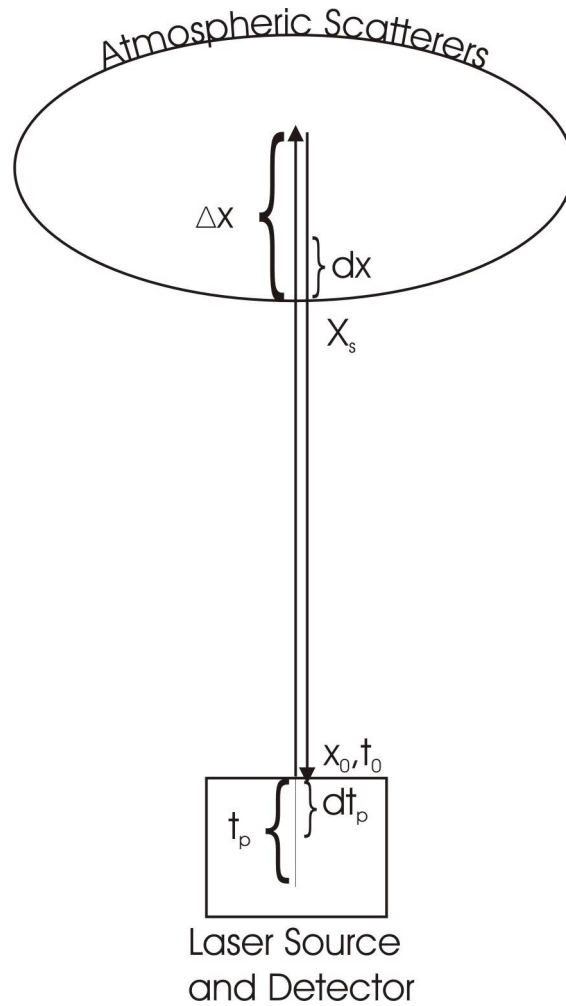


Figure 5.1. Time of flight

The diagram above details the times and distances associated with the waves flight through the atmosphere and back to the detector. Here x_s is the starting point of the region of atmosphere being sampled, dx is the location within those set of points and x_0 is the location of the source. The equation for the phase change due to the wave's travel through the atmosphere is:

$$\phi_{\omega,d} = k_{\omega} (x - x_0 - 2x_s - 2dx) = \frac{2\pi\omega}{c} (x - x_0 - 2x_s - 2dx) = \frac{2\pi\omega}{c} d \quad (5.1)$$

This expression shows how the phase for a given distance depends on the frequency

as well as the distance traveled. Using this phase change due to distance, the single tone FM expression for the return at time t can be written as:

$$E_{return}(t, d) = E_0 \left[1 + M \sin(\omega_m (t - t_0 - t_p) + \phi_{\omega_m, d}) \right] e^{i(\omega_0 (t - t_0 - t_p) + \phi_{\omega_0, d} + B \sin(\omega_m (t - t_0 - t_p) + \phi_{\omega_m, d}))} \quad (5.2)$$

The time the leading edge of the pulse is emitted is t_0 and the location within the pulse is dt_p . Since the light emitted at the source has a width in time, the pulsewidth, the value dt_p is added to t_0 to represent the specific temporal location within the pulse.

At any instant the same time will have passed for any wave received at the detector. That is, $t - t_0 - t_p$ will be the same for all waves arriving at the same time. That portion of the phase of the return waves will be the same for all of them. However, the distance the waves traveled will be different since the value of dx will be different for each scattered wave. Since the phase is determined by both the time of flight and the distance, the waves received at the same time from different distances will have different phases. Depending on the specific phase (a specific distance) the waves will interfere.

Dubinsky, et al [29,42] have performed an analysis of the currents on the detector caused by the return signal and concluded that although the waves themselves don't interfere, the AM component does. The result is that in the presence of scatterers the AM signal is diminished. He performs an experiment with a single tone FM signal scattered at different distances from the detector to show the following result.

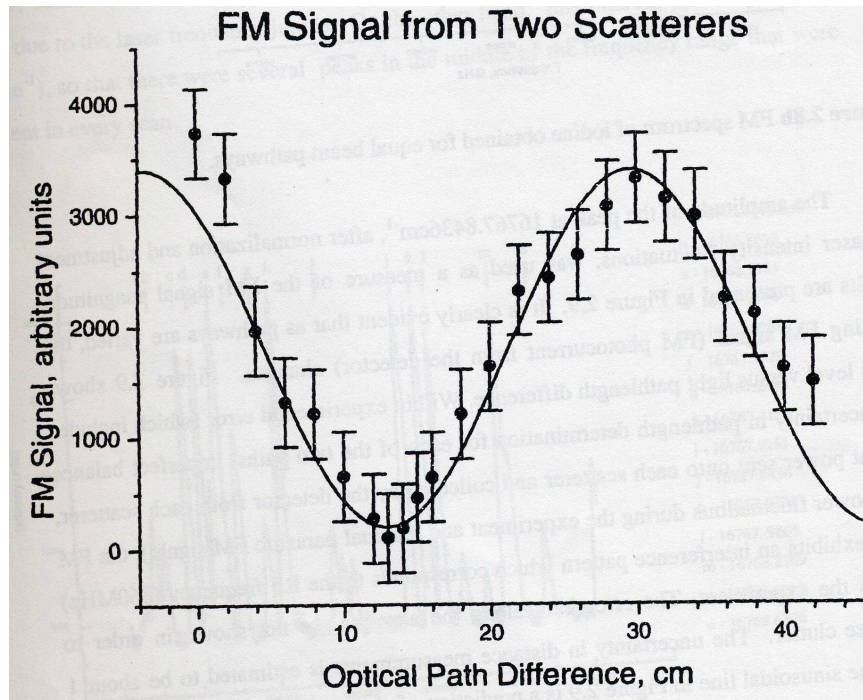


Figure 5.2. Dubinsky FM signal from Two Scatterers [36]

The single tone FM signal is passed through an absorber to attenuate one sideband. The resulting laser signal is directed at two scatterers. One scatterer is kept fixed while the other is moved. They combine on a detector and the magnitude of the detector output is plotted against the optical path difference between the signals. This process is repeated for various optical path distances and plotted. The result is a plot showing the variation of the detector current as a result of the interference between the two scattered waves.

Dubinsky's concludes from his analysis and experiment that the AM part of the FM signal will exist in the return only when the light pulse is still entering a cloud. Once the light pulse is completely in the cloud, the return signal will average out to a dc value. The cloud is a region of absorption and scattering. His analysis focuses on the existence of discrete areas of scattering (the clouds) and no scattering outside those areas. His results

show that the phase of the returning waves effect the resulting detector current. However, for a general remote sensing experiment the concept of a cloud is not an appropriate distinction. Scattering will occur over the entire path of the light pulse. In order to determine the feasibility of FM remote sensing, the effects of this scattering and subsequent combination of the different phased waves at the detector will have to be determined in greater detail. That is the aim of this section.

5.3. Lossless, equally spaced scatterers

The simplest case is a serious of equally spaced scatterers without loss due to atmospheric effects or r^2 losses. The equally spaced scatterers result in return waves with equally spaced phases due to the travel distance. Without loss each return wave has the same amplitude. More complex cases will be treated after this simple one.

A single tone FM laser source with an FM modulation index of 0.1 produces the following spectrum.

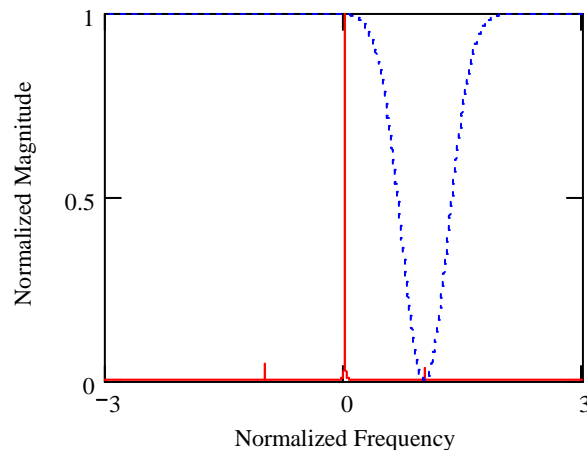


Figure 5.3. Source and Absorption

The magnitude has been normalized to the carrier. The frequency has been normalized such that the carrier is zero frequency and the sidebands are one.

Superimposed on the source spectrum is the absorption feature profile. The absorption is modeled as a Gaussian centered on the higher sideband.

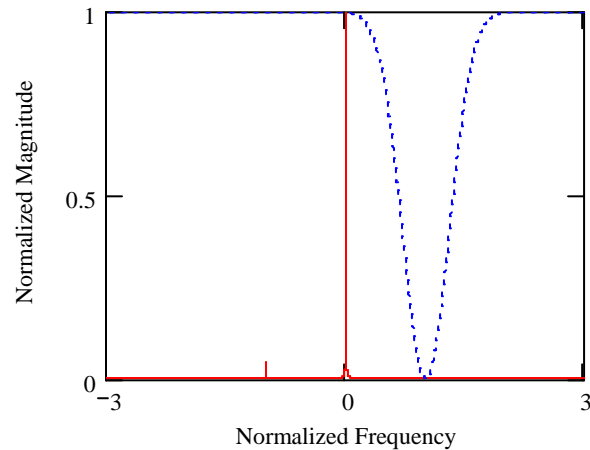


Figure 5.4. Sideband Absorption

The absorption of the higher sideband results in the attenuation of the sideband which unbalances the FM signal causing the generation of AM signals at the frequency of the sideband modulation frequency.

The return laser light hits the detector and is converted into a current. The detector doesn't have the bandwidth to detect the frequency of the light itself. If no AM were on the return signal, the detector would produce only an unvarying (dc) current dependent on the intensity of the return. The AM signal, however, is within the bandwidth of the detector and results in a current at that signal proportional to the signal on the return light. So the output of the detector is a dc current proportional to the intensity of the return signal and an ac current proportional to the AM modulation on the return signal. The

inverse Fourier transform current spectrum results in the following time domain plot of the resulting current.

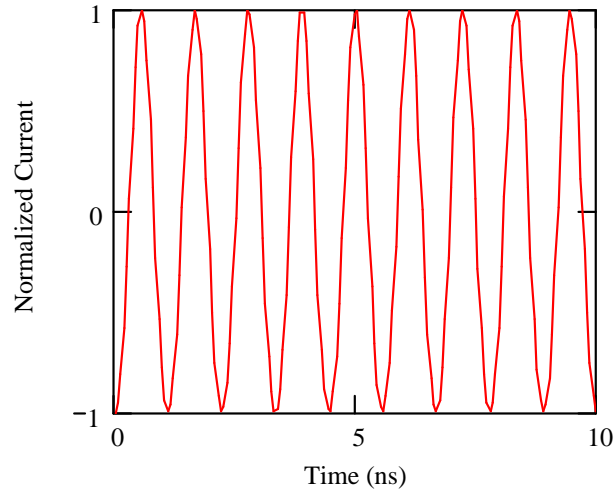


Figure 5.5. Return current in time domain

The normalized current has been plotted against time. The single tone FM modulation frequency for this example is 900MHz.

This return current is for one wavefront returning from one scattering point in the atmosphere. Each wavefront will arrive with a different phase due to its different travel time through the atmosphere. Since this case is for lossless scattering, it is as if the waves impinge upon mirrors in the atmosphere that reflect all energy in that wave back to the detector. An example of this is given in the plot below. The plot shows three different detector currents with three different relative phases due to the different distances traveled by the waves before reaching the detector. At any given time they will add to a value dependent on the phase difference between them.

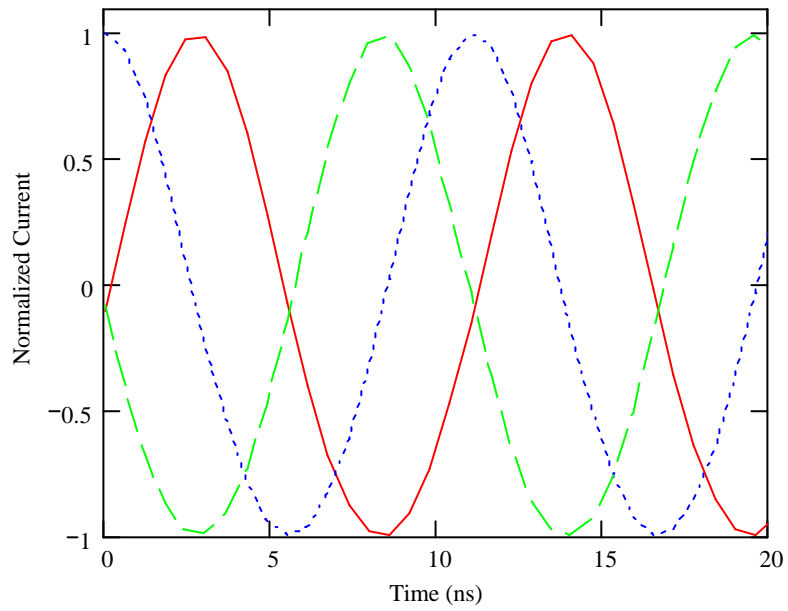


Figure 5.6 Detector currents of different phases versus time

The diagram below illustrates the physical model behind this plot.

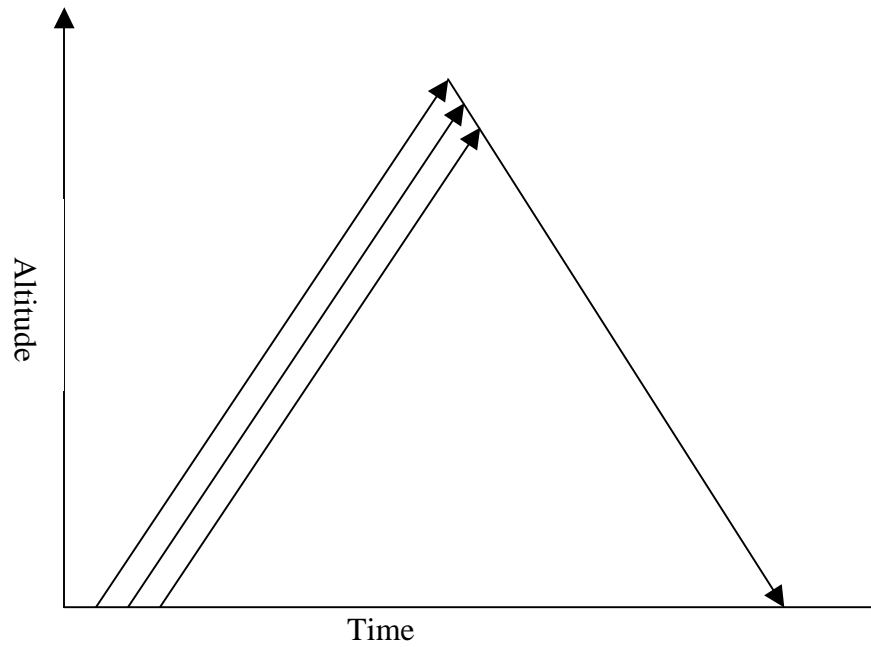


Figure 5.7. Time-Distance diagram

Each wave is emitted at a different time by the laser. The earlier ones travel farther than the later ones so that they all arrive at the detector at the same time. The scatterers are equal distances apart. The waveform plot is what you would see at the detector if the individual waves could be separated. However, they will actually add together.

In the next plot the return signal plotted is summed over 1 (no sum), 2 and 3 scattered returns in the following plot. Each summation contains waves equally spaced in phase over a period equal to the period of the modulation frequency.

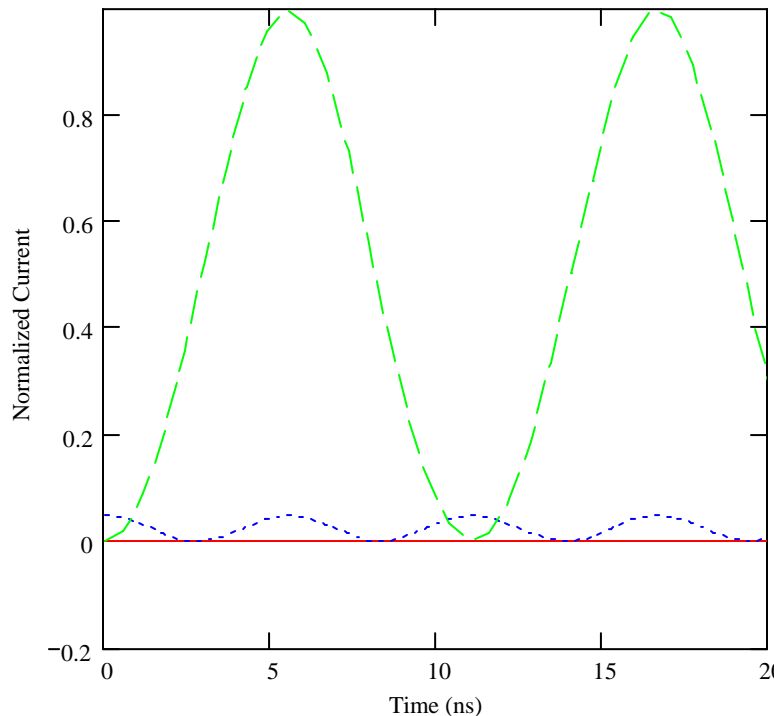


Figure 5.8. Summation of return

The drop in the level of the modulation with increasing number of scatterers is clearly visible. After 2 sums, the signal has dropped to zero. After 3 the signal is very small relative to the single wave case.

Assuming each return is due to one scatterer and those scatterers are equally

distributed in space, the linear density of scatterers this represents can be calculated. In this particular case the frequency is 900MHz. That represents a reasonable value for a single tone modulation frequency. The period of that signal is 1.1 ns. This corresponds to a travel time for the wave of $\frac{1}{2} (c)$ (1.1 ns) or 0.17 meters. So the sums can be expressed as 1, 2 and 3 reflections over 0.17 meters. These correspond to linear scattering densities of 6/m, 12/m, 3/m and 24/m. This is a low density of scatterers. It indicates that the loss of signal due to interference is a problem even at low densities.

In general, for M scatterers in a single period T of the single tone signal of frequency f the linear density of scatterers is:

$$\rho_l = \frac{M}{\frac{1}{2}cT} = \frac{Mf}{\frac{1}{2}c} \quad (5.3)$$

Increasing the frequency of the single tone signal, f, increases the number of scatterers within a period of the wave and generally reduces the AM detector current. Increasing M increases the linear density of scatterers and generally reduces the AM detector current. Increasing either M or f has the effect of increasing the relative density of scatterers per period of the single tone signal which causes the signal to decrease.

However, this decrease is not monotonic. As the number of scatterers per period increases, some of the scattered waves may add constructively and some destructively. Even if a uniform distribution of scatterers is assumed the resulting detector current has jumps and dips due to constructive and destructive interference.

For the general case of waves at many different phase differences, the summation of the return is dependent on the phase differences between the returning waves and how many waves of each phase sum. If the phase difference is a multiple of 2π then the waves

add constructively to an amplitude equal to the number of waves times the amplitude of one. For other phases the summation is more complicated depending on what that phase is and how many waves are summed. Since the phase difference between the waves is directly proportional to the different distances they have traveled, we can plot the current on the detector against this distance induced phase difference.

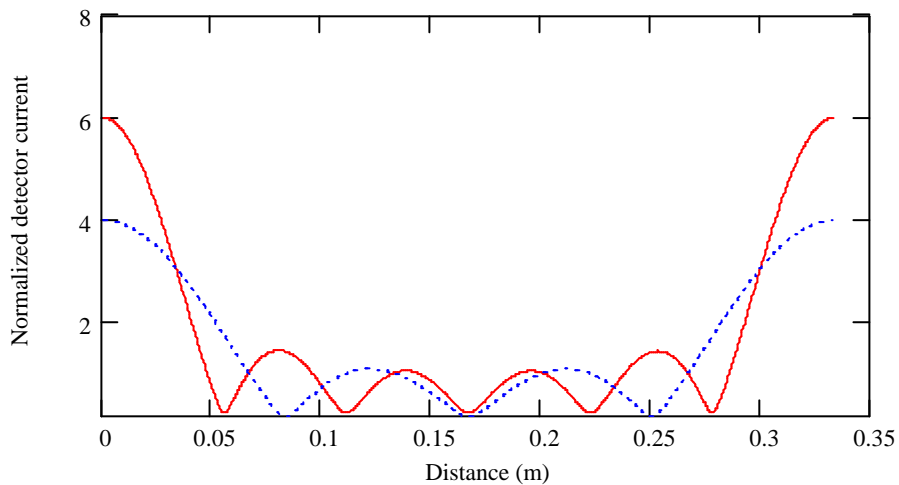


Figure 5.9. Detector current vs. distance induced phase difference of return waves

The plots are normalized to the case of no summing of waves. The curve with six peaks that reaches a normalized level of six is for six sums of equidistant waves. The other curve is for four sums of equidistant waves.

The x-axis represents the phase difference between successive waves received at the detector. The phase difference has been converted to the corresponding distance

$(\frac{\Delta\phi \times c}{2\pi \times \Delta f})$ between the scatterers. So, for example, if the scatterers are 0.1 m apart and there are six of them, the six waves scattered from them will reach the detector and add to the value shown by the red line above 0.1 m on the x-axis.

From this plot we can see that as the distance between scatterers changes, the phases

change and the sum of the waves produces different current amplitudes on the detector. When the phase difference due to distance is a multiple of 2π the waves add constructively and the resultant current is maximum. For all other phase differences the current is lower than this value.

The interference pattern shown on this plot of the AM components follows the basic pattern of the interference of a number of waves of equal amplitudes and equal phase differences. It can be represented in closed form by the general equation describing this type of interference [37]:

$$I(M, \varphi) = I_0 \sqrt{\frac{\sin^2\left(\frac{M\varphi}{2}\right)}{\sin^2\left(\frac{\varphi}{2}\right)}} \quad (5.4)$$

The parameters in this equation are the current, I , the phase difference between waves, φ , and the number of waves added, M . If the phase and M terms are expressed in terms of FM remote sensing parameters, this equation can be used to model the detector current as a function of the distance (or time) traveled by each wave and number of waves return to the detector. The expression for the phase is dependent on the distance or time traveled as follows.

$$\varphi = \frac{2\pi\omega}{c}d = 2\pi\omega t \quad (5.5)$$

M is equal to the number of waves scattered back to the detector. I and I_0 are the current and current for one wave (no interference), respectively. In the plots above M is 4 and 6. So the maximum level, which occurs at phase differences of $n\pi$ (n an integer), is four times and six times the current that would be detected for no summation.

This establishes the important result that the AM detector currents will interfere depending on the phase characteristics, and therefore the distance between scatterers, for each wave arriving at the detector at a given time. The total detector current will depend on the number of scatterers, the distance between the scatterers (which determines the distance traveled for a given wave and its phase relative to the other waves) and the frequency of the single tone signal. If it were somehow possible to fix the scatterers such that they were all lined up at equal distances from each other, the return level would depend on the phase difference between successive waves as shown in the plot above. The absorption level would cause the plot to move up and down as the absorption changed. It would be possible then, assuming the scatterers were arranged in such a way that the nulls were avoided, to measure the absorption by observing the detector currents. An example of this is plotted below for absorptions of 1 and 0.5. The magnitude of the detector current is linearly related to the absorption except at the null points.

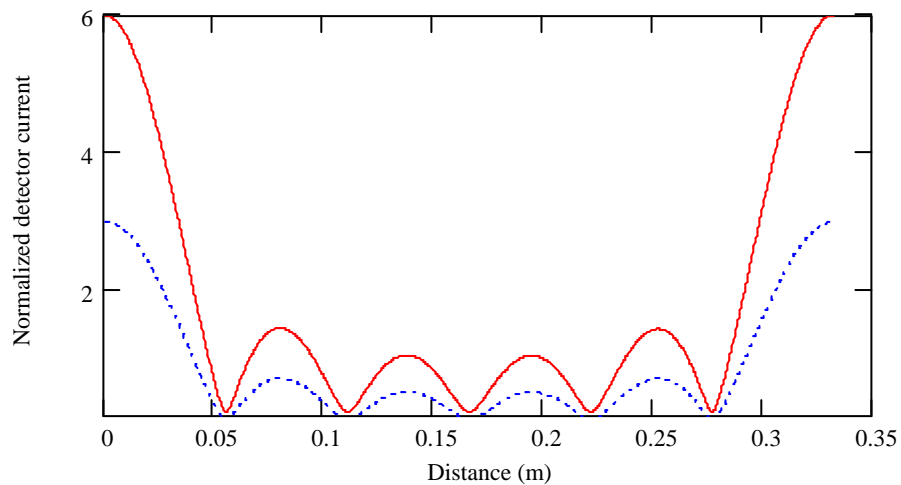


Figure 5.10. Interference of return currents for absorptions of 1 and 0.5

In any practical atmospheric sensing system, however, the number and location of

scatterers isn't fixed by the experimenter. In addition, the number and location would vary with time. The result is a detector current magnitude that varies as the number and location of the scatterers varies. As the scatterers move, the distances between them change and a new position on the x-axis is established. Therefore, the effect of scatterer movement on the plot above is movement along the x-axis. As the scatterers move, the signal level rises and falls depending on the differential distance between them. Since the movement is random, the result is a signal level variation from zero to the maximum value determined by the relative distances of the scatterers. An experimenter looking at a detector current will observe a large variation in signal over time as the scatterers move about. Without knowing the number and location of the scatterers at any given time, the absorption information can't be extracted. Since the number and location of the scatterers is exactly what the experiment is trying to detect (the concentration) this would make the FM remote sensing technique difficult to use.

As the number of summations increases, the problem gets worse. For ten sums we get:

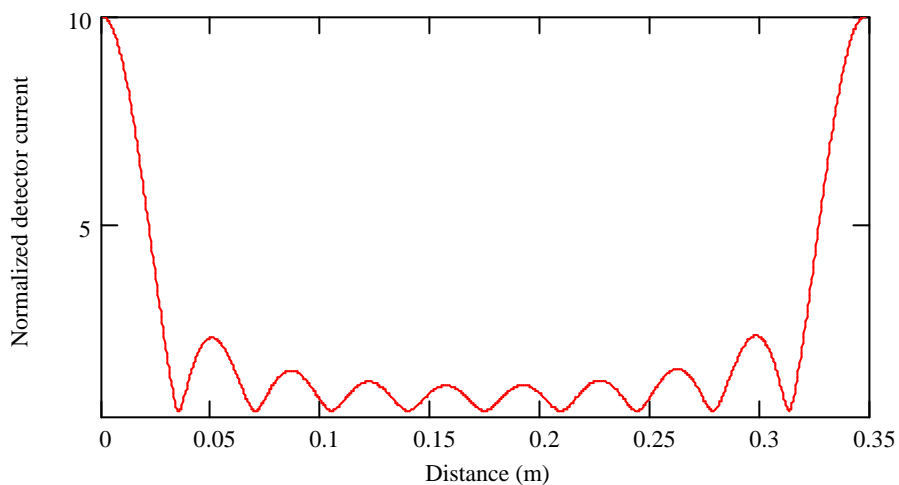


Figure 5.11. Interference of detector currents for summation of 10 waves

Comparing this to the plots with four and six summations, we can see that both the number of peaks and the height of the largest peaks increases proportionally to the number of summations. As a result there are more and sharper peaks. With more and sharper peaks the changes from one point on the plot to an adjacent point become larger. Since the x-axis represents scatterer position, the FM signal becomes more and more sensitive to the scatterer position as the number of scatterers (summations) increases.

Summing a large number of waves shows an extreme case of this below.

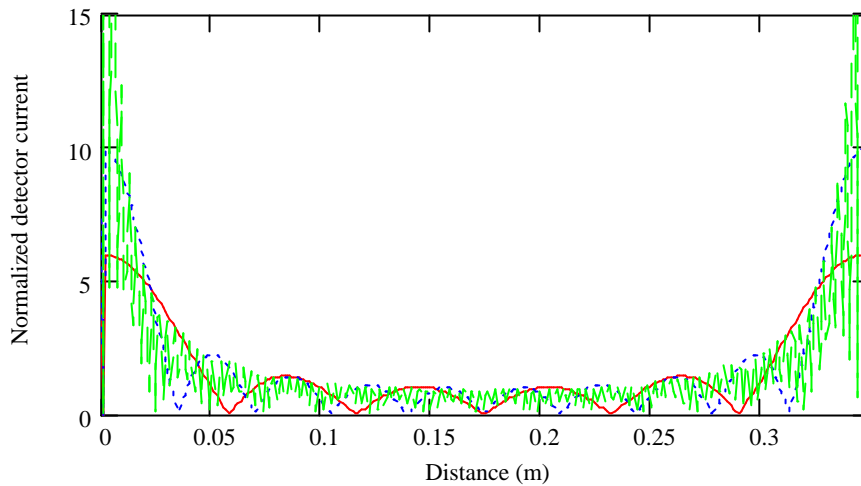


Figure 5.12. Interference of detector current for 100 waves (1)

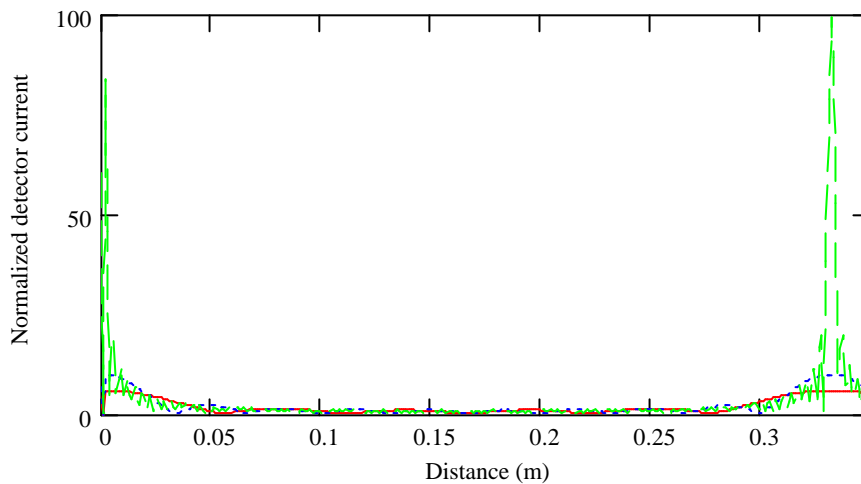


Figure 5.13. Interference of detector currents for 100 waves (2)

These plots are the return current for six, ten and one hundred summations. That is, for six, ten and one hundred equidistant scatterers. The difference between them is only the scale of the y-axis. On the upper one we can see that the difference between the highest and lowest points increases as the number of summations increases (the lower chart emphasizes this difference). The number of peaks also increases with increasing number of summations. The result is a large number of peaks with large slopes. At the maximum displayed here of one hundred scatterers, very slight movements of the scatterers would result in large variations in the signal intensity as you get near the peaks on the sides.

However, this is a simple case and the additional considerations involved in a more complex treatment have the potential to mitigate these limitations. Specifically, the returns are not all the same magnitude. Since they return from different points in the sky, they have different losses due to atmospheric attenuation and scattering loss. These losses are large, so the signals will have significantly different magnitudes when they arrive at

the detector. The resulting interference pattern will be dominated, therefore, by the waves coming from the closest points in the sky since they are the strongest. Thus, as the relative travel distances increase, the relative phase changes increase but the signal strength decreases. The result is that the summation of currents at the detector is weighted more heavily toward waves of similar phase. The result is a stronger FM component of the signal. In the next section this effect will be investigated.

5.4. Lossy, Equally Spaced Scatterers

For this case the scatterers will remain equally spaced, but the losses will not be neglected. An earlier section included a discussion of the losses experienced by laser signals traveling through the Martian atmosphere.

$$T_{all} = T_{1/r^2} + T_{\lambda} \quad (5.6)$$

The first term is the $1/r^2$ loss dependent on the distance from the scatterer to the detector and the cross section of the scatterer. The second is due to absorption at a particular wavelength. For an ideal FM system, the absorption loss is limited to the sideband that is tuned to or sweeps through the absorption feature. It is exponentially dependent on the distance traveled through the atmosphere and the strength of the absorption feature. For the short distances represented by a single period of a wave, the scattering losses will dominate. So over one wave period three waves equally spaced apart experience different scattering losses and return to the detector with different amplitudes.

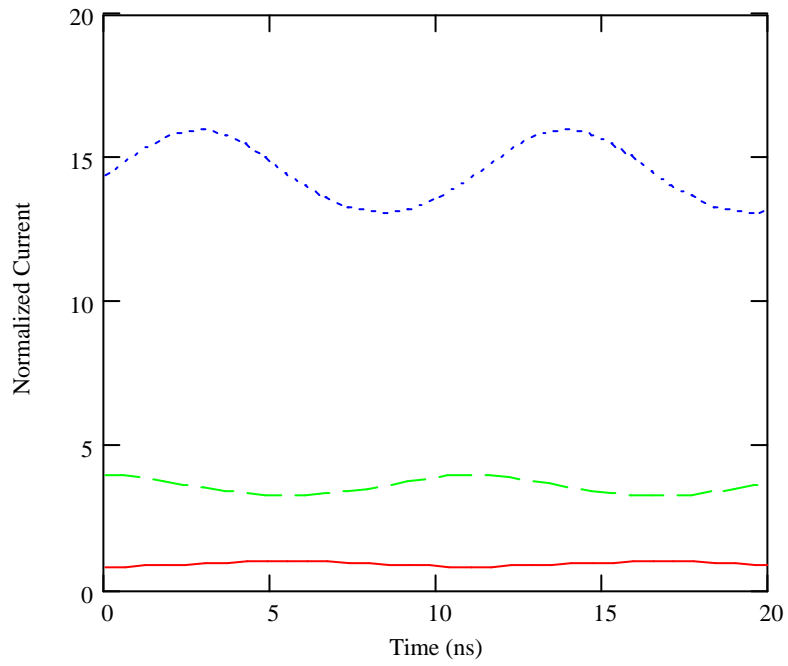


Figure 5.14. Return waveform including scattering loss

The waveforms have been displayed for loss increasing from top to bottom.

Summing these return waves at the detector gives the following plot.

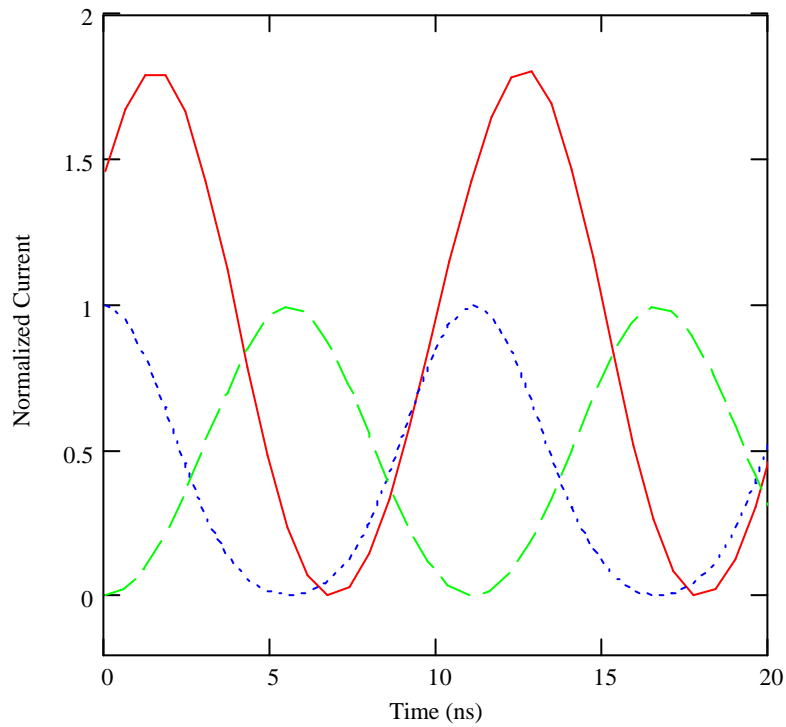


Figure 5.15. Return waveforms summed

This plot displays the same curves as the earlier one with loss. The largest signal has no summation. The next two are for two and three summations. Comparing this to the plot for lossless returns demonstrates how the loss has dramatically increased the magnitude of the current on the detector.

Plotting the current against distance induced phase change over distances similar to the period of the modulation frequency results in the following plot.

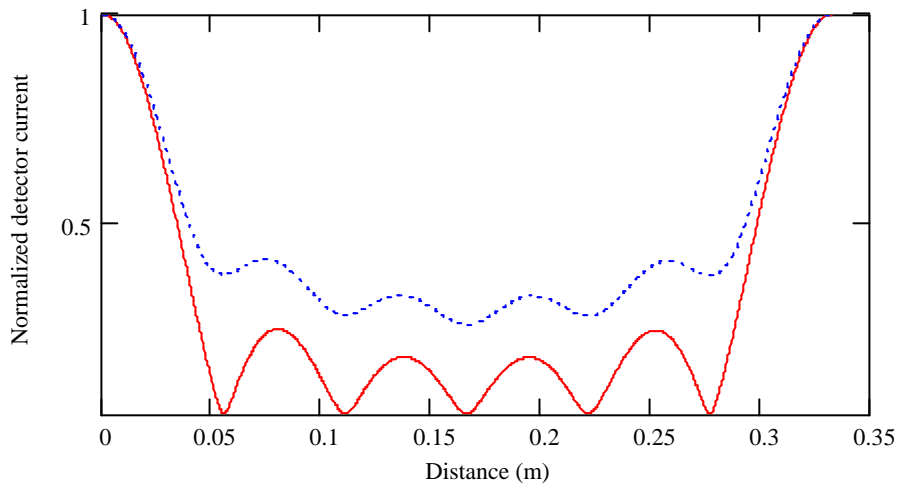


Figure 5.16. Detector current vs. distance induced phase difference

The solid line is the lossless example displayed earlier. The dotted line is the same case with losses included. The signal with loss is less affected by interference than the signal without loss.

The reason for the better result with loss is that both loss and phase are dependent on the distance to the scatterer. The result is that waves coming from a given scatterer have both the same loss and the same phase. Waves coming from farther away have a different phase, and therefore will interfere with the first set of waves, but they also have a lower magnitude. So when they interfere the effect is less than if there was no loss. The interference is less, so the FM signal is better preserved. The nulls have been eliminated and the signal level raised for all scattering distance differences. In the case for no loss, moving scatterers had the effect of moving along the x-axis, causing the signal to vary. Here the moving scatterers still cause movement along the x-axis, but the variation is much less. In particular, the nodes are gone.

However, this plot only is good for short distances. The span of the plot above

corresponds to the distance the wave travels in one period of the single tone modulation frequency, about 0.3 meters for the 900 MHz frequency. This is the appropriate scale to illustrate phase effects since the plot will repeat for distances greater than that. The period of the modulation frequency is what matters as far as the phase properties of the return go. However, using this distance scale results in a plot that is only valid for short distances. As the distance to the scatterer increases, the distance corresponding to the period of the modulation signal becomes small in comparison. At a distance of 150 meters, the effect of the phase difference is negligible. The plot below shows this.

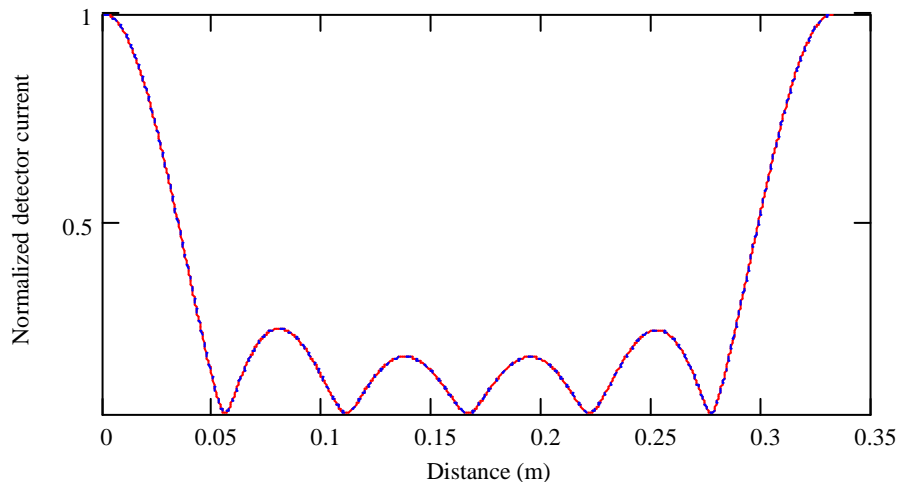


Figure 5.17. Detector current vs. distance induced phase difference at 150 meters

The traces in this plot fall on top of each other. The longer distance, more representative of a practical implementation, has eliminated the improvement in the signal seen in the preceding plot of the lossless versus lossy cases.

For ease of comparison, the above plot normalizes the return lossless or lossy detector current to the respective maximum of the return, lossless or lossy. As a result, the lower overall signal level of the lossy case is normalized out. In the following plot, the normalization is done with respect to the lossy case for both lossy and lossless return detector currents.

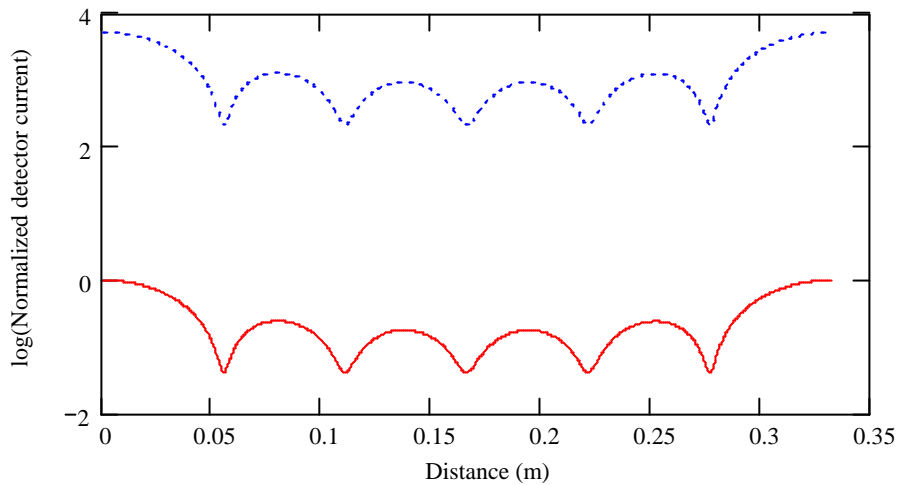


Figure 5.18. Detector current vs. distance induced phase difference at
150 meters (log scale)

This is the same plot as the one above, but now normalized to the same baseline, the lossy case. In this plot the log of the detector current is displayed to better show the large difference in magnitude between the two curves. The top curve is the lossless case. The bottom curve is the lossy one assuming a distance of 150 meters from source to scatterers. We can see that the losses the signal experiences are quite large. For 150 meters of distance the signal drops by almost four orders of magnitude. From this and the previous plot it can be concluded that the addition of losses, a more realistic case than the

lossless one, still doesn't improve the situation if the distances of a real experiment are taken into account.

5.5. Two Tone Results: Lossy, Equally Spaced Scatterers

The analysis just done for single tone FM remote sensing with regard to phase differences caused by flight distance differences can be performed for two tone FM as well. The analysis follows the same pattern as single tone. The final result is the plot of magnitude against distance that was originally generated for single tone.

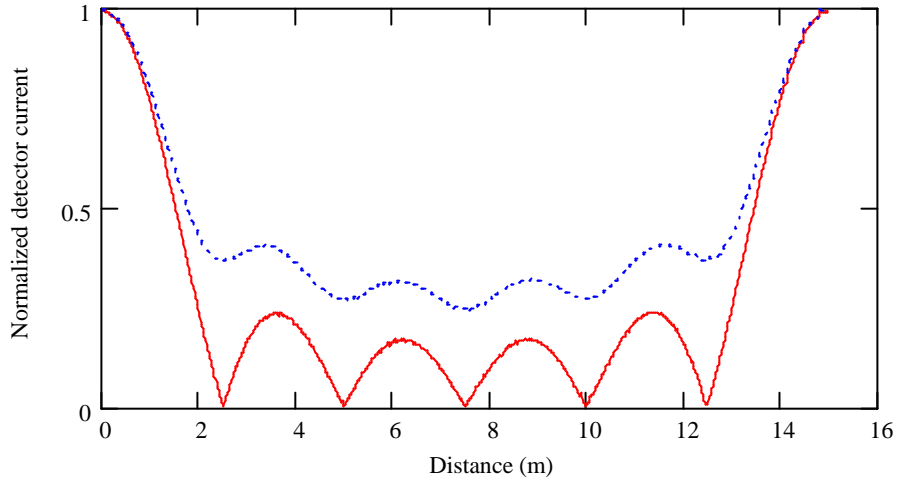


Figure 5.19. Current vs. distance induced phase difference, two tone

Again, the solid line is the result without loss, the dotted line with loss. The result is the same as for single tone FM. The signal exhibits interference effects due to the phase differences the waves develop as they travel different distances through the atmosphere. The losses matter again, but only at the short distances shown on this plot. At longer distances the signals are the same as shown in the following plots.

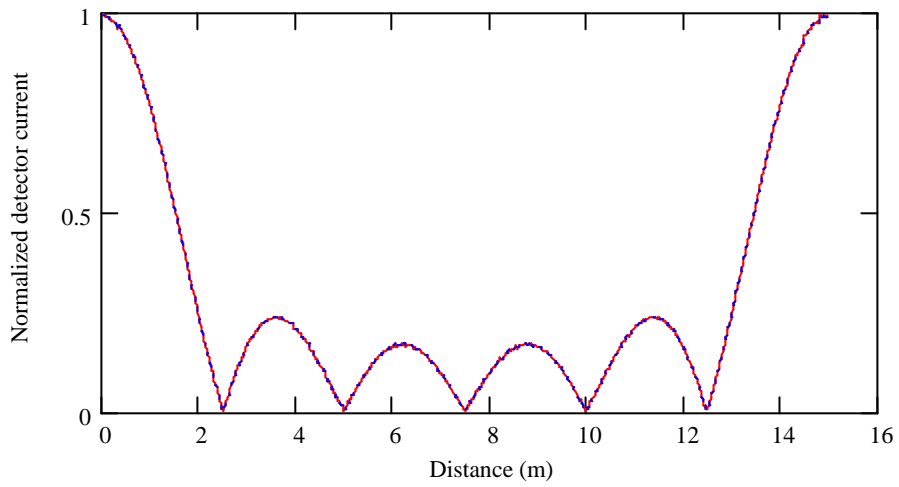


Figure 5.20. Detector current vs. distance induced phase difference at 150 meters

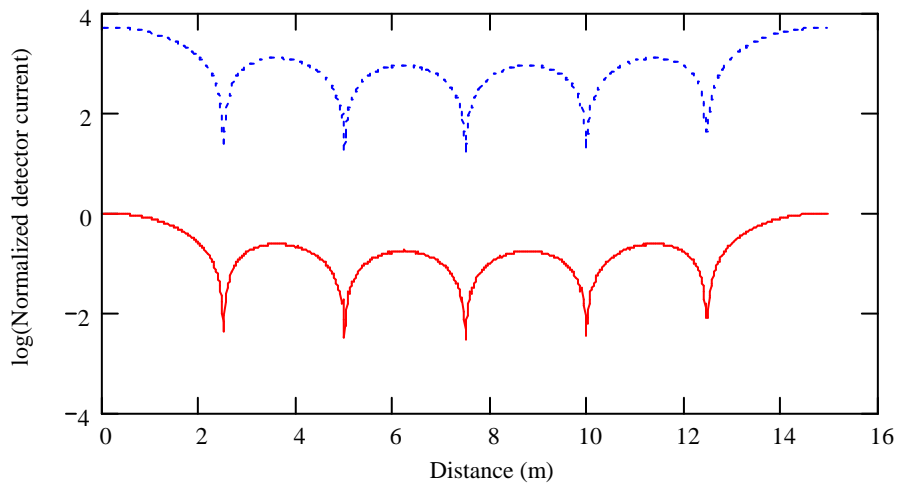


Figure 5.21. Detector current vs. distance induced phase difference at 150 meters (log scale)

The results for two tone are the same as for single tone. The improvement in the lossy case is only over short distances. Over distances corresponding to a practical FM remote

sensing experiment the improvement goes away.

There is one difference between single tone and two tone. The frequency of the single tone modulation frequency is 900 MHz. The two tone modulation frequency is 20 MHz. The result is that the distance over which the interference effects repeat, is larger for the two tone FM technique. It is thus easier to detect the FM signal on the detector current for a two tone than a single tone frequency. The peaks are further apart.

5.6. Summary

It is important to the use of FM in remote sensing to establish under what conditions the return signal will retain the phase characteristics necessary to measure atmospheric constituents. The question is to what extent the waves reaching the detector after being scattered in the atmosphere will constructively add. If the phase information is lost the FM technique won't work in a remote sensing environment. This section starts with a description of the phase characteristics of a laboratory FM setting, where the phases of the detected signal are known to add constructively, and builds on that to show that the AM signal on an FM modulated source, caused by selective absorption of a sideband, will interfere at the detector due to the different distances the waves have traveled. Both the analytic and numerical model of the FM remote sensing process are used to establish this result.

Looking at only the lossless case, it can be concluded that summing the return waves will result in the loss of the amplitude modulation on the return and, therefore, the loss of the atmospheric data, thus making the FM remote sensing technique difficult to use. Further investigation into a more realistic lossy case shows that the addition of those

losses doesn't help the situation. These results indicate that the use of FM remote sensing that relies on atmospheric scattering is severely limited due to these phase effects.

In the next section the model will be compared to experimental data from the literature as well as an experiment conducted by the author. This will establish the models validity and will allow the progression to a discussion of how FM remote sensing can be used that avoids the phase effects.

6. Experiment Description and Results

6.1. Introduction

The last section established the limitations of the FM Remote Sensing system based on a scattered return. These limitations are based on the reduction of the signal at the detector due to the phase differences of the returning waves. In this section the model will be validated by comparing its predictions to previous published results as well as to a new experiment conducted by the author.

6.2. Comparison to Previously Published Experimental Data

Dubinsky's data presented earlier in this section can be used to verify the model. Dubinsky scattered light off of two targets and varied the pathlength between one of them and the detector. By doing so he was able to measure the resulting detector current due to the reception of waves from different locations that had traveled different distances to get to the detector. His result showed that the waves interfere. The amplitude of the detector current depends on the pathlength.

The result we would expect can be calculated using the numerical model developed here. Calculating the current on the detector as a function of the optical path difference between the waves results in the following plot.

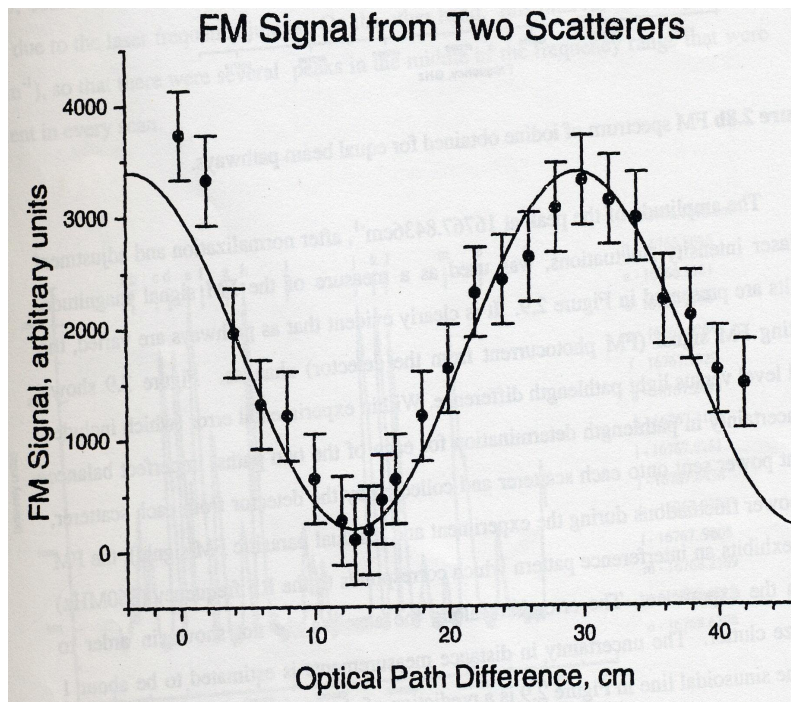
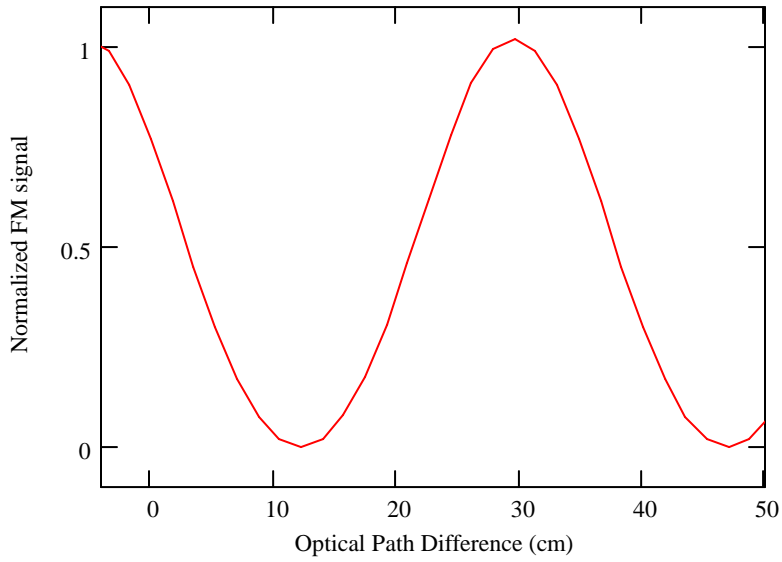


Figure 6.1. Computed FM signal from Two Scatterers (top) compared to Dubinsky's laboratory data (bottom)

If we compare the model result with Dubinsky's we see that the numerical model

correctly predicts this basic case of detector current due to two scatterers as a function of the relative pathlength between them and the detector.

6.3. Current Modulation Phase Experiment Introduction

The experiment conducted by the author and reported on in this section will expand upon the results above. This experiment is intended to explore the effects of phase on the RAM component of a current modulated semiconductor laser. The laboratory FM version of a current modulated system has been described in an earlier section of this paper. The advantages of such a system for spaceflight are significant. An external modulator is not required along with the high voltage power supply that is necessary to drive it. This saves mass and power. It also lowers the parts count and complexity of the system which increases its reliability, an important consideration on a mission to Mars. The design of the modulator itself is also a reliability concern. The need to keep the components on a spaceflight mission small and low mass drives the use of electro-optic modulators. These modulators are susceptible to failure during mechanical shock. Care must be taken to design the system so that the modulator can survive the shock environment of a spacecraft, which can be in the range of 2000 g's at the box level. For these reasons the behavior of a current modulated system will be explored further here.

The characteristic of a current modulated system that will be important to this experiment is the creation of Residual Amplitude Modulation (RAM). This is the amplitude modulation of the laser due to the direct modulation of the semiconductor laser power supply. This modulation of the laser input current produces both FM sidebands

and an AM signal. This AM signal, called Residual AM (RAM), is a noise source for an FM sensing technique. In this experiment, the characteristics of the RAM signal as a result of phase addition will be investigated. It will be determined that the RAM signal exhibits the same phase effects as the AM signal due to the absorption. The model accurately predicts this value.

6.4. Experiment Description and Preliminary Measurements

6.4.1. Setup

A general block diagram of the laboratory setup is show below.

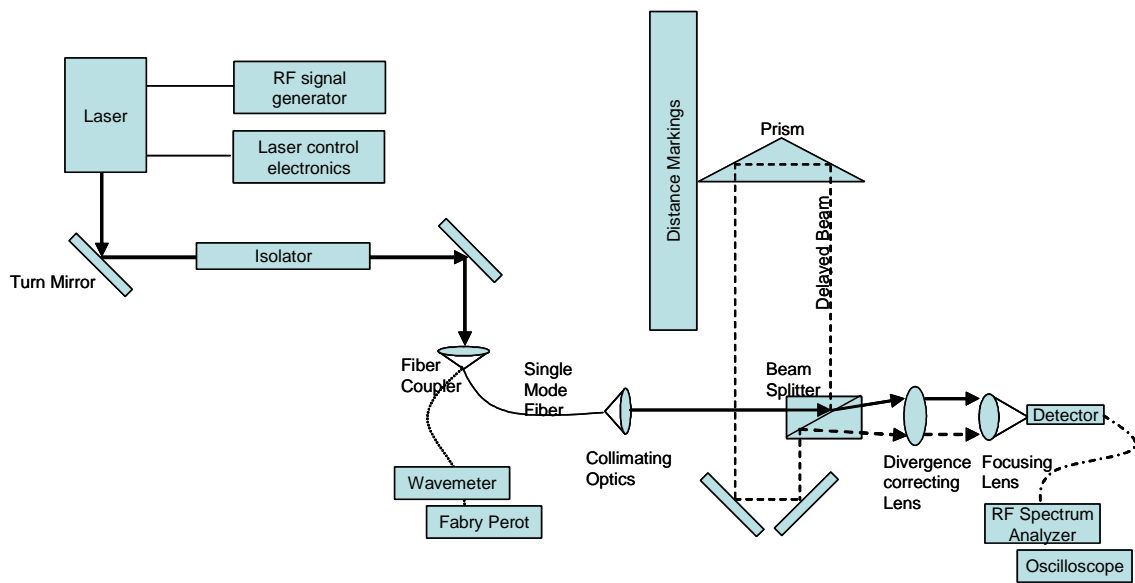


Figure 6.2. Experiment Block Diagram

The laser temperature and current control are in the laser control electronics. The laser current is modulated by the RF signal generator through a bias-T contained within the laser itself. The light output of the laser is reflected off of a turn mirror and passes through the isolator. The turn mirror is used to align the laser beam to the isolator while

the isolator prevents back reflections from the optical components from affecting the stability of the laser. Without it the laser will oscillate at two frequencies determined by the laser cavity size as well as the extended cavity size determined by the external optical components. The second turn mirror is used to align the output of the isolator to the fiber coupler. The light is coupled into a single mode fiber. It is then directed into a wavemeter and the control electronics power and temperature controls used to adjust the frequency to the required 935.686nm. After that the fiber can be connected to a scanning fiber Fabry Perot device that shows the finer structure of the laser, down to around 20 MHz. The fiber Fabry Perot is used to view the sidebands in greater detail than is possible with the wavemeter. It also is used to measure the linewidth of the laser.

After making these measurements, the output of the fiber is connected to the collimating optics. The collimated light is divided by a beam splitter into two parts. One part travels through to the optics on the other side. The other part is delayed using a prism and turn mirrors and brought back to the beamsplitter. The two beams, the original and the delayed, exit the beam splitter on slightly divergent paths. The first lens brings them to parallel paths and the second to focus together on the detector. The detector output can be monitored by an oscilloscope or RF spectrum analyzer to measure the power at the detector as a function of the delayed beam distance.

The first photo below is of the laser (top left), first turn mirror (middle left) and isolator (middle right).

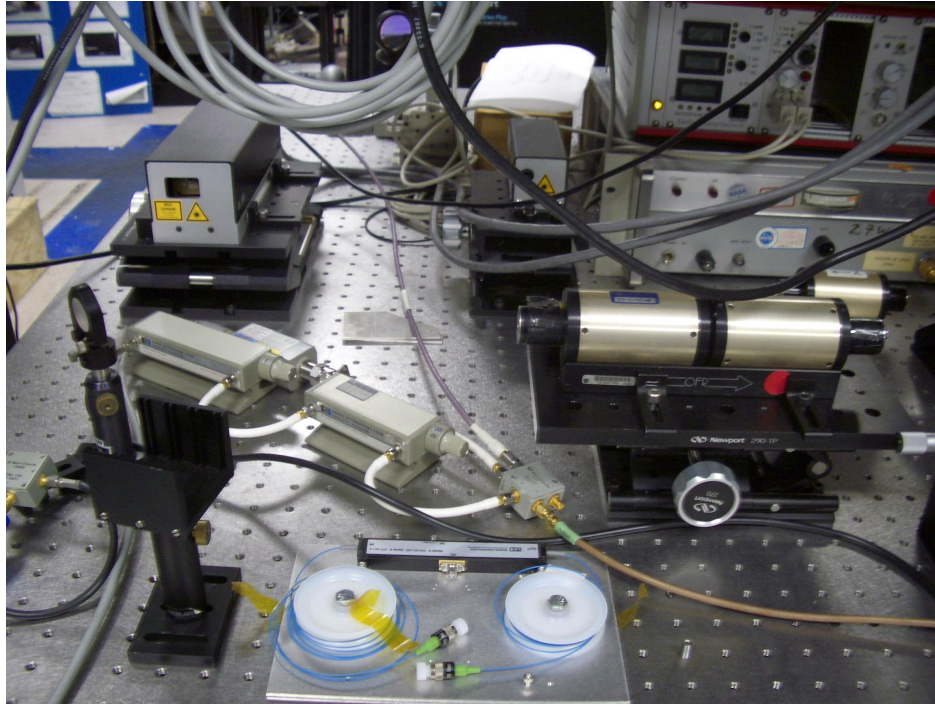


Figure 6.3. Laser and isolator

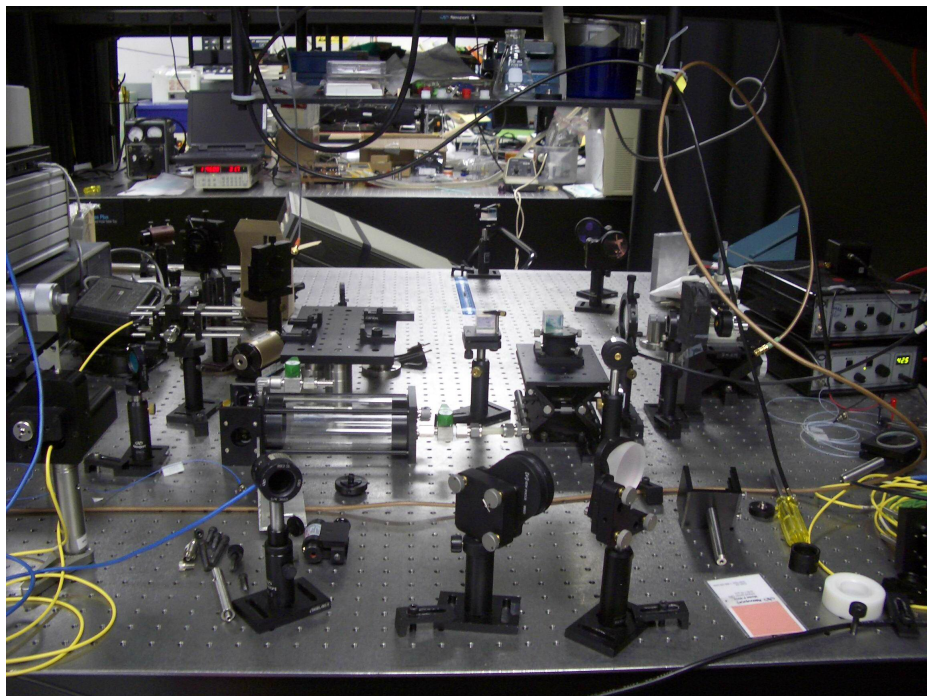


Figure 6.4. Beamsplitting, delay path and recombination

The bottom picture shows the fiber and collimating optics (left center), beamsplitter (center), prism (top center), the turn mirrors that direct the delayed signal (bottom center) and the divergence correcting lens (right of the beamsplitter), the focusing lens (to the right of that) and the detector (to the right of the focusing lens).

The following photograph shows the entire experiment.

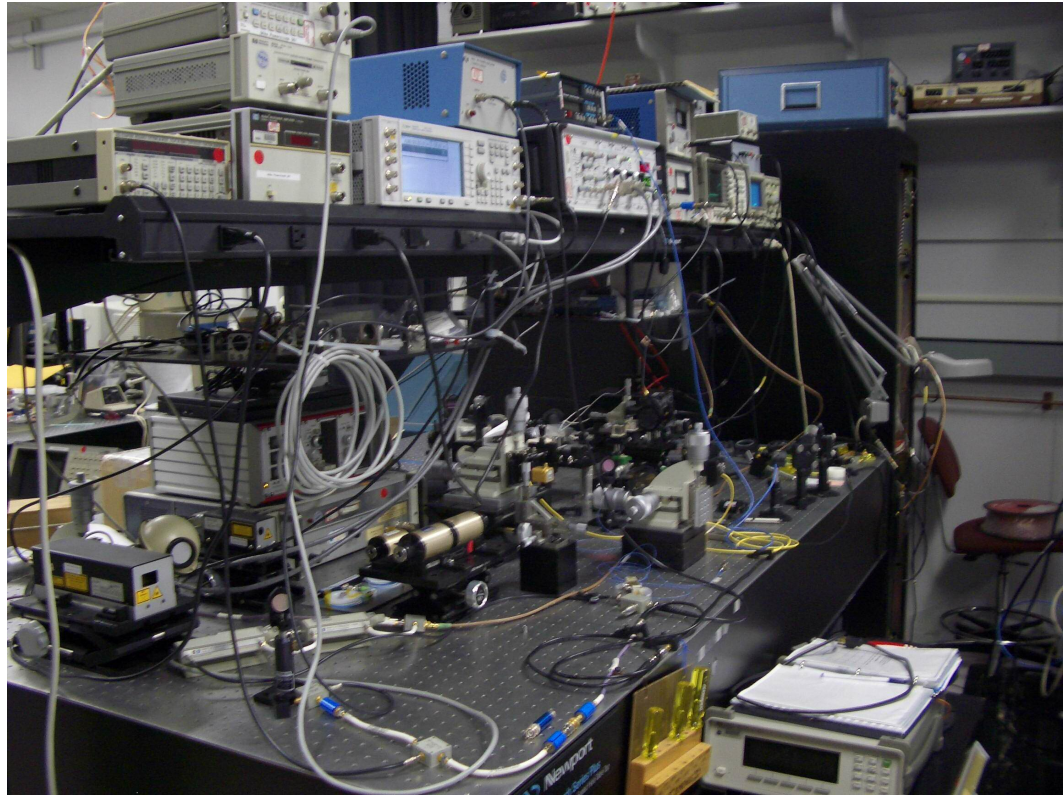


Figure 6.5. Entire Experimental Setup

6.4.2. *Laser Frequency Adjustment*

Semiconductor lasers at 935.68nm are hard to obtain. The one used for this experiment is an external cavity device from a company called TUI in Germany. It is no longer produced. To get it to oscillate at the required 935.68nm frequency requires adjustment of the internal grating position, the temperature and the current input into the

laser.

The single mode fiber output was connected to a HP Wavemeter. This device displays the wavelengths and power levels of the laser output. This process requires some time, but is straightforward. The internal grating position was first set, then the current and temperature were varied to get the laser as close to 935.68 as possible. The laser mode hopping complicated this effort. The frequency change between mode hops is on the order of 0.02 nm. It was often the case that temperature and current adjustments caused the laser mode to hop before reaching 935.68nm. This necessitated a few iterations of grating position adjustment along with further temperature and current adjustment to establish a stable, single linewidth at 935.68nm. This was obtained at 57mA and 21.6 degrees C. At this current, the laser output is about 6 mW of total optical power.

6.4.3. Linewidth Measurement

The next step taken was to measure the linewidth of the laser. This is necessary to make certain that the modulation frequency used is sufficient to keep the sideband away from the center frequency of the laser. The method used was to feed the single mode fiber input into the Micron Optics Fiber Fabry Perot device. This device consists of a Fabry Perot cavity which can be scanned over frequency using the controller electronics. The cavity can be changed out to allow for different laser frequencies, free spectral ranges and bandwidths. The cavity used for this experiment has a maximum free spectral range of 10GHz and a bandwidth of 20 MHz. It was purchased for use at 935 nm, but the manufacturer didn't have a 935nm source, so it was calibrated at 1064nm. As a result, the linewidth of the laser determined using this device isn't exact. However, it will determine

the bandwidth to the extent necessary to ensure that the modulation is away from the center frequency.

The Micron Optics controller is easiest to use in conjunction with a variable intensity analog oscilloscope to display the Fabry Perot output. This makes it inconvenient to get the data in digital form with a computer, so a digital camera was used to take a photograph of the screen. The following is a photograph of the oscilloscope output while the cavity is scanning the laser line.

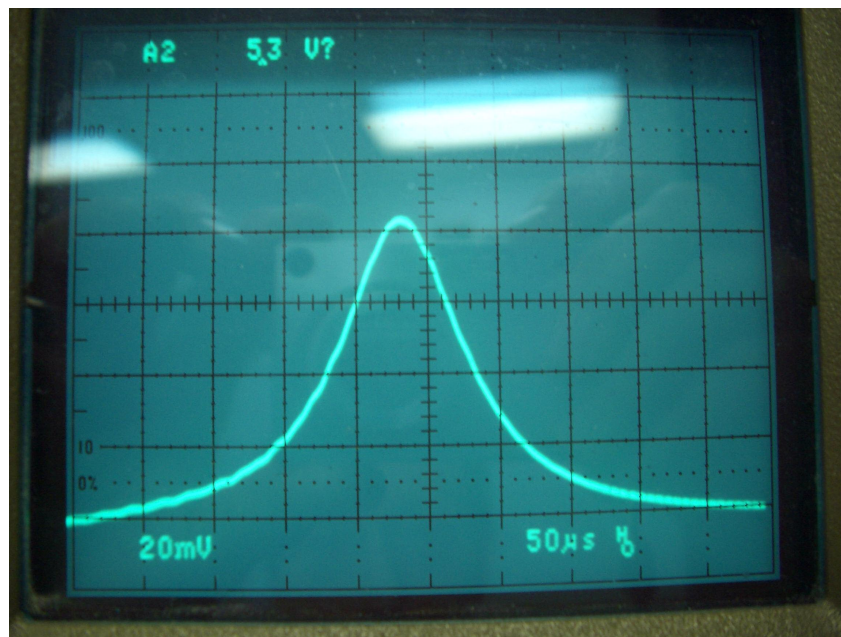


Figure 6.6. Laser linewidth

The time axis was calibrated by applying a series of known modulation frequencies to the laser modulation port using an Agilent 4437B RF signal source. In this case the automatic scanning mode was set to scan from 100MHz to 1GHz in 100 MHz steps. From this it was determined that the conversion factor for frequency to scan time was about 660MHz per millisecond. The above photo shows a FWHM of the laser of 100

μs . Using the conversion factor the result is a linewidth of 66 MHz. With the uncertainties due to the calibration of the Fabry Perot at 1064nm, this measurement is likely limited by the Fabry Perot itself, rather than the laser. The laser is a TUI Littman-Metcalf external cavity laser specified at a few MHz linewidth. However, this measurement is sufficient to allow a determination of the modulation frequency. Based on a linewidth of at most 66 MHz, a modulation frequency greater than 100 MHz will be sufficient to stay away from the central peak.

6.4.4. Modulation Response of Laser vs Frequency

The next step determined the response of the laser to the modulation frequency as a function of the frequency. The purpose of this measurement is to determine the limits of the laser modulation capability. This is necessary information so that a modulation frequency can be chosen that is within the capabilities of the laser.

The single mode fiber was connected to the collimation optics and the resulting collimated beam focused on the detector. The delayed path was blocked to remove that contributor to the signal at the detector. The RF power out of the detector was measured using a spectrum analyzer. The detector responsivity is 0.55 A/W at 935nm is used along with the 50ohm termination impedance to convert the RF power at the spectrum analyzer to the optical power at the detector.

The results are shown in the following plot for a 0 dBm RF modulating power into the laser bias-T port.

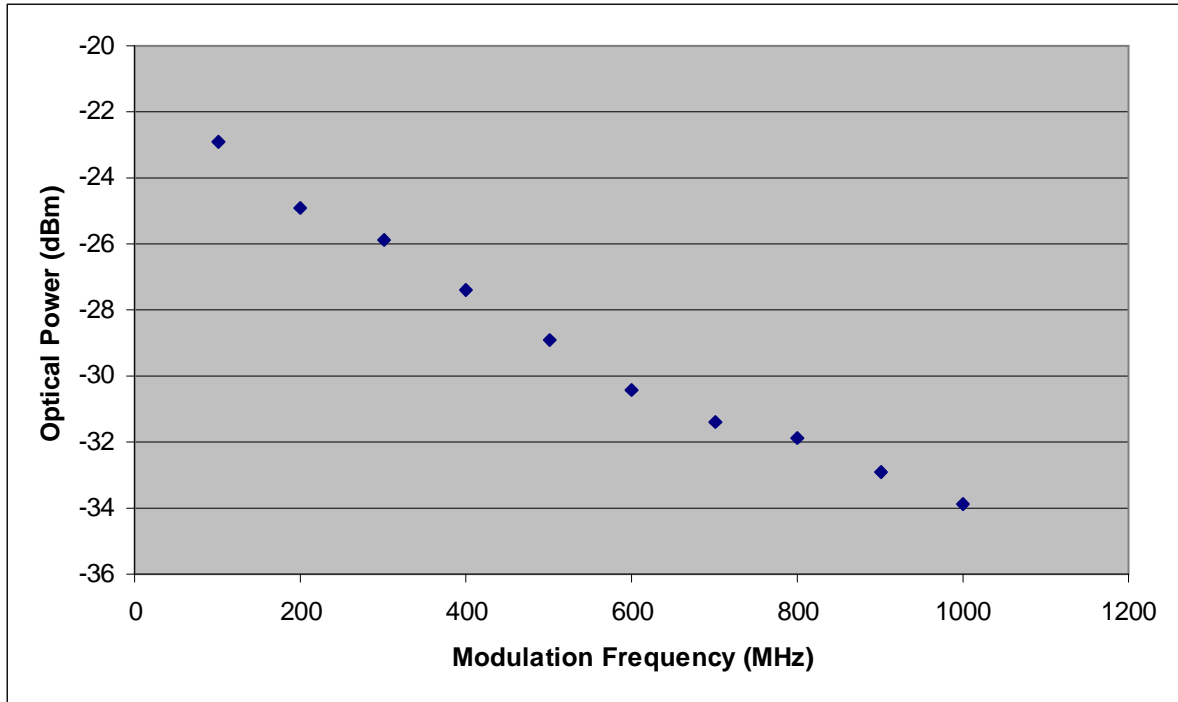


Figure 6.7. Optical power as a function of frequency

The optical power of the AM signal caused by the laser current modulation through the bias-T decreases as the frequency of the modulation increases. Given the linewidth of the laser is at maximum 66 MHz, this laser can easily meet the requirements for modulation at frequencies that allow for separation between the center peak and sidebands. This performance was actually unexpectedly good. Although the laser had been purchased specifying a modulation capability of up to 1GHz, the vendor had expressed some doubts as to whether it would perform to the frequency. It did.

6.4.5. Modulation Response of the Laser vs. Power

The next part of the experiment uses the same setup but varies the RF power input to the laser rather than the frequency. This will give information on the response of the

laser to RF modulation at the bias-T with respect to the RF power applied there at a given frequency. Three frequencies determined by the range in the previous plot will be used: 200MHz, 500MHz and 1GHz.

The result of these measurements is plotted below.

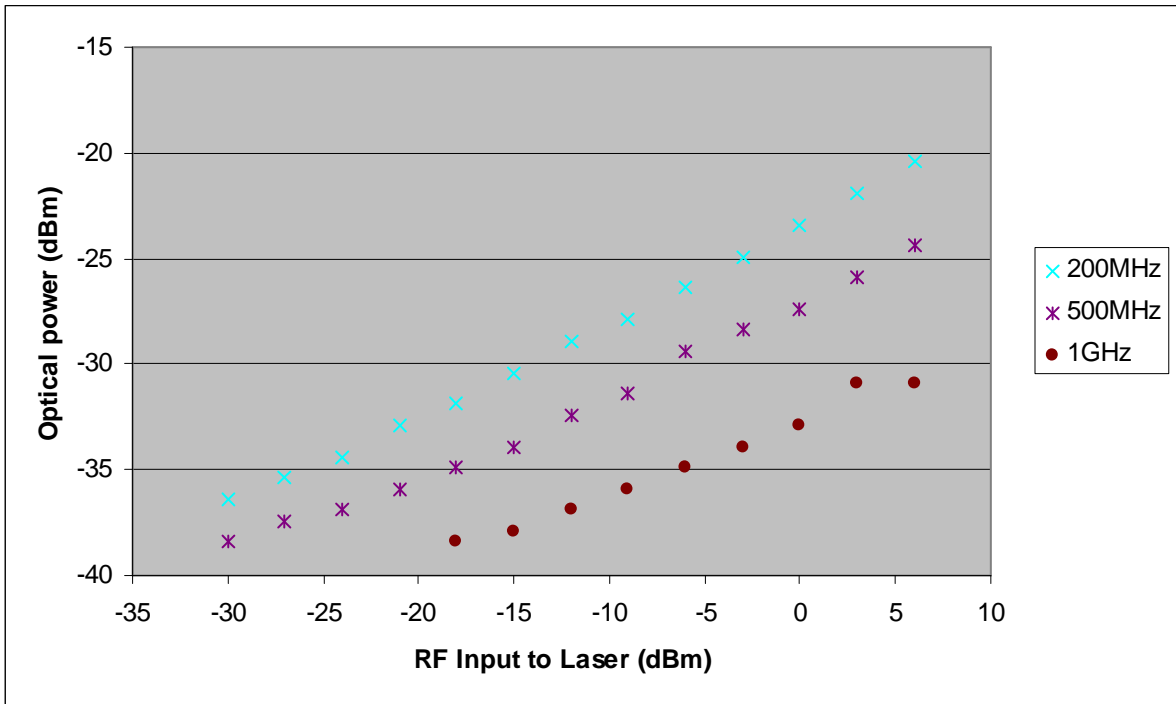


Figure 6.8. Optical power as a function of RF power

The RF modulation of the laser is more effective at lower frequencies. The optical power output at a given frequency is linear for decreasing ranges of input RF power as the frequency of modulation increases. At 200MHz the range is from -25dBm to +6dBm. At 500MHz it's -15dBm to +6dBm. At 1GHz the range starts at -15dBm but ends at 0dBm. Operation in the linear ranges will set limits to the RF input power levels that can be used depending on the frequency of operation required. A value of 0dBm falls in the

linear range of all and would maximize the modulation power for all these frequencies.

6.4.6. Summary of preliminary results

The results obtained so far define the limits of operation of the system that will be used in the following experiments. The laser temperature and power settings have been established that result in stable single frequency 935.68nm operation. The modulation characteristics of the laser have been determined as well. To keep the sidebands away from the center frequency but still generate reasonable optical power in the AM signal, a modulation frequency of 500 MHz at 0dBm will be used in the experiment that follows. These values were used to obtain the following photo of the Fabry Perot measured spectrum of the modulated laser beam. The sideband to the right of the center frequency can be clearly seen. The other sideband is off the trace.

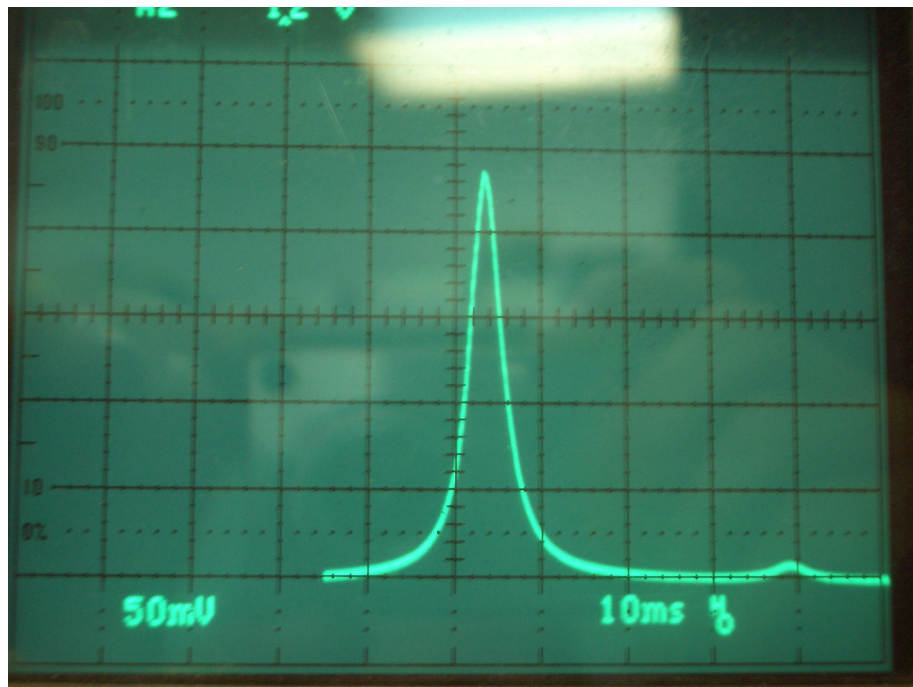


Figure 6.9. Modulated laser

6.5. Experiment Results

The prism was moved along the distance marker and the power at the detector measured. At one point during the experiment another detector was placed in the delayed beam to measure the phase difference relative to the other beam. The two waveforms were displayed on the oscilloscope. A photograph of this is displayed below. This clearly illustrates the phase difference that results from the differing travel distances of the two signals.

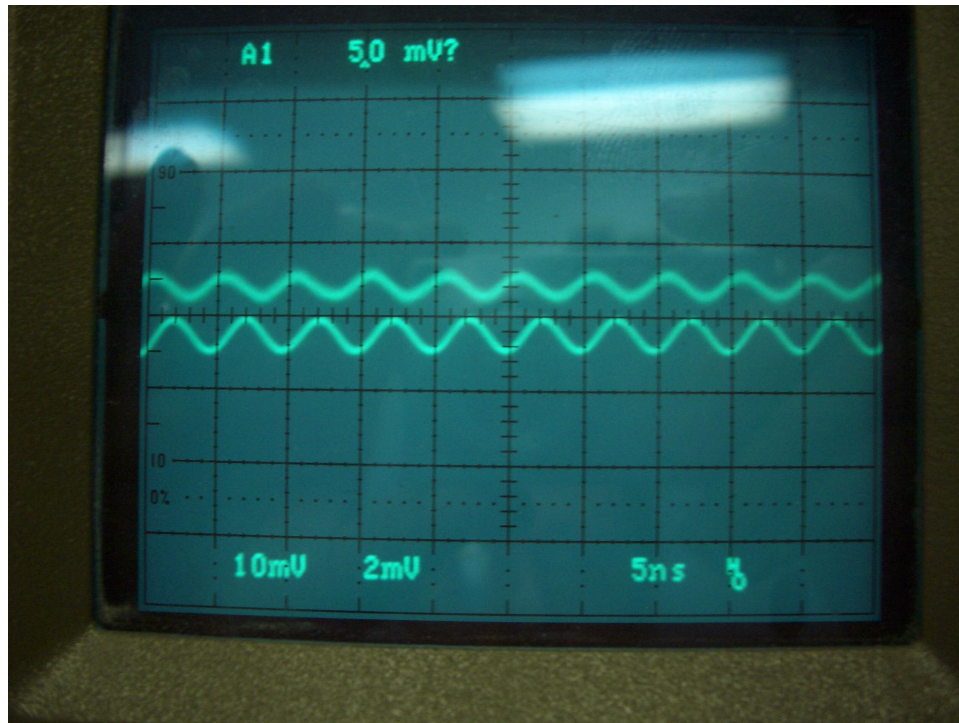


Figure 6.10. Delay-non Delay phase difference

The results of moving the prism and measuring the power at the detector are shown in the following plot.

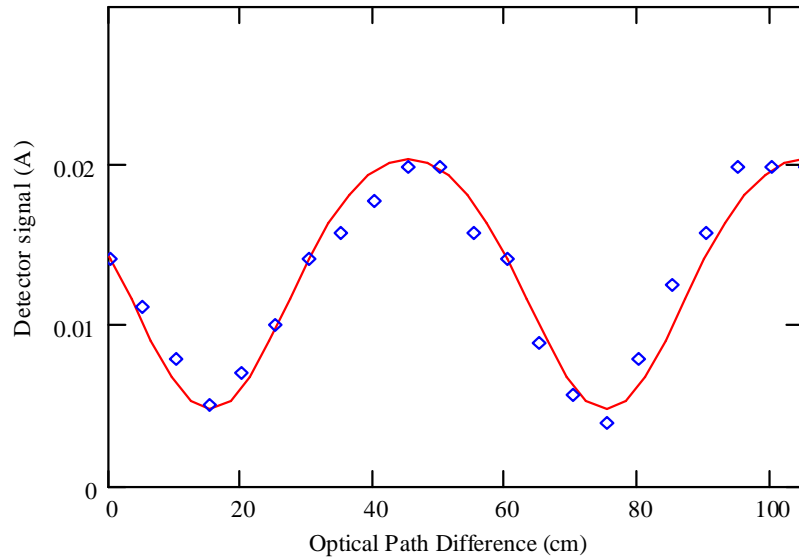


Figure 6.11. Detector signal as a function of differential distance

The solid line is the calculated value using the computer model. The diamonds are the values measured in the experiment. The results shows that the RAM behaves in the same fashion as the signal derived from the suppression of one of the FM sidebands. It also shows that the model correctly predicts this behavior.

6.6. Discussion and Conclusions

This experiment establishes that the differing travel distances of two waves with AM modulation impressed on them through the use of current modulation will cause a phase difference between them that will result in the interference of those signals at the detector. The computer model correctly predicts this result. In addition, the model correctly predicts the outcome of the experiment conducted by Dubinsky. Both these results validate the computer model as correctly modeling the FM remote sensing technique. The conclusion that follows from the modeling results are now supported by the experimental data. An FM remote sensing system which relies on scattering for the return will experience signal degradation due to the phase differences between the returning waves. The different distances these waves travel cause these phase differences. The issue in using FM for remote sensing is to avoid generating these phase differences.

The key is to avoid the multiple scatterings of the outgoing wave that result in phase differences between the waves received at the detector at a given time, causing cancellation of the signal due to destructive interference. Sounding offers a way around that limitation. In a sounding configuration, the FM signal is bounced off of the planet's surface and returned to the detector. As a result the return waves all travel the same distance and have the same phase when they are detected. The destructive interference caused by the differing phases of the return waves is avoided. The result is a readily detectable FM signal that will reflect the total concentration of water vapor in the column of atmosphere through which the light traveled. Since this is more similar to a laboratory configuration than the scattering option that has been discussed so far, the best way to

analyze the performance of such a system on Mars is to modify the laboratory signal to noise equations to accommodate the remote sensing parameters. This will be done in the next section.

7. FM Sounding SNR Equation Development

7.1. Introduction

It has been established that interference at the detector due to distance induced phase differences will significantly reduce the signal current for a scattering based form of FM remote sensing. Another form of FM remote sensing, FM sounding, avoids the problems that earlier sections of this paper have identified. The rest of this paper will address the FM sounding method and its expected performance. This section will undertake to develop a SNR equation that will allow performance calculations and design tradeoffs. The method of producing an FM specific remote sensing Signal to Noise Ratio (SNR) will be to develop an equation for the SNR of an FM remote sensing system based on a laboratory version already developed [38,39,40,41].

7.2. Sounding

Sounding methods reflect light from a surface back to the detector. In this they are closer in principle to the laboratory FM techniques described earlier. An FM sounding experiment would send light down onto a planet's surface and use that surface reflectance, its albedo, to return the light back to the orbiting satellite.

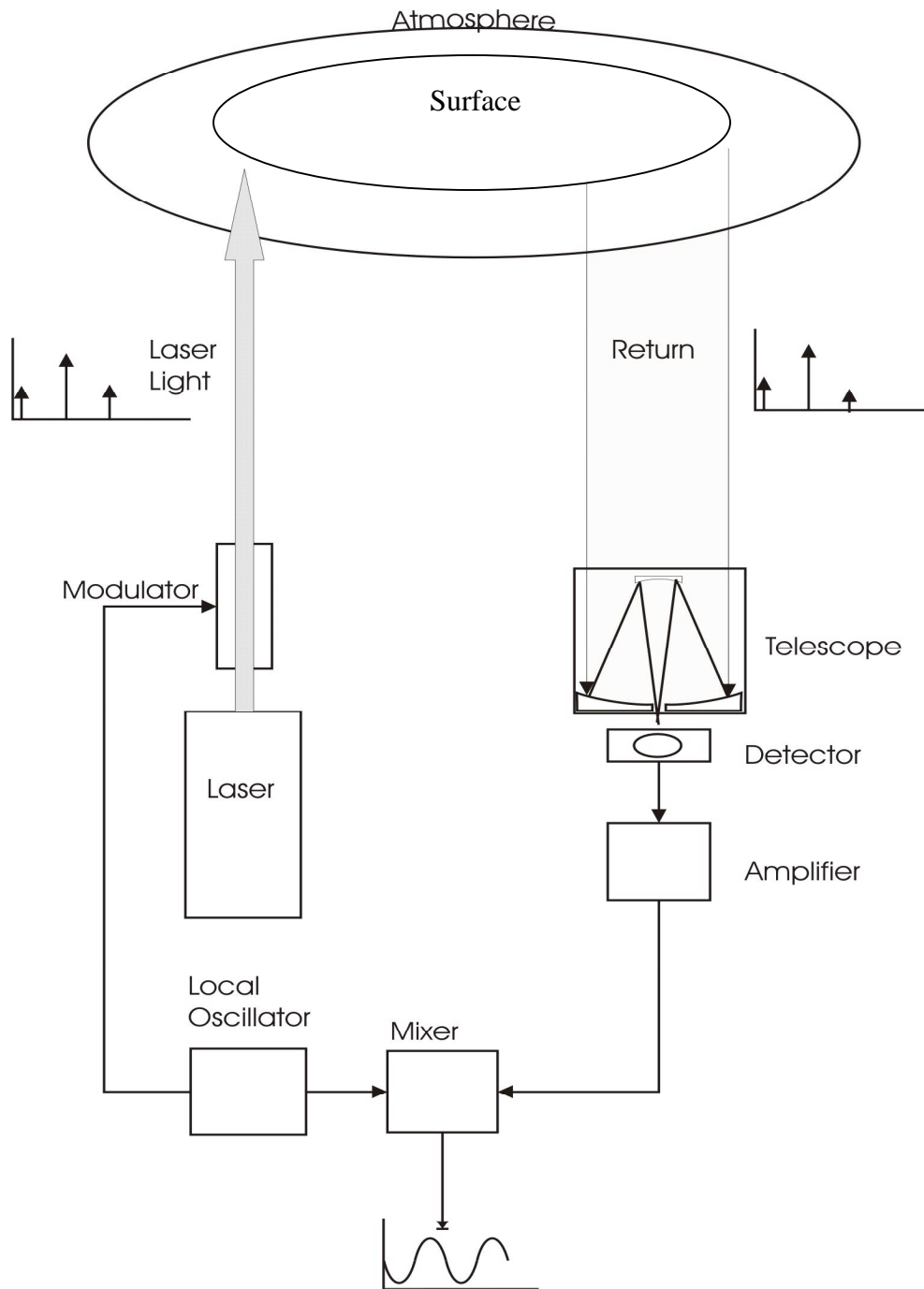


Figure 7.1. FM Sounding

7.3. Laboratory FM SNR Equation

The starting point will be the basic expression for the SNR (Signal to Noise Ratio),

which is:

$$SNR = \frac{\overline{i_{return}^2}}{\overline{i_{SN}^2 + i_{thermal}^2 + i_{RAM}^2 + i_{y_f}^2}} \quad (7.1)$$

The basic Laboratory FM equation has been derived by many authors from this starting point. The form of the equation used here is from [42]. In order to use this equation for FM remote sensing applications some modifications are necessary.

The first modifications are straightforward changes to the parameters used. One is the addition of a term for the gain, G . The other is to add a term for the noise figure of the amplifying electronics, F_N . When added to the basic Laboratory FM SNR equation we have:

$$SNR = \frac{G \left(\frac{e\eta_{qe}}{h\nu_0} \right)^2 2P_0^2 |Q|^2}{2e\Delta f G \left[\frac{e\eta_{qe}}{h\nu_0} P_0 \left(1 + \frac{M^2}{2} \right)^N + \frac{2kTF_N}{eR_L} \right] + \left(\frac{e\eta_{qe}}{h\nu_0} \right)^2 G \left(2R^2 (M) \sigma_p^2 + \frac{\Delta f}{f^b} \sigma_{ex}^2 \right)} \quad (7.2)$$

Each term will now be discussed in more detail. After the discussion of each term is complete, the entire equation will be analyzed in greater detail and more substantial modifications made to accommodate a remote sensing application.

7.3.1. Return Current Term

The numerator in the SNR equation is the square of the current generated by the return signal.

$$i_{return}^2 = G \left(\frac{e\eta_{qe}}{h\nu_0} \right)^2 2P_0^2 |Q|^2 \quad (7.3)$$

where η_{qe} is the quantum efficiency of the detector, G is the gain, h is Planck's constant, ν_0 is the frequency of the light and P_0 is the power of the source signal.

In a laboratory FM experiment the value of P_0 is close to the value of the laser light emitted. Since the emitter and detector are in line with each other, little power is lost. In sounding the returned power will be smaller than in a laboratory experiment. As a result the value of P_0 will have to be replaced with a value, P_{RS} , reflecting the current expected in a remote sensing experiment.

Without the Q term, the parameters in the return current combine to give the number of electrons per second counted by the detector. Q is the parameter representing how much of this current is in the sidebands of interest. It is the return term containing FM specific characteristics. It will be discussed next.

7.3.2. Q term

The Q term is expressed as:

$$Q(\alpha) = \sum_{n,m} r_n r_m r_{n-1}^* r_{m+1}^* \exp(-2\alpha(n+m)\overline{\nu_m}) - M^2 \quad (7.4)$$

Each pair of n and m defines a frequency distance from ν_m , where ν_m is the modulation frequency for FM, and the amplitude of the contribution at that frequency $r_n r_m r_{n-1} r_{m+1}$. At each frequency there is an attenuation defined by the attenuation coefficient $\alpha(n+m)$.

The specific expression for r is:

$$r_n(B, M, \Psi) = \sum_{k=-1}^1 a_k J_{n-k}(B) \quad (7.5)$$

where the a 's are:

$$\begin{aligned}
 a_0 &= 1 \\
 a_{\pm 1} &= \pm \frac{M}{2i} \exp(\pm i\Psi)
 \end{aligned}
 \tag{7.6}$$

The r_n terms are the amplitudes of the frequency components of the FM signal at the detection frequency of interest. Their magnitudes follow the Bessel functions. This pattern is familiar from laboratory FM. The sidebands have amplitudes determined by Bessel functions.

The Q term multiplies each of these components by an attenuation factor dependent on the modulation frequency. The attenuation factor assumes a Gaussian line shape with peak value α occurring when ν_m is zero. The parameter ν_m is the modulation frequency divided by the linewidth, the normalized modulation frequency.

As n and m increase, the exponential gets smaller and the contribution to Q decreases. That is, sidebands farther from the carrier are lower in amplitude and contribute less. This first part of Q (the part without the M factor) represents the power in the sidebands.

M is the amplitude modulation index. Its value squared represents the power in the residual AM. This is power lost to the sidebands, so it is subtracted out.

The overall result for Q is that it represents the fraction of power in the sidebands that isn't due to residual AM. When it is multiplied by the number of electrons counted at the detector, the result is the number of electrons counted at the detector due to the sidebands. It represents the FM signal received. Along with P_{RS} , a Q_{RS} will have to be calculated to include remote sensing information. Both of these will be calculated after the review of the SNR equation is complete.

7.3.3. Noise Terms

The first noise term is the shot noise:

$$i_{SN} = 2e\Delta fG \left[\frac{e\eta_{qe}}{h\nu_0} P_0 \left(1 + \frac{M^2}{2} \right)^N \right] \quad (7.7)$$

The shot noise is due to the quantum nature of the light arriving at the detector. The random distribution in the rate of arrival of photons at the detector results in noise. Shot noise defines the lowest noise level possible in a photon detection system. In this expression e is the charge of an electron, Δf is the bandwidth of the detector and N is one or two for single or two tone FM. The term with M represents the additional contribution to the shot noise due to the current generated by the RAM signal. M is the amplitude modulation index of this residual AM.

The second noise term is the thermal noise of the detector:

$$i_{th} = 2e\Delta fG \left(\frac{2kTF_N}{eR_L} \right) \quad (7.8)$$

where Δf is the bandwidth, e is the electron charge, G is the gain, k is Boltmann's constant, F_N is the noise figure for the electronic amplifier and R_L is the detector impedance.

The last noise term is the RAM noise and the $1/f$ noise or excess noise.

$$i_{1/f}^2 = G \left(\frac{e\eta_{qe}}{h\nu_0} \right)^2 \left(2R^2(M)\sigma_p^2 + \frac{\Delta f}{f^b} \sigma_{ex}^2 \right) \quad (7.9)$$

The excess noise term falls off rapidly as the modulation frequency increases. At the frequencies used for single tone and two tone, in the GHz range, the noise is much smaller than the other sources of noise in the system and is usually neglected. The excess

noise at a bandwidth of 1 Hz of bandwidth and 1 Hz of frequency is σ_{ex} . The standard deviation of the laser power within the bandwidth of the detector is σ_p .

The RAM noise function $R(M)$ is defined as:

$$R_{\text{sin gltone}}(M) = M \sin(\theta + \Psi) \quad (7.10)$$

$$R_{\text{two tone}}(M) = M^2 \cos(\theta) \quad (7.11)$$

Here Ψ is the phase angle between the RAM and the FM impressed on the signal. The parameter θ is the phase angle between the return signal and the local oscillator.

Investigations by Lenth indicate that the value of Ψ is about:

$$\Psi = \begin{cases} n\pi + \pi/2 & \text{for } 2\pi\omega_m < 750\text{MHz} \\ n\pi & \text{for } 2\pi\omega_m > 2\text{GHz} \end{cases} \quad (7.12)$$

Between these two extremes the phase angle smoothly changes from one to the other. The 2GHz frequency is the relaxation oscillation frequency of the semiconductor diode used in Lenth's experiments. These values would be shifted for another diode. It can be seen from these equations that the single tone RAM/FM phase angle can be offset by the local oscillator phase angle. In two tone FM this isn't possible.

The following relationship for RAM and excess noise terms can be found in Silver:

$$\sigma_p = k_p P_0 \quad (7.13)$$

$$\sigma_{ex} = \frac{\sigma_p}{k_{ex}} = \frac{k_p P_0}{k_{ex}} \quad (7.14)$$

These can be substituted into the SNR equation to give:

$$SNR = \frac{G \left(\frac{e\eta_{qe}}{h\nu_0} \right)^2 2P_0^2 |Q|^2}{2e\Delta f G \left[\frac{e\eta_{qe}}{h\nu_0} P_0 \left(1 + \frac{M^2}{2} \right)^N + \frac{2kTF_N}{eR_L} \right] + \left(\frac{e\eta_{qe}}{h\nu_0} \right)^2 GP_0^2 \left(2R^2 (M) k_p^2 + \frac{\Delta f}{f^b} \left(\frac{k_p}{k_{ex}} \right)^2 \right)} \quad (7.15)$$

7.3.4. Summary of Laboratory SNR Equation

Before modifying this equation for FM remote sensing it is instructive to qualitatively analyze the effects of the parameters on the SNR.

The RAM noise can be reduced by decreasing the magnitude of the amplitude modulation or by increasing the power going to the sidebands. This is a straightforward application of more power to the signal wavelength, the sideband, to increase the SNR. If RAM is a problem, it is also possible to set the local oscillator phase to offset the difference in phase between the RAM and FM modulation, at least for single tone. Of course, the excess noise decreases with increasing modulation frequency, which is the reason for using large modulation frequencies to move the sideband signal far away from the center frequency. The excess noise also increases with increasing bandwidth. Also, putting more power into the sidebands, which increases Q, moves the power away from the noise.

The shot noise decreases linearly with increasing photon count rate while the thermal noise decreases with the square of the increasing photon count rate. Reducing the bandwidth of the detector decreases this noise source. Increasing the power to the sidebands also reduces this noise source.

The SNR equation presented will now be used as the basis of developing an FM

specific sounding SNR using the Martian sounding model developed earlier. The primary method of combining these results will be in the modification of the P_0 and Q parameters to be P_{RS} and Q_{RS} through the use of the Martian LIDAR equation.

7.4. FM Remote Sensing Sounding Equation

The development of an SNR equation for Martian water vapor remote sensing using FM sounding involves combining a modified Martian LIDAR equation with a modified Laboratory FM SNR equation.

7.4.1. LIDAR equation modifications for sounding

The Martian LIDAR equation discussed earlier was for the case of scattered returns:

$$N_{photons}(\lambda_L, R) = \frac{E_L}{hc/\lambda_L} \frac{A}{R^2} \xi(R) \xi(\lambda_L) \beta(\lambda_L, R) \Delta R f e^{-2 \int_0^R \kappa(\lambda_L, R) dR} \quad (7.16)$$

This equation changes for a sounding application.

Instead of scattering from an atmospheric constituent, the return is a reflection of a laser beam from the surface. As a result, there is no longer the R^2 losses that result from the scattering process. Instead there is loss due to the divergence of the laser. As the beam travels from the source to the ground and back it widens. The result is that the telescope in front of the detector doesn't intercept the whole beam. The area of the receiving telescope determines how much of the beam is gathered. The fraction intercepted is:

$$fraction = \frac{A_{rec}}{\pi (2h_{sc} \tan(\theta_{div}))^2} \quad (7.17)$$

The numerator is the area of the receiving telescope. The denominator is the area of

the beam at the receiver due to divergence of the laser. The angle θ_{div} is the divergence of the laser beam coming out of the instrument. The power of the laser is distributed over this beam. As the beam travels from the spacecraft altitude, h_{sc} , and back it widens to the area represented by the denominator.

In addition the backscatter term is replaced by the reflection from the surface. This surface reflection is called the albedo. Making these changes in the equation results in the following sounding equation.

$$N_{photons}(\lambda_L, R) = \frac{E_L}{hc/\lambda_L} \frac{A_{rec}}{\pi(2h_{sc} \tan(\theta_{div}))^2} \xi(R) \xi(\lambda_L) r_{albedo} \Delta R f e^{-2 \int_0^R \kappa(\lambda_L, R) dR} \quad (7.18)$$

This is the basic Martian sounding equation for sounding applications that will be used in the following sections to develop the SNR equation for sounding.

7.4.2. FN SNR modifications for sounding

The laboratory FM SNR equation as we've just seen and discussed is:

$$SNR = \frac{G \left(\frac{e\eta_{qe}}{h\nu_0} \right)^2 2P_0^2 |Q|^2}{2e\Delta f G \left[\frac{e\eta_{qe}}{h\nu_0} P_0 \left(1 + \frac{M^2}{2} \right)^N + \frac{2kTF_N}{eR_L} \right] + \left(\frac{e\eta_{qe}}{h\nu_0} \right)^2 GP_0^2 \left(2R^2 (M) k_p^2 + \frac{\Delta f}{f^b} \left(\frac{k_p}{k_{ex}} \right)^2 \right)} \quad (7.19)$$

The Martian sounding equation contains the information about water vapor on Mars and the strength of the return signal. The FM SNR equation contains the information specific to the FM technique. Modifying the FM SNR equation and combining these two equations will give an expression for the SNR of an FM water vapor sounding

experiment on Mars. Looking closely at the laboratory FM SNR equation it can be seen that two of the parameters, P and Q , are dependent on the magnitude of the return.

The power of the detected signal, P_0 , is large in a laboratory setting but small in a remote sensing setting. In a laboratory setting it is essentially a constant equal to cross sectional area of the detector multiplied by the power density of the emitted beam. That is, how much power is intercepted by the detector in the straight line path of the laser beam. In a remote sensing sounding application it is the amount of reflected light collected by a telescope and incident on the detector. It will be calculated from the Martian sounding equation and called P_{RS} .

The other term that depends on the magnitude of the return is Q . The term Q in a laboratory is just the fraction of the light that is in the sideband of interest. This will be the same in a remote sensing sounding application. However, the expression for the loss in a sideband used in the Martian sounding equation is a peak loss. The assumption is that the on and off line frequencies are far enough apart that it isn't necessary to map out the absorption profile exactly. This is not the case in FM remote sensing. In FM remote sensing experiment the frequencies of the sidebands are close enough together that the width of the absorption feature is important. The Martian sounding model will be augmented to include the absorption profile. Adding this will give the new term for remote sensing, Q_{RS} .

The method of combining these two equations is to replace the P_0 and Q terms with P_{RS} and Q_{RS} . The result will be an FM sounding SNR equation for Martian water vapor.

7.4.3. Calculating P_{RS}

The Martian sounding equation can be separated into two parts. One part determines the magnitude of the overall return signal for use in determining the P_{RS} , the other is the absorption particular to the sidebands for use in determining Q_{RS} . The terms that determine the overall return signal can be grouped together to give the following expression.

$$P(\lambda_0, R) = \frac{A_{rec}}{\pi(2h_{sc} \tan(\theta_{div}))^2} \xi(R) \xi(\lambda_0) r_{albedo} P_0 \quad (7.20)$$

Here λ_0 is the carrier frequency. A is the area of the receiver, $\xi(R)$ is the target telescope field of view overlap, $\xi(\lambda)$ is the transmission through the receiver system, r_{albedo} is the surface reflection, θ_{div} is the divergence of the laser beam, h_{sc} is the altitude of the spacecraft and P_0 is the laser power emitted. All these terms are independent of the sideband structure. The effect the return power overall, but not the fraction of power in any particular sideband.

After removing these terms the remaining part of the LIDAR equation is:

$$T_{total}(\lambda_L, R) = e^{-2 \int_0^R \kappa(\lambda_L, R) dR} \quad (7.21)$$

This is the total transmission expected due to backscatter and absorption effects at a given wavelength and height above the surface of Mars. Expressing this in frequency and separating out the backscatter and absorption components gives:

$$T_{total}(\lambda, R) = T_b(\lambda, R) T_\lambda(\lambda, \nu_m, R) = e^{-2 \int_0^R \kappa_b(\lambda, R) dR} e^{-2 \int_0^R \kappa_\lambda(\lambda, \nu_m, R) dR} \quad (7.22)$$

The parameter ν_m is the modulation frequency. The backscatter term can be approximated

at the carrier frequency. Doing this removes any dependence on sidebands. This allows the backscatter term to be included in the return power equation above to give:

$$P_{RS}(\lambda_0, R) = \frac{A_{rec}}{\pi(2h_{sc} \tan(\theta_{div}))^2} \xi(R) \xi(\lambda_0) r_{albedo} T_b(\lambda_0, R) P_0 \quad (7.23)$$

The sounding method will integrate the losses over the distance the light travels in the Martian atmosphere. As a result P_{RS} will be evaluated at the maximum atmospheric height for the model.

$$P_{RS}(\lambda_0) = GP_0 \frac{A_{rec}}{\pi(2h_{sc} \tan(\theta_{div}))^2} \xi(R) \xi(\lambda_0) r_{albedo} T_b(\lambda_0, R_{max}) \quad (7.24)$$

This expression now contains all the terms not specific to any particular sideband. The backscatter and transmission terms have to be calculated using the Martian sounding model developed in an earlier section.

7.4.4. Calculating Q_{RS}

This parameter contains the information on the effects of absorption on the sidebands. That is, it is the parameter that contains the effects on the FM signal due to the atmospheric constituent of interest. To calculate it for the sounding configuration, the parts of the Martian sounding equation pertinent to the FM sideband absorption will be identified and incorporated into the Q term to give the Q_{RS} term that will replace the Q term for sounding configurations.

There was one sideband dependent term left after creating the expression for P_{RS} .

$$T_\lambda(\lambda, R) = e^{-2 \int_0^R \kappa_\lambda(\lambda, v_m, R) dR} \quad (7.25)$$

This absorption term can be used in Q to represent the absorption experienced by a

sideband. Q is the factor that contains the information peculiar to FM.

Q for laboratory FM is expressed as:

$$Q(\alpha) = \sum_{n,m} r_n r_m r_{n-1}^* r_{m+1}^* \exp(-2\alpha(n+m)\overline{v_m}) - M^2 \quad (7.26)$$

So Q_{RS} can be written in a similar way using the sideband atmospheric attenuation from the Martian sounding equation:

$$Q_{RS}(\alpha) = \sum_{n,m} r_n r_m r_{n-1}^* r_{m+1}^* e^{-2 \int_0^R \kappa_\lambda(\lambda, v_m, R) dR} - M^2 \quad (7.27)$$

Here λ is the wavelength of the particular wave corresponding to a given set of n and l. To make the combination of the Martian sounding equation and the FM SNR equation easier, it will be convenient to express the term in the integral in terms of the frequency of modulation v_m normalized to the linewidth of the absorption feature.

$$Q_{RS}(v_m) = \sum_{n,m} r_n r_m r_{n-1}^* r_{m+1}^* e^{-2 \int_0^R \kappa_\lambda((n+m)\overline{v_m}, R) dR} - M^2 \quad (7.28)$$

Earlier in this paper it was mentioned that it would be necessary to create an absorption profile for an FM remote sensing sounding model rather than use only the absorption peak as was done in the Martian LIDAR equation. The Martian LIDAR model was used only to show on and off absorption line behavior. The value of the absorption parameter κ_λ doesn't include a frequency dependent component. The assumption in the earlier Martian LIDAR model is that the on and offline frequencies are so far apart that it isn't necessary to include the absorption profile explicitly in the model. This limitation is carried over into the Martian sounding equation. As a consequence, if we use this model directly the selective absorption of the sideband won't be accounted for in our model. In

an FM model the sidebands are close to the carrier frequency, so the absorption profile must be explicitly included in the calculations.

In the Martian sounding equation the peak absorption was given as:

$$g(h, \lambda) = \frac{1}{\gamma_D(h, \lambda)} \left(\frac{\ln(2)}{\pi} \right)^{1/2} \quad (7.29)$$

This must be modified to be a profile, not just a peak. Using a Gaussian profile for low density atmospheres (like Mars) along with this peak value gives the remote sensing replacement for α :

$$\alpha_{RS}(h, \nu_m) = g(h, \lambda_0) \exp \left[- \left(\frac{\nu_m}{\gamma_D(h, \nu_m)} \right)^2 \ln(2) \right] \quad (7.30)$$

To enable an easy transition from the Q to Q_{RS} the absorption profile has been expressed in frequency. The parameter g changes negligibly from the carrier to the carrier plus modulation frequency. For simplicity, therefore, it is expressed in terms of the carrier only.

This formulation of the absorption profile not only contains the variation of the absorption profile peak value g with altitude, but also the variation in the linewidth γ_D with altitude. This expression will replace g in the subsequent derivation of the absorption parameter. Following through with the rest of the derivation in the same way as was done with the Martian LIDAR equation results in the replacement for the absorption cross section σ :

$$\sigma_{H_2O_{-RS}}(h, \nu_m) = S \cdot \alpha_{RS}(h, \nu_m) \quad (7.31)$$

This in turn can be inserted into the expression for the absorption coefficient due to

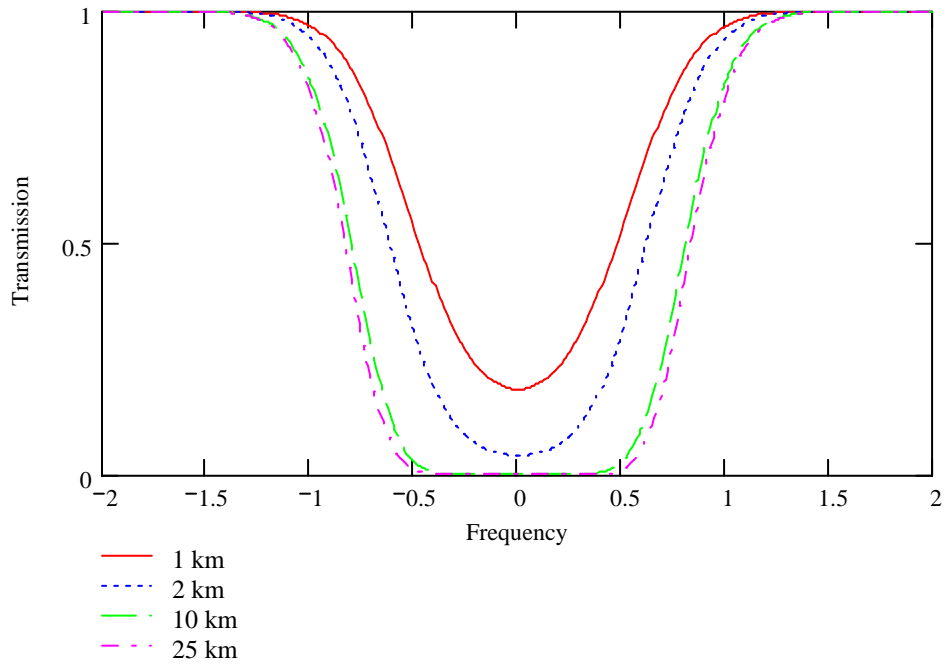


Figure 7.2. Transmission versus Relative Frequency

water vapor κ to give its remote sensing replacement:

$$\kappa_{RS}(h, \nu_m) = \sigma_{H_2O_RS}(h, \nu_m) \rho_{H_2O}(h) = S \cdot \alpha_{RS}(h, \nu_m) \rho(h) \quad (7.32)$$

Now the remote sensing sounding replacement for the transmission can be calculated and plotted:

$$T_{RS}(\lambda, R) = e^{-2 \int_0^R \kappa_{RS}(\lambda, \nu_m, R) dR} \quad (7.33)$$

The plot shows the dependence on frequency and altitude that has been added to the basic model by the author. The original expression in the Martian sounding equation didn't have this necessary feature.

Using this result the absorption linewidth and depth variation with altitude can now be incorporated into the Q equation. The final step is to use this expression to get the expression for the remote sensing replacement for Q:

$$Q_{RS}(h, \nu_m) = \sum_{n,m} r_n r_m r_{n-1}^* r_{m+1}^* e^{-2 \int_0^R \kappa_{RS}((n+m)\nu_m, R) dR} - M^2 \quad (7.34)$$

The FM sounding system will integrate over the total height of the atmosphere. So the equation is evaluated at the maximum height in the atmospheric model:

$$Q_{RS}(\nu_m) = \sum_{n,m} r_n r_m r_{n-1}^* r_{m+1}^* e^{-2 \int_0^{R_{\max}} \kappa_{RS}((n+m)\nu_m, R) dR} - M^2 \quad (7.35)$$

Now that Q_{RS} has been calculated, it can be combined with P_{RS} to give an expression for the SNR for FM of Mars.

7.4.5. FM Remote Sensing SNR equations summary

Putting Q_{RS} and P_{RS} into the equation for the laboratory FM SNR gives the equation for the FM remote sensing SNR.

$$SNR_{RS}(\nu_m) = \frac{\left(\frac{e\eta_{qe}}{h\nu_0}\right)^2 2P_{RS}^2 |Q_{RS}(\nu_m)|^2}{2e\Delta f \left[\frac{e\eta_{qe}}{h\nu_0} P_{RS} \left(1 + \frac{M^2}{2}\right)^N + \frac{2kT_{eff}}{eR_L} \right] + \left(\frac{e\eta_{qe}}{h\nu_0}\right)^2 \left(2R^2(M)\sigma_p^2 + \frac{\Delta f}{f^b} \sigma_{ex}^2\right)} \quad (7.36)$$

This expression for the SNR adds the effects due to sounding to the model for FM. This model incorporates a vertical (altitude) model of the Martian atmosphere allowing for modeling of the absorption profile linewidth, absorption profile peak, backscatter coefficients and absorption coefficients as a function of spacecraft altitude and laser wavelength. The addition of the absorption linewidth profile function allows for the

accurate modeling of the sidebands characteristics of the FM technique. The model can be used for single tone and two tone techniques. It can be generalized to other atmospheres and other atmospheric constituents by replacing the density profiles and absorption line center frequencies with ones appropriate to the items of interest.

8. FM Sounding SNR analysis

Now that an FM Remote Sensing Sounding SNR equation has been developed, it can be used to determine the capabilities of a practical FM Martian water vapor detection system using sounding. The SNR equation will be used in conjunction with the Martian sounding model developed earlier to produce plots of SNR versus altitude dependent on various parameters.

In the first part of this section the parameters that go into the SNR equation will be discussed. In the parts following the first these parameters will be used to determine the performance of the FM system as a function of various important parameters.

8.1. SNR Parameters

In order to use the SNR equation to determine the performance of such a system on Mars, the values of certain parameters in the SNR equation must be set. They are divided into two groups. The first group contains the parameters associated with the characteristics of the Martian atmosphere and water vapor in that atmosphere. The second contains the parameters determined by the science measurement requirements and the available technology. This second group is divided further into those parameters for the emitter, the telescope and the detector system. In addition, the available technology will be restricted to that which can survive a trip to Mars. It must be rugged, small, low power and radiation tolerant.

The first group is the group of Martian atmosphere water vapor parameters.

$$\begin{aligned}
\sigma_0 &= 0.025 \text{ km}^{-1} \\
b' &= 5.0 \text{ km} \\
a &= 0.4 \\
S_p &= 30 \text{ sr} \\
b &= 3.2 \text{ km} \\
f &= 6 \times 10^{-6} \text{ km}^{-1} \\
a' &= 2981 \\
n &= 1.0007 \\
m_{\text{H}_2\text{O}} &= 2.993 \times 10^{-23} \text{ gm} \\
S_l &= 5.419 \times 10^{-22} \text{ cm}^{-1} \text{ cm}^2
\end{aligned}$$

Figure 8.1. Martian Water Vapor Parameters

These parameters have been discussed as part of the development of the Martian LIDAR equation. They are the result of earlier scientific investigations of Mars that have allowed the creation of models of the Martian atmosphere, such as the one reflected in the Martian LIDAR equation in this paper. They relate to the backscatter and transmission of light in the presence of water vapor in the Martian atmosphere. For the purposes of this paper they define what the FM remote system must be capable of detecting through their incorporation into the Martian atmospheric model developed earlier. They aren't controlled by the experimenter.

The second group contains parameters determined by the scientific requirements for the mission which are limited by the available of current technology. The first set of these scientific measurement parameters determine the range resolution of the experiment and the frequency of firing of the laser. These are grouped together since they are commonly used values for remote sensing experiments.

$$rate = 50Hz$$

$$pulsewidth = 1.28\mu s$$

$$\Delta R = 192m$$

Figure 8.2. Science Requirements: Range Resolution and Firing Rate

The next set of scientific measurement parameters determines the capabilities of the laser emitter. These have been discussed in more detail in the section on the terms in the SNR equation. The power output of the laser is assumed to be around 1W using an external optical amplifier. This is an attainable power level with currently available semiconductor lasers and flared amplifiers operating at the 935.68nm wavelength. The modulation frequency can be attained with external modulators.

$$P_0 = 1W$$

$$\lambda = 935.68nm$$

$$\nu_m = 1GHz$$

Figure 8.3. Science Requirements: Laser

The next group of science measurement determining parameters includes those associated with the detector system.

$$\eta = 0.84$$

$$G = 10^6$$

$$\Psi = \frac{\pi}{2}$$

$$\theta = 0$$

$$Area = 0.292m^2$$

$$h_{sc} = 400km$$

$$\theta_{div} = 100\mu rad$$

$$\xi(h) = 1$$

$$\xi(\lambda) = 0.30$$

Figure 8.4. Science Requirements: Receiver/Detector

These parameters provide a reasonable basis for solving the FM remote sensing SNR equation. They are representative of what is currently available for spaceflight type applications. They are based on using semiconductor laser and detector technology in the 935.68nm wavelength region. Using these we can now proceed to solve the FM remote sensing SNR equation.

8.2. Noise Currents

Taking the parameter above and calculating the noise currents for a single tone FM sounding system versus laser power gives the following plot.

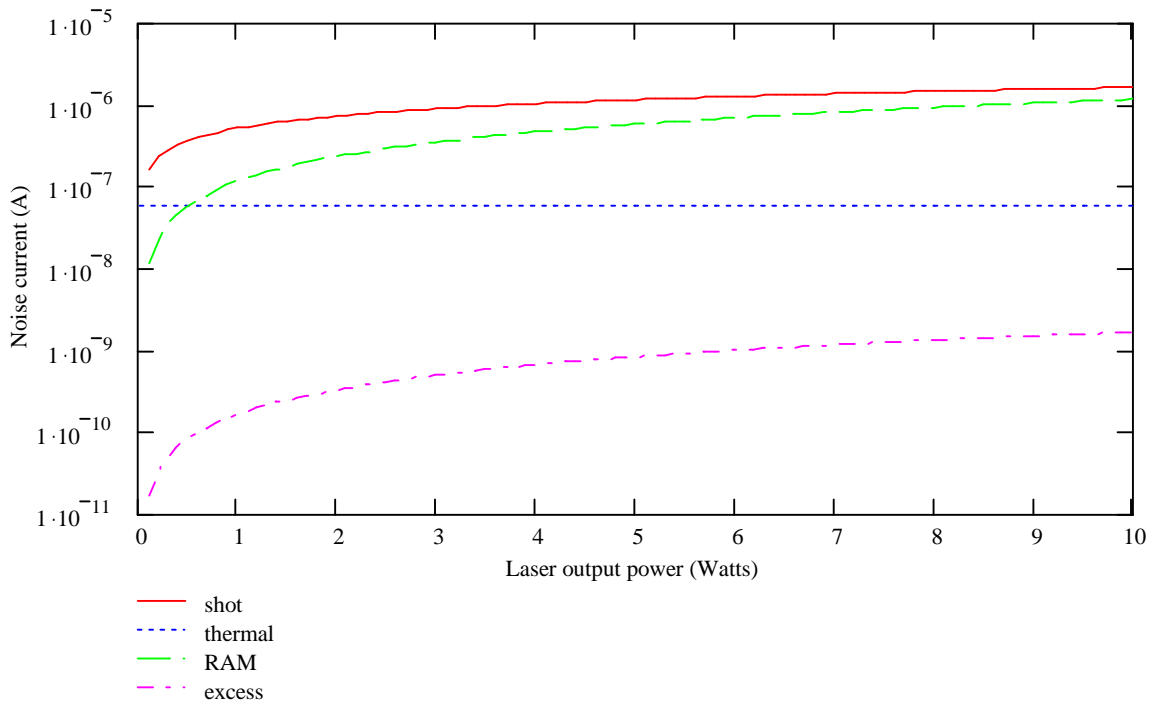


Figure 8.5. Noise Current vs Laser power for single mode FM sounding

The plot shows the noise levels are dominated by shot noise for laser power levels above about 0.5 W. The excess noise is lowest, as expected. Reducing the excess noise contribution is one of the advantages of using FM techniques. For the rest of the analysis the excess noise contribution will not be analyzed further.

The thermal noise is lower than the shot noise for any power above 0.5W and the temperature of 295 degrees K. Calculating the noise currents for a range of temperatures results in the following plot.

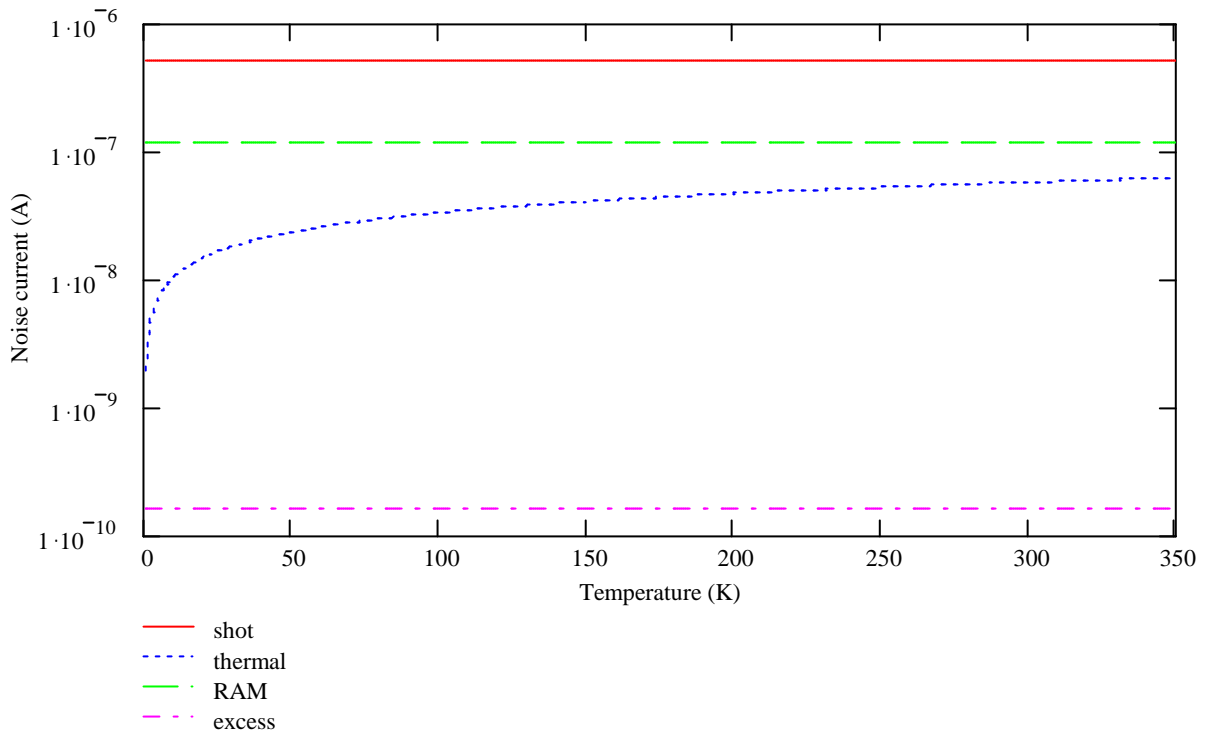


Figure 8.6. Noise currents vs temperature for FM sounding at 1W laser power

This plot shows that the detection system isn't thermal noise limited for a wide range of operational temperatures that cover any reasonable detector operational temperatures. If necessary, detectors can be cooled to lower the thermal noise contribution. However, that won't be necessary in this system.

The primary source of noise is the RAM noise due to unwanted amplitude modulation of the signal. The RAM noise must be kept below the shot noise limit to maximize the FM sounding systems sensitivity. Plotting the RAM noise against the RAM modulation index, M , results in the following plot.

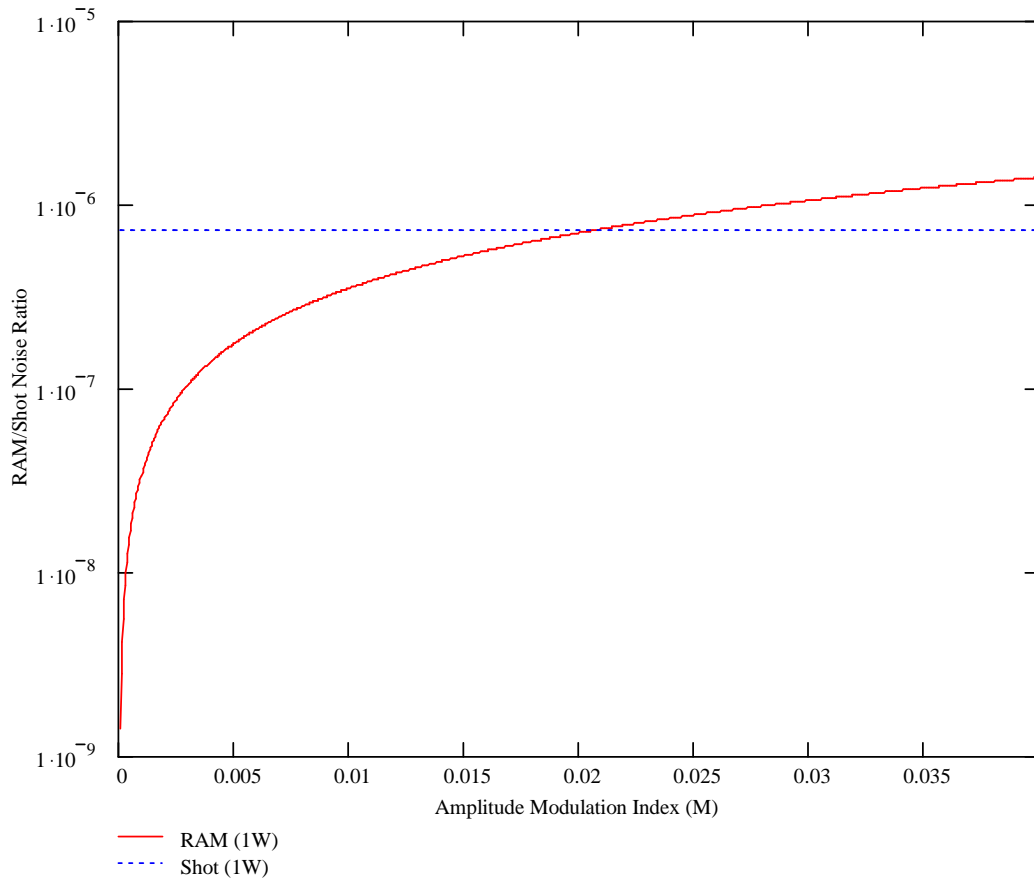


Figure 8.7. RAM and shot noise comparison as a function of M

The excess noise and thermal noise contributions have been removed since they don't drive the system performance.

The RAM noise becomes equal to the shot noise above $M \sim 0.02$. To increase the SNR we might try increasing the laser power. Increasing the power of the laser results in increasing the overall power to the center frequency and sidebands, but also increases the RAM noise current. To see what the overall effect is we plot the ratio of RAM noise to shot noise for various laser power levels.

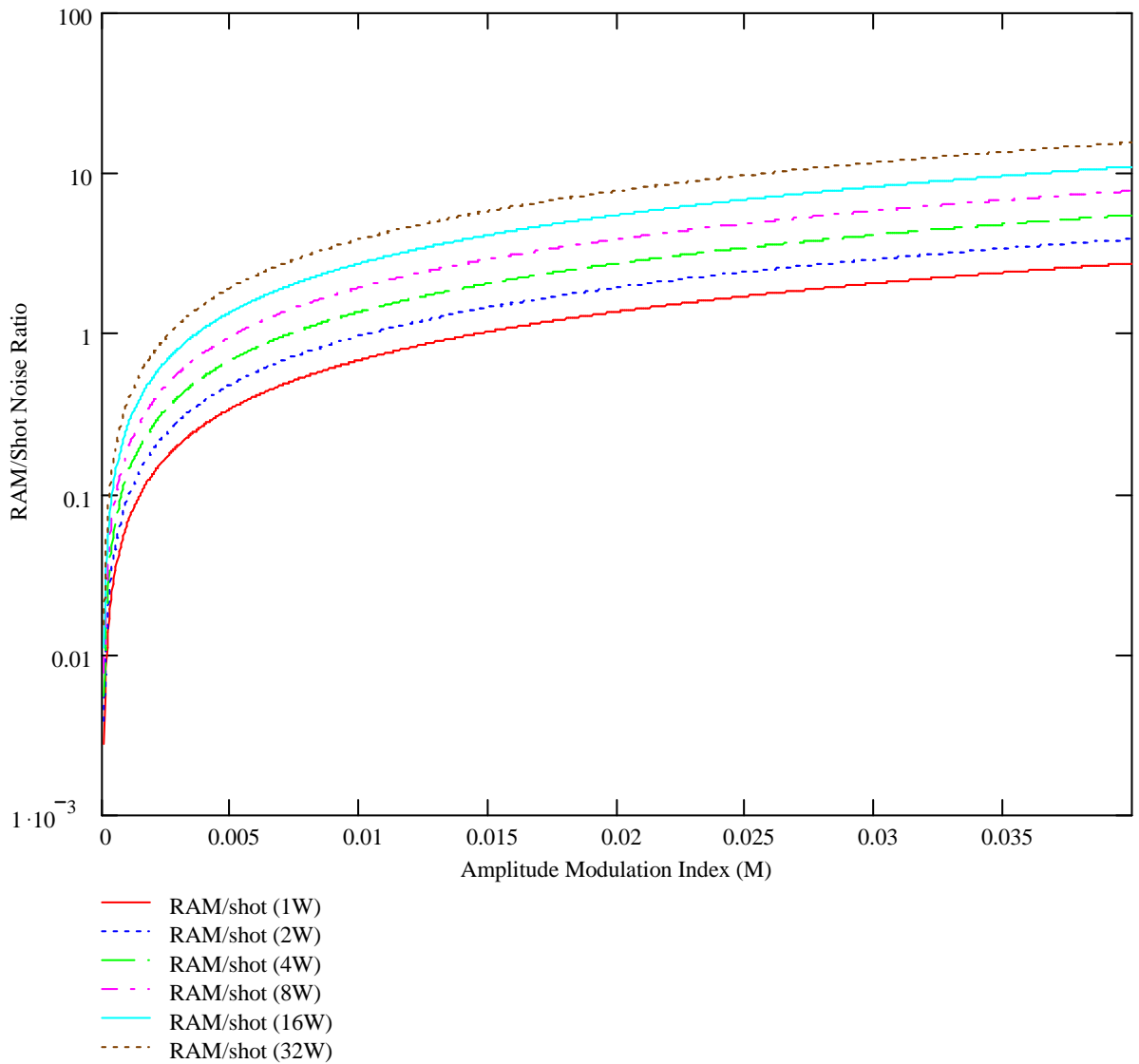


Figure 8.8. RAM/shot noise ratio as a function of laser power

As the laser power increases the RAM increases faster than the shot noise increases. The result is that increasing the laser power makes the system more susceptible to RAM noise. A current modulated system, suited to spaceflight for reasons discussed earlier, has to be particularly careful about balancing increasing laser power against increasing RAM noise.

From the plot it can be seen that doubling of the laser power increases the RAM/shot noise ratio by the same amount. This means that at higher power levels an additional increase in power has less effect on the ratio than at lower power levels. The SNR equation can be used to determine the balance between power and the noise sources.

This noise analysis has shown that the key noise contributors will be the RAM and shot noise. The shot noise is the lowest possible noise level that can be reached using the FM sounding technique. Any increase in RAM noise above the shot noise level will degrade an FM system's performance. The concentration on the RAM and shot noises determines that the focus in the SNR analysis that follows will be on those parameters that affect those two noise sources. These include the frequency modulation index (B), the amplitude modulation index of the RAM (M) and the power of the laser source.

8.3. SNR Equation Analysis

The SNR equation will now be used to analyze the FM sounding system further. The SNR will be plotted as a function of the parameters of the system to determine how the system performance varies with parameter value changes.

8.3.1. *FM modulation index*

One of the critical parameters for an FM sounding system is the FM modulation index. The SNR equation will now be used to determine the ideal FM index. Plotting the SNR versus FM index of gives the following plot.

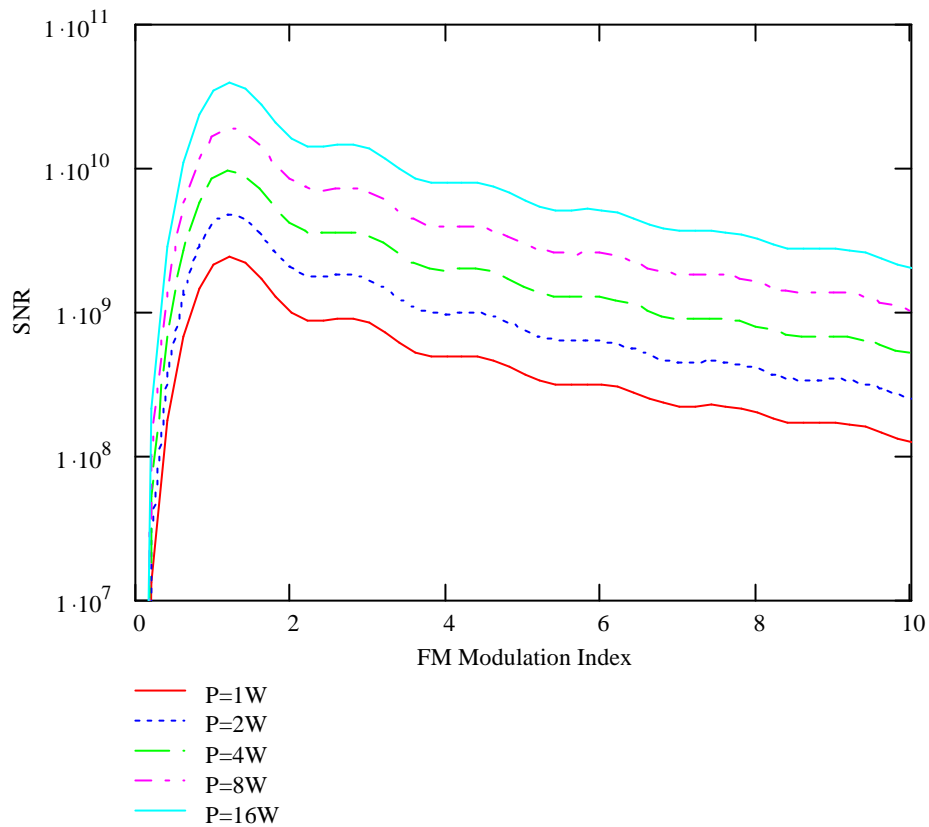


Figure 8.9. SNR vs. Power showing maximum at $B=1.2$

For all powers represented by these curves the peak SNR occurs at the same value. Determining the maximum's numerically gives a result of $B=1.2$ for the maximum value. This value of the FM modulation index will maximize the sensitivity of the technique. For smaller values of B the SNR drop off is steep. For larger values of B the drop off is gradual. However, larger values of B are more difficult to obtain, so the designer will have to trade off B for SNR.

8.3.2. AM modulation index

Now that an ideal FM modulation index has been identified, it can be used to help further

evaluate the AM modulation index. This index is associated with unwanted AM that is impressed on the laser beam. Current modulation of the laser is one source of this noise signal. Plotting the SNR against the amplitude modulation index (M) for values of the frequency modulation index (B) around 1.2 gives the following result.

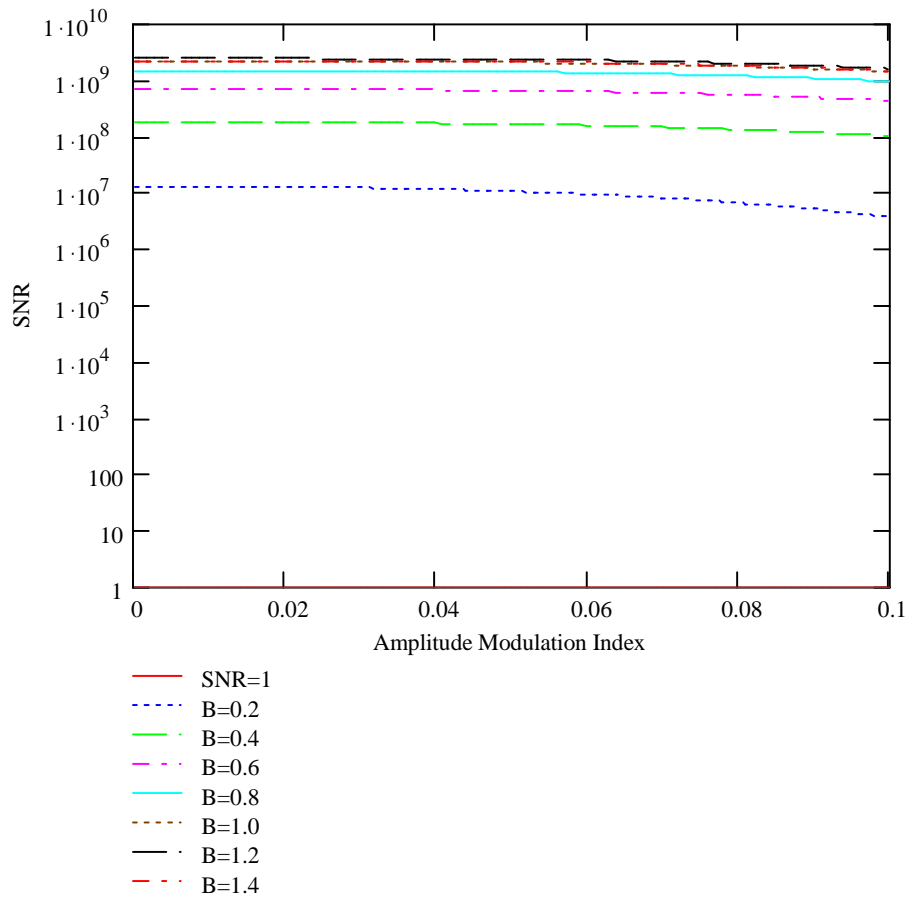


Figure 8.10. SNR as a function of M for various B around 1.2

The laser power is 1W.

It can be seen on the plot that the SNR decreases in general with increasing M. This is to be expected. As the amplitude modulation increases the noise increases and the SNR goes down. At this power level the SNR doesn't drop below 1 for any value of M.

This indicates one of the advantageous of sounding over scattering. The return power is much higher and, therefore, the signal to noise ratio can be maintained at much higher noise powers than would be the case with the low returns from scattered light.

8.3.3. *Laser power*

In laboratory FM the next step is often to calculate the sensitivity of the system. However, in this case we have a given, the Martian atmosphere, with the characteristics established in earlier sections using the LIDAR equation and its sounding variant. Since the Martian atmosphere is a given, instead of calculating the sensitivity we'll calculate the parameters that allow the system to maintain a SNR of at least one. This will establish the boundaries of the requirements for a Martian water vapor system.

These calculations are based on determining the minimum power levels required to maintain a minimum SNR, defined as $SNR=1$. Other parameters will be varied to determine how they affect his minimum power requirement.

The FM modulation index that results in the best SNR has been established to be $B=1.2$. That value and values around it will be used to determine the minimum power levels required and how that level varies with B.

Calculating the SNR as a function of laser power for various B results in the following plot.

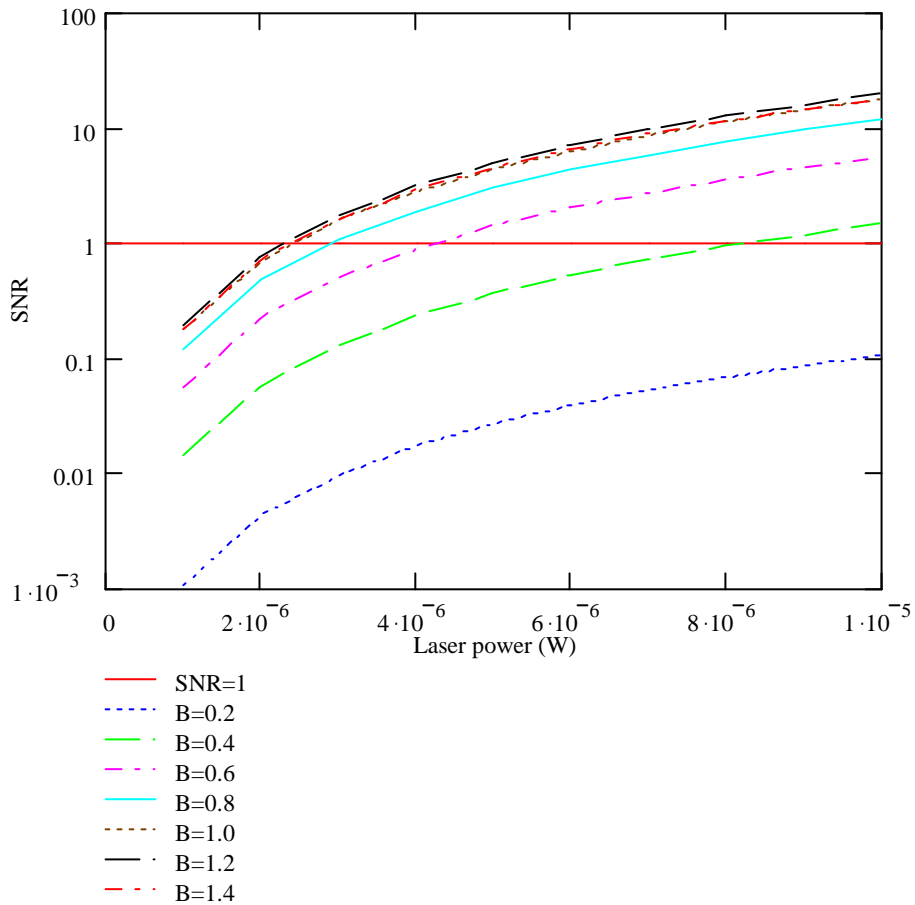


Figure 8.11. SNR as a function of power for various FM indices

As expected, as the laser power decreases the SNR decreases. The top curve on the plot is the B=1.2 curve. This has the best performance as a function of power. It crosses the SNR=1 line at about 2 μ W. For lower and higher values of B the power at SNR=1 is higher. For B=0.4 the power is 8 μ W. For B=1.4 it is 4 μ W. All these curves demonstrate that the signal can be detected down to very low laser power levels. This is an advantage on spaceflight systems. It could, for example, make it unnecessary to have an amplifier stage to increase the power output from a semiconductor amplifier. This reduces complexity and increases reliability. Reliability is also increase by the low power

levels required since power implies increased heat dissipation and a consequent reduction in reliability due to the effects of elevated temperatures. Lower temperatures also imply fewer cooling requirements and less complexity in the laser support system.

The above plot evaluates the dependence on the FM modulation index. The one below does the same for different values of the AM modulation index.

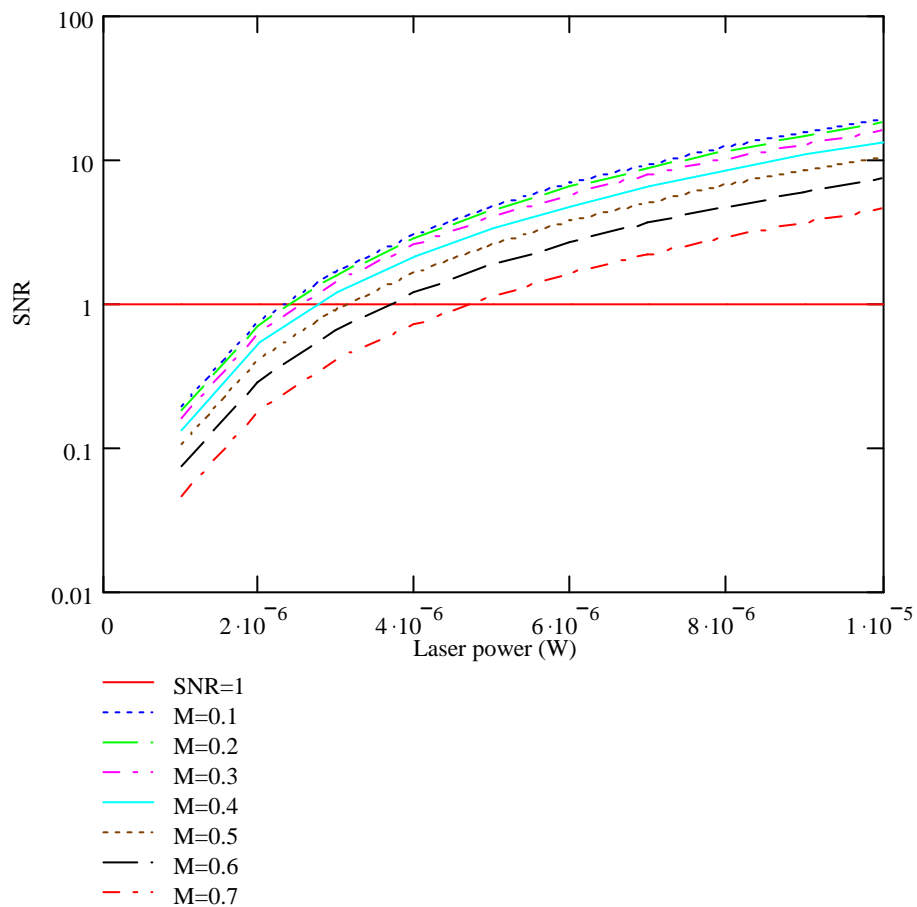


Figure 8.12 SNR as a function of power for various AM indices

These plots are all for $B=1.2$, the best case for B . As expected, the SNR decreases as the amount of AM modulation, represented by M , increases. The power level at which the SNR is equal to one increases as well. For the maximum level displayed, $M=0.7$, the

power level has climbed to 5 μW from 2 μW for $M=0.1$. These are fairly large values of M and so bound the problem well. Lowering M always improves the SNR, but relatively high values of M still allow the system to perform above noise limits at reasonable power levels.

8.4. Summary

This section has used the SNR equation developed in earlier sections to establish how the performance of an FM system depends on the major FM parameters, the FM and AM modulation indices, and the laser power output. It was concluded that the laser power output required to be able to detect the signal in the return is 2 μW for the best FM index value of 1.2. Plots were used to show the variation in power levels required for other levels of the FM index. Then the value of the AM modulation index was varied to determine the sensitivity of the required laser power level on it. The result showed, as expected, that less AM modulation on the source results in a higher SNR. More importantly, it showed that the SNR can be maintained at acceptable levels for relatively high values of the AM index. As a result, a designer can trade off AM modulation index for sensitivity or laser power.

This is particularly important if the advantageous of current modulation of the laser are important to the design. Current modulation necessarily involves the generation of unwanted AM. It is simpler and perhaps more reliable to implement, however. These results provide a basis for understanding the trade-offs between the FM index, the AM index, the laser power and SNR.

9. Summary

The goal set out at the beginning of this paper was to evaluate the use of FM techniques for remote sensing applications, specifically the detection of water vapor on Mars. FM techniques have demonstrated in the laboratory. However, the laboratory environment differs in important respects from the remote sensing environment. A sophisticated analysis of the FM technique as it applies to remote sensing is necessary. This paper accomplishes that through the use of complex analytic and computer modeling supported by experimental data. This data is both previously published data as well as a unique experiment.

Specifically, we recognize the key point that the FM technique depends on maintaining stable phase relationships between the source and detected signals. In order to mix the detected signal with the local oscillator it is necessary that the local oscillator can be maintained at the same frequency and phase as the detected signal. If this cannot be accomplished, it won't be possible to extract the return signal from the currents on the detector. We also recognized that in the case of a scattered return the phase of the return changes dependent on the distance the wave travels. As a result, when the waves arrive at the detector they will have different phases and could potentially degrade the FM signal.

A sophisticated analytic model was developed that allowed the calculation of the return current depending on the distance traveled. Limitations to this model led to the development of a comprehensive computer model that addressed these limitations. The analytic model was used to evaluate the computer model in the simpler cases and provided a valuable tool to ensure the computer model validity. These models were both

then used to calculate the effects of the scattered light on the phase of the return.

The models made the key prediction that the returns scattered from different points in the sky would interfere as currents on the detector. The result is a degradation of the signal due to destructive interference of the waves. It was noted that losses experienced by the light as it travels and is scattered might alleviate the problem by effectively matching the waves of a given phase in amplitude, reducing the destructive interference. Although the models demonstrated that this effect does occur, its contribution to the overall signal was negligible due to the long distances involved. Overall, the reduction in signal due to the interference of the detector currents was not reduced. The important conclusion is that using the FM techniques for remote sensing with scattered return is not practically feasible due to the interference of the waves of different phase at the detector.

Experimental data was required to support these conclusions and validate the model. Previously published data showing the results of combining two waves, one delayed relative to the other, on a detector was compared to the results predicted by the model. The comparison demonstrated that the model correctly predicted the results of the experiment.

We expanded upon that result in a unique experiment. This experiment was designed to test a part of the model not addressed by the previously published data but important to spacecraft applications, the current modulation of the laser. The use of current modulation has significant benefits in mass, power and reliability over the use of an external modulator for spaceflight applications, especially to a distant location like Mars. To further evaluate this option, to evaluate the effects of phase on the current modulated signal and to extend the validation of the model into this case, an experiment was

conducted by the author using the AM signal impressed on a semiconductor laser when it is modulated to produce sidebands. It was determined that this Residual AM (RAM) behaves like the AM produced by selective absorption of the sidebands. The model correctly predicts this. This result validates another important aspect of the model, the RAM contribution and the phase effects on it. It also demonstrates that the signal generated by absorption of an FM sideband behaves exactly like pure AM modulation of the signal. This makes quite clear that there are no differences between the absorption generated signal and the pure AM signal. The problem of adding the return signals at the detector reduces to that of adding delayed pure AM signals, which results in the interference and signal degradation predicted by the model and confirmed in experiment.

We then identified the FM sounding technique as a method that avoids the phase addition problem while still retaining the advantageous of the FM technique. We recognized that the FM sounding technique is similar to the laboratory technique in some important respects, which allowed the use of the laboratory SNR equation as a basis for our FM sounding SNR equation development. We extensively modified the FM laboratory SNR equation and the Martian LIDAR equation presented earlier in the paper and combined them into an FM sounding SNR equation. This equation incorporates both the FM sounding technique parameters and those of the Martian atmosphere to allow calculation of the performance of an FM sounding experiment to detect water vapor on Mars.

We then used the FM sounding SNR equation to address the main goal of this research, detection of water vapor on Mars. The results are a series of plots describing the performance of the system as a function of FM modulation index, AM modulation

index and laser power. These plots describe the basic design considerations that need to be addressed by the designer of such a system. They show the basic trade offs that will need to be made to achieve a given SNR.

The overall result is that analysis, modeling and experimentation presented here have established FM sounding as the best method for using FM techniques to measure water vapor on Mars.

10. Conclusions

The purpose of the analysis and experiments presented in this paper is to investigate using FM techniques in remote sensing applications, specifically to detect water vapor on Mars. To address this issue an analytic model and a sophisticated computer model were developed. Previously published data and a unique experiment both validated the models and confirmed the conclusions directly.

The first main conclusion is that FM remote sensing based on returns from scattered light has significant limitations that prevent the technique from achieving sensitive measurements of atmospheric constituents. The analysis and experiments support the conclusion that the scattered light is detected with differing phases due to the differing travel times to a given scatterer and back to the detector. As a result the detector current is reduced. Few scatterers are required to lower the current significantly. Not only is the signal lowered, but it fluctuates with scatterer position and number, making the extraction of the data on the absorption difficult. Comparison with previously published data and new experiments validate the model as well as support the general conclusion for the case of two scatterers. The experiment also establishes that a pure AM signal behaves exactly the same as the FM signal with absorption. The interaction of the FM return signals can be reduced to the interference of delayed AM wavefronts. The result, predicted by the models and confirmed in these experiments, is degradation of the signal due to interference of the delayed wavefronts.

The second main conclusion is the FM sounding can achieve high sensitivity to laser power ratios for water vapor detection on Mars. In this paper the Martian water vapor

model controlled the atmospheric parameters. The value of the FM technique for sounding was reflected in the lower powers required to get acceptable performance. Based on these results, laser power on the order of a few mW would be quite sufficient to measure water vapor columns in the Martian atmosphere. The data presented in this paper also establish the ideal value of the FM modulation index. The ideal value may be unattainable, however, so data was also presented allowing for tradeoffs between laser power, FM modulation and AM modulation. Thus, the basic design parameters have been established for building a Martian FM sounding system for detecting water vapor.

The goal of evaluating the FM technique for use in detecting Martian water vapor has been accomplished by determining that the FM sounding approach retains the advantageous of the FM technique without the disadvantages, analyzed in this research effort, of the scattering based approach. The determination of the limitations of the FM remote sensing technique using scattering and the capabilities of the FM sounding technique are significant contributions to the development of sensitive techniques for measuring water vapor on Mars as well as other constituents on other planets.

11. Recommendations for Future Work

This research established that the FM sounding technique holds the greatest promise for measuring water vapor on Mars using FM techniques. One of the main issues that will need to be investigated further is the capabilities of current modulated systems relative to externally modulated systems. There are advantages to current modulated systems in lower parts count, less complexity and more robust component design (due to the lack of electro-optic modulators), but they could be offset by reductions in sensitivity due to the increase in amplitude modulation noise. A detailed test program of an externally modulated system which addresses power and modulation requirements necessary to achieve a given sensitivity would establish the baseline for comparison. Similar testing of a current modulated system would determine if the sensitivity of the current modulated system is significantly degraded by the amplitude noise and, if so, by how much. All this testing would be best performed in a remote sensing mode. That is, with a target reflector set up at some distance away and a telescope. This would mimic a remote sensing mode of operation.

Once the basic concept has been shown to be sound an aircraft experiment can be built up. Such a system could have both external modulation and current modulation capabilities to enable direct comparison by switching back and forth between them. For this experiment, the laser light would be directed down toward the earth and reflected back. The water vapor in the column of atmosphere between the aircraft and the ground would be measured. This system could easily be configured to allow for conventional absorption measurements as well by turning off the modulation and allowing direct

detection of the carrier. This would allow direct comparison of the FM techniques, both current and external modulation, and a conventional direct absorption technique using the same setup. The results from this experiment would determine the capabilities of the FM sounding technique and prepare the way for a spaceflight design.

Analysis of the aircraft experiment data would determine the expected performance on Mars. This data and analysis could then be used to develop a proposal for a Martian water vapor system that is robust enough to fly to Mars and fits within the power and mass constraints typical of such a mission.

The analysis and experimental data presented in this paper were focused on the use of an FM system to detect water vapor on Mars. However, the models developed and verified as a consequence of this research are applicable to any atmospheric constituent and any atmosphere. Future work could include the analysis of the performance of an FM system for other atmospheric constituents and the comparison of the results to current methods. The columnar data obtained by FM sounding might be useful in the detection of other atmospheric constituents or pollutants. These other applications could be identified, the analysis performed using the models used in this research, and experiments conducted. In particular, the low power levels required to perform FM sounding might open up opportunities in low power, remotely activated and read devices for trace gas detection, such as pollutants.

The research presented here provides a firm basis for continued efforts to develop FM techniques for remote sensing applications.

12. References

- [1] Michael H. Carr, "Water on Mars", Oxford University Press, New York, 1996, p. 59.
- [2] Michael H. Carr, "Water on Mars", Oxford University Press, New York, 1996, p. 21.
- [3] Michael H. Carr, "Water on Mars", Oxford University Press, New York, 1996, p. 183.
- [4] Bjorkland, Gary C., "Frequency-modulation spectroscopy: a new method for measuring weak absorptions and dispersions", Optics Letters, Vol. 5., No. 1, p. 15-17, 1980.
- [5] D.S. Colburn, J.B. Pollack, R.M. Haberle, "Diurnal variations in optical depth at Mars: Observations and Interpretations", NASA Technical Memorandum 100057, May 1998.
- [6] Michael H. Carr, "Water on Mars", Oxford University Press, New York, 1996, p. 9.
- [7] R.M. Measures, "Laser Remote Sensing", Wiley Publishing, New York, 1984, pp. 238-243.
- [8] Avalanche Photodiodes: A User's Guide, optoelectronics.perkinelmer.com/library/papers/tp5.asp, 1998.
- [9] Gregory W. Switzer, "Semiconductor Laser Transmitter for Water Vapor LIDAR on Mars", Montana State University, Bozeman, Montana, Nov. 1998, p. 105.

-
- [10] Gregory W. Switzer, "Semiconductor Laser Transmitter for Water Vapor LIDAR on Mars", Montana State University, Bozeman, Montana, Nov. 1998, p. 106.
- [11] HiTran-PC, version 2.51, August 1997, Ontar Corporation, North Andover, MA.
- [12] Spiegelberg, et al, "Compact 100mW fiber laser with 2kHz bandwidth", OFC 2003, Atlanta, GA.
- [13] Koheras Product Catalog, available at www.koheras.com.
- [14] R.M. Measures, "Laser Remote Sensing", Krieger Publishing Company, 1992.
- [15] J.A. Reagan et al, "Assessment of extinction to backscatter ratio measurements made at 694.3nm in Tucson, Arizona", Aerosol Science Technology, Vol. 8, 1984.
- [16] J.D. Spinhirne, "Micro Pulse Lidar", IEEE Transactions on Geoscience and Remote Sensing, Vol. 31, No 1, January 1993.
- [17] P.H. Smith et al., "Results from the Mars Pathfinder Camera", Science, Vol. 278, December 5, 1997.
- [18] J.A. Reagan et al., "Lidar sensing of aerosols and clouds in the troposphere and stratosphere", Proceedings of the IEEE, Vol. 77, 1989.
- [19] J.D. Spinhirne et al., "Vertical distribution of aerosol extinction cross section and inference of aerosol imaginary index in the troposphere by lidar technique", Journal of Applied Meteorology, Vol. 19, 1980.
- [20] R.M. Measures, "Laser Remote Sensing", Krieger Publishing Company, 1992, p. 42.

-
- [21] Collis, R.T.H. and P.B. Russell, "LIDAR Measurement of Particles and Gases by Elastic Backscattering and Differential Absorption", Laser Monitoring of the Atmosphere, E.D. Hinckley, Ed. , Spring Verlag, 1976, pg. 89.
- [22] R.M. Measures, "Laser Remote Sensing", Krieger Publishing Company, 1992, p. 43.
- [23] R.M. Measures, "Laser Remote Sensing", Krieger Publishing Company, 1992, p. 37 and 138.
- [24] R.M. Measures, "Laser Remote Sensing", Krieger Publishing Company, 1992, p. 99.
- [25] Dubinsky, Ilia A., "Application of Highly Sensitive Spectroscopic Techniques to the Study of Intramolecular Dynamics and Remote Sensing", Doctoral Dissertation, MIT, February 1998.
- [26] Janik, G.R., C.B. Carlisle and T. F. Gallagher,"Two-tone frequency-modulation spectroscopy",J.Opt.Soc.Am.B, Vol. 3, No.8, pp.1070-1074, 1986.
- [27] Cooper, David E. and Russell E. Warren, "Two-tone optical heterodyne spectroscopy with diode lasers: theory of line shapes and experimental results", J.Opt. Soc. Am. B, Vol. 4, No. 4, pp. 470-480, 1987.
- [28] Cooper, David E. and Russel E. Warren, "Frequency modulation spectroscopy with lead-salt diode lasers: a comparison of single-tone and two-tone techniques", Applied Optics, Vol. 26, No. 17, pp. 3726-3732, 1987.
- [29] Cooper, David E. and Clinton B. Carlisle,"High-sensitivity FM spectroscopy with a lead-salt diode laser",Optics Letters, Vol. 13, No. 9, pp. 719-721, 1988.

-
- [30] Silver, Joel A., "Frequency-modulation spectroscopy for trace species detection: theory and comparison among experimental methods", *Applied Optics*, Vol. 31, No. 6, pp. 707-717, 1992.
- [31] Lenth, Wilfried,"Optical heterodyne spectroscopy with frequency and amplitude modulated semiconductor lasers", *Optics Letters*, Vol. 8, No. 11, pp. 575-577, 1983.
- [32] Lenth, W,"High Frequency Heterodyne Spectroscopy with Current-Modulated Diode Lasers", *IEEE Journal of Quantum Electronics*, Vol. QE-20, No. 9, pp. 1045-1050, 1984.
- [33] Lenth, W and M. Gehrtz,"Sensitive detection of NO₂ using high-frequency heterodyne spectroscopy with a GaAlAs diode laser",*Applied Physics Letters*, Vol. 47, No. 12, pp.1263-1265, 1985.
- [34] Cooper, David E. and J.P. Watjen,"Two-tone optical heterodyne spectroscopy with a tunable lead-salt diode laser",*Optics Letters*, Vol. 11, No. 10, pp. 606-608, 1986.
- [35] Dubinsky, I., K. Rybak, J.I. Steinfeld, R.W. Field,"Frequency-modulation-enhanced remote sensing", *Applied Physics B*, Vol. B 67, pp. 481-492.
- [36] Dubinsky, Ilia A., "Application of Highly Sensitive Spectroscopic Techniques to the Study of Intramolecular Dynamics and Remote Sensing", *Doctoral Dissertation, MIT*, February 1998, p. 68.
- [37] Saleh and Teich, "Fundamentals of Photonics", *John Wiley & Sons, Inc*, 1991, p. 69.

[38] Powers, P.E., C.A. Taatjes and Thomas J. Kulp, "Two-tone frequency modulation spectroscopy from laser light scattered off a hard target", *Applied Optics*, p. 4735, 1996.

[39] Carlisle, Clinton B., David Cooper and Horst Preier," Quantum noise-limited FM spectroscopy with a lead-salt diode laser", *Applied Optics*, Vol. 28, No. 13, pp. 2567-2576, 1989.

[40] Bomse, David S., Alan C. Stanton, and Joel Silver, "Frequency modulation and wavelength modulation spectroscopies: comparison of experimental methods using a lead-salt diode laser", *Applied Optics*, Vol. 31, No. 6, pp. 718-731, 1992.

[41] Modugno, G., C. Corsi, M. Gabrysch, F. Marin, M. Inguscio, "Fundamental noise sources in a high-sensitivity two-tone frequency modulation spectrometer and detection of CO₂ at 1.6 μm and 2 μm", *Applied Physics B* 67, p. 289-296, 1998.

[42] Silver, Joel A., "Frequency-modulation spectroscopy for trace species detection: theory and comparison among experimental methods", *Applied Optics*, Vol. 31, No. 6, p. 712, 1992.